

THE RELATION BETWEEN QUASAR AND MERGING GALAXY LUMINOSITY FUNCTIONS AND THE MERGER-INDUCED STAR FORMATION RATE OF THE UNIVERSE

PHILIP F. HOPKINS¹, RACHEL S. SOMERVILLE², LARS HERNQUIST¹, THOMAS J. COX¹, BRANT ROBERTSON¹, & YUEXING LI¹

Submitted to ApJ, February 13, 2006

ABSTRACT

Using a model for the self-regulated growth of supermassive black holes in mergers involving gas-rich galaxies, we study the relationship between quasars and the population of merging galaxies and, as a consequence, predict the merger-induced star formation rate density of the Universe. These mergers drive nuclear inflows of gas, fueling starbursts and “buried” quasar activity until feedback energy from black hole growth expels the gas, rendering the quasar briefly visible as a bright optical source. As black hole accretion declines, the quasar dies, and the stellar remnant relaxes as a passively evolving spheroid with properties and correlations typical of red, elliptical galaxies. Based on the time history of these events in our simulations, we demonstrate that the observed *statistics* of merger rates/fractions, luminosity functions, mass functions, star formation rate distributions, specific star formation rates, quasar luminosity functions, quasar host galaxy luminosity functions, and elliptical/red galaxy luminosity and mass functions are self-consistent and follow from one another as predicted by the merger hypothesis. We use our simulations to de-convolve both the quasar and merging galaxy luminosity functions to determine the birthrate of black holes of a given final mass and merger rates as a function of the total stellar mass and the mass of new stars formed during the merger. We use this to predict the merging galaxy luminosity function in several observed wavebands (e.g. UV, optical, and near-IR), color-magnitude relations, mass functions, absolute and specific star formation rate distributions and star formation rate density, and quasar host galaxy luminosity function, as a function of redshift from $z = 0 - 6$. We invert this prescription and predict e.g. quasar luminosity functions from observed merger luminosity functions or star formation rate distributions. Our results show good agreement with observations, but idealized models of quasar lightcurves give inaccurate estimates and are ruled out by comparison of merging galaxy and quasar observations at $> 99.9\%$ confidence, provided that quasars are triggered in mergers. Using only observations of quasars, we estimate the contribution of mergers to the star formation rate density of the Universe even to high redshifts $z \sim 4$ and constrain the evolution in the characteristic initial gas fractions of quasar and spheroid-producing mergers.

Subject headings: quasars: general — galaxies: active — galaxies: evolution — cosmology: theory

1. INTRODUCTION

It is now widely believed that structure in our Universe grew hierarchically, as small objects merged to form progressively larger systems. Direct observations of interactions between galaxies led to the formulation of the “merger hypothesis” (Toomre & Toomre 1972; Toomre 1977), according to which ellipticals originate when spiral galaxies collide, as suggested by simulations (for reviews, see e.g. Barnes & Hernquist 1992; Barnes 1998). Observations also show that most galaxies contain supermassive black holes (e.g. Kormendy & Richstone 1995; Richstone et al. 1998; Kormendy & Gebhardt 2001) and that the masses of these black holes are correlated with either the mass (Magorrian et al. 1998) or the velocity dispersion (i.e. the $M_{\text{BH}}-\sigma$ relation: Ferrarese & Merritt 2000; Gebhardt et al. 2000) of their host spheroids. These correlations imply that the evolution of supermassive black holes and galaxies are linked, a point of view supported by simulations showing that the energy released by self-regulated black hole growth in a galaxy merger has a significant impact on the structure of the remnant (Di Matteo et al. 2005).

Many observations indicate that galaxy mergers trigger starbursts and black hole growth and play a role in structuring ellipticals. Infrared luminous galaxies are thought to

be powered by nuclear starbursts (e.g. Soifer et al. 1984a,b; Sanders et al. 1986, 1988a,b; for a review, see e.g. Soifer et al. 1987), and the most intense of these, ultraluminous infrared galaxies (ULIRGs), are invariably associated with mergers (e.g. Allen et al. 1985; Joseph & Wright 1985; Armus et al. 1987; Kleinmann et al. 1988; Melnick & Mirabel 1990; for reviews, see Sanders & Mirabel 1996 and Jogege 2005). Radio observations identify large quantities of dense gas in the centers of ULIRGs, (e.g. Scoville et al. 1986; Sargent et al. 1987, 1989), supplying fuel to feed black hole growth, and providing a mechanism for boosting the concentration and central phase space density to resemble those typical of ellipticals (see, e.g. Carlberg 1986; Gunn 1987; Lake 1989; Hernquist 1992, 1993a; Hernquist et al. 1993; Robertson et al. 2005c). Some ULIRGs have “warm” IR spectral energy distributions (SEDs), which have been interpreted as evidence that they harbor buried quasars (e.g. Sanders et al. 1988c), as indicated by X-ray observations of growing black holes in e.g. NGC6240 and other ULIRGs (e.g. Komossa et al. 2003), which are heavily obscured at optical and infrared wavelengths (e.g. Gerssen et al. 2004; Max et al. 2005; Alexander et al. 2005a,b; Borys et al. 2005). These facts, and the overlap between bolometric luminosities of ULIRGs and quasars, suggest that quasars originate from an IR luminous phase of galaxy evolution caused by mergers (Sanders et al. 1988a), a proposal supported by observations of quasar hosts (e.g. Stockton 1978; Heckman et al. 1984; Stockton & MacKenty 1987; Stockton & Ridgway 1991; Hutchings

¹ Harvard-Smithsonian Center for Astrophysics, 60 Garden Street, Cambridge, MA 02138

² Max-Planck-Institut für Astronomie, Königstuhl 17, D-69117 Heidelberg, Germany

& Neff 1992; Bahcall et al. 1994, 1995, 1997; Canalizo & Stockton 2001).

Observations of individual merging galaxies and merger remnants (e.g., Lake & Dressler 1986; Doyon et al. 1994; Oliva et al. 1995; Shier & Fischer 1998; James et al. 1999) have shown that their kinematic and photometric properties, including velocity dispersions, concentrations, stellar masses, light profiles, and phase space densities, are consistent with their eventual evolution into typical $\sim L_*$ elliptical galaxies. Furthermore, the correlations obeyed by these mergers and remnants (e.g., Genzel et al. 2001; Rothberg & Joseph 2004, 2005), are observed to be quite similar to e.g. the observed fundamental plane and Kormendy relations for relaxed ellipticals, and consistent with relaxation onto these relations as stellar populations age.

While these various studies have plausibly established that gas-rich mergers pass through starburst and quasar phases and evolve into spheroidal galaxies, little is known about the *statistics* of galaxy mergers. For example, it is not clear if there are sufficient numbers of mergers to account for the present density of spheroids or whether all gas-rich mergers or elliptical-producing mergers undergo an infrared luminous starburst phase. Various observational studies have estimated the galaxy merger rate and its evolution (e.g., Xu & Sulentic 1991; Burkley et al. 1994; Carlberg et al. 1994; Sulentic & Rabaca 1994; Keel & Wu 1995; Soares et al. 1995; Yee & Ellington 1995; Patton et al. 1997; Zepf & Koo 1989; Toledo et al. 1999; Le Fèvre et al. 2000; Patton et al. 2000, 2002; Conselice et al. 2003; Xu et al. 2004; Lin et al. 2004; Bundy et al. 2004; Conselice et al. 2005), but the uncertainties in the measurements are large, and it is not known if the merger rates are consistent with the growth of the remnant red/elliptical galaxy population and the number of bright quasars observed.

Recent measurements of galaxy stellar mass functions separated by color or morphology (Bundy et al. 2005a,b; Franceschini et al. 2006; Pannella et al. 2006) have shown that “transition mass,” above which the red galaxy population dominates the galaxy mass function, increases with redshift, tracing a general trend of “cosmic downsizing.” As low-mass, red galaxies build up, the mass of the largest star-forming galaxies, although less well-constrained, decreases correspondingly, further supporting the idea that star formation is “quenched” in these systems and that they move to the red sequence (Bundy et al. 2005b). Comparing observations of the transition or quenching mass with the characteristic masses of quasars (corresponding to the break in the observed quasar luminosity function) and merging galaxies, Hopkins et al. (2006) have shown that these trace the same mass and evolve together over the range $0 < z \lesssim 3$, further suggesting that the populations must be linked. Such a suggestive connection demands a more detailed analysis to understand the relationships between observed merger and quasar distributions.

While many ULIRGs display some (generally moderate or low) level of X-ray activity characteristic of active galactic nuclei (AGN), it is not clear whether all such events terminate in a bright, optical quasar phase. Nearby hosts of bright quasars exhibit features characteristic of mergers (e.g., Bahcall et al. 1997; Canalizo & Stockton 2001) and starbursts (e.g., Brotherton et al. 1999, 2002; Canalizo et al. 2000; Yip et al. 2004; Vanden Berk et al. 2005), but at higher redshifts such determinations are difficult and the observations are less conclusive (e.g., Schweizer 1982; Dunlop et al.

2003; Floyd et al. 2004). Thus, it is not clear if most bright quasar activity at high redshifts is caused by mergers, or even if there is sufficient merger activity to account for the observed quasar population. Moreover, the few observational studies of the distribution of quasar host luminosities (Bahcall et al. 1997; McLure et al. 1999; Falomo et al. 2001; Hamilton et al. 2002; Jahnke & Wisotzki 2003; Dunlop et al. 2003; Floyd et al. 2004; Vanden Berk et al. 2005) have not yet determined whether this distribution is expected (as a subset of the merging galaxy population), or whether it implies further, specific requirements for quasar hosts beyond their being interacting systems with reservoirs of cold gas or different modes of quasar fueling. More recent observations (Straughn et al. 2005) and simulations (Hopkins et al. 2005a) suggest that the stages most likely to be identified as mergers can be quite distinct from the merger-driven AGN phase, further complicating such comparisons.

The contribution of merger activity to the star formation density of the Universe is not well known, particularly at high redshifts (e.g., Brinchmann et al. 1998; Menanteau et al. 2001, 2005; Bell et al. 2005a), and traditional observational measurements which require morphological identification of star-forming galaxies are difficult to extend to these redshifts and are likely incomplete (Wolf et al. 2005), making particularly valuable any independent constraints that do not require direct morphological information, such as those from quasar populations. Even fewer estimates exist for the distribution of star formation rates in merging systems (e.g., Bell et al. 2005a), and whether or not these distributions are consistent with the notion that gas-rich mergers pass through a starburst phase and build up the stellar mass observed in the elliptical galaxy population.

These large and important uncertainties in the relation of elliptical galaxy, merger remnant, LIRG/ULIRG, merging (peculiar/interacting) galaxy, starburst, and quasar populations are related to the same fundamental question: Are the luminosity and mass distributions of quasars, quasar host galaxies, merging galaxies, starbursts, and elliptical systems self-consistent? If the primary mechanism for the creation of red/elliptical galaxies is through gas-rich mergers, resulting in an intermediate starburst phase which is terminated when black hole growth exceeds a critical threshold and expels gas from the central regions of the remnant, then these populations must be self-consistent at all redshifts.

One major obstacle to relating these populations has been the lack of theoretical models which incorporate all the relevant physical processes. Large-scale cosmological simulations (e.g., Cen et al. 1994; Zhang et al. 1995; Hernquist et al. 1996; Katz et al. 1996a,b; Navarro et al. 1996; Croft et al. 1998, 1999, 2002; Davé et al. 1999; McDonald et al. 2000, 2004; Hui et al. 2001; Viel et al. 2003, 2004) and semi-analytic models (e.g., Kauffmann & Haehnelt 2000; Cole et al. 2000; Somerville et al. 2001; Volonteri et al. 2003; Wyithe & Loeb 2003; Granato et al. 2004; Somerville et al. 2004a; Baugh et al. 2005; Croton et al. 2005) have provided a framework for understanding the intergalactic medium in the context of hierarchical structure formation, but have not been able to resolve the small scales within individual galaxies associated with star formation, supernova feedback, black hole accretion and feedback, and dust obscuration, which are critical for inferring the relation between e.g. quasar and starburst populations and overall merger rates. Therefore, these processes currently must be treated via simplified, tunable parameterizations rather than modeled

physically. Ideally, the prescriptions should be determined from physically motivated analytical or numerical models, which themselves have been tested against observations.

By using high-resolution simulations of individual galaxies and mergers between them, we can gain the necessary resolution to study the physical processes of interest. These simulations, which dynamically incorporate the effects of star formation and pressurization of multi-phase interstellar gas by supernova feedback (Springel & Hernquist 2003a) as well as black hole growth and feedback (Springel et al. 2005b), allow us to study the evolution of mergers and quantify the relation between various phases. Di Matteo et al. (2005) and Springel et al. (2005a,b) have shown that the gas inflows produced by gravitational torques during a merger both trigger starbursts and fuel rapid black hole growth. However, for most of this period, the black hole is obscured (Hopkins et al. 2005a). The growth of the black hole is determined by the gas supply and terminates abruptly when significant gas is expelled owing to the impact of feedback energy from black hole accretion on the surrounding gas, resulting in a bright but brief optical quasar phase. Eventually, as the gas is heated and driven out, the accretion rate falls, leaving a dead quasar in an ordinary galaxy. The self-regulated nature of black hole growth in mergers explains observed correlations between black hole mass and properties of normal galaxies (Di Matteo et al. 2005), as well as the color distribution of ellipticals (Springel et al. 2005a).

Previously (Hopkins et al. 2005a-e, g; Lidz et al. 2005), we considered the implications of this modeling and showed that it enables a self-consistent reproduction of many quasar observables, with no dependence on a particular prior cosmological distribution. We measured the differential luminosity-dependent quasar lifetime, i.e. the amount of time a given quasar (with a fixed peak luminosity or final, post-merger black hole mass) spends in a given luminosity interval, as a function of luminosity. We found that the quasar lifetime for a given peak luminosity *increases* at lower luminosities – i.e. quasars spend most of their lives in phases fainter than their peak luminosities. This yields a different interpretation of the quasar luminosity function than implied by idealized models of quasar lightcurves (in which quasars grow/decay in a step function or pure exponential manner), namely that the steep, bright end of the quasar luminosity function traces quasars accreting at high Eddington ratios near their peak luminosities, but the shallow, faint end is dominated by quasars with high peak luminosities but which are seen in less luminous states. The distribution of quasar birthrates as a function of their peak luminosities (final black hole masses), which is directly related to e.g. the gas-rich galaxy merger rate as a function of final galaxy mass, is *peaked* at a luminosity/mass corresponding to the break in the observed quasar luminosity function, with objects near the peak in this distribution dominating the observed faint-end quasar luminosity function in their fainter (luminosity well below peak) phases.

In Hopkins et al. (2005f), we extended our modeling to predict the distribution of remnant elliptical galaxies formed in mergers. Because the spheroid stellar mass or velocity dispersion is correlated with the final black hole mass in our simulations, we can use our modeling of quasar lifetimes and our determination of the birthrate of quasars as a function of their peak luminosity (final black hole mass) to infer the rate at which spheroids with given properties are formed in mergers as a function of e.g. mass, velocity dispersion, size, and redshift. This allows us to accurately reproduce spheroid

mass, luminosity, and velocity dispersion functions, age distributions, mass-radius and luminosity-size relations, mass-to-light ratios, color-magnitude relations, and distributions of young (blue) spheroids at redshifts $z = 0-6$. The co-evolution of star formation, black hole growth, and obscuration is a key element in this analysis, and corresponding predictions made either neglecting the role of black hole feedback in terminating star formation or by modeling the quasar lightcurve in an idealized manner are inaccurate.

Because, in principle, the merger hypothesis provides a self-consistent framework for describing the co-formation of quasars and spheroids that reproduces a wide range of observations, it is of interest to apply such modeling to statistics and properties of merging systems. In this paper, we use the modeling described above to study the implied relation between the quasar luminosity function (QLF), merging galaxy luminosity function (MGLF), quasar host galaxy luminosity function (HGLF), distribution of star formation rates in mergers (SFRF), and the cumulative merger rates and star formation rate density triggered by mergers.

In § 2, we describe our simulations, and in § 3 we use them to determine the evolution of near-IR and optical/UV luminosities (§ 3.1), colors (§ 3.2), and star formation rates (§ 3.3) during mergers, as a function of host galaxy properties. In § 4 we use our modeling to predict the quasar luminosity function from the observed merging galaxy function (at the same redshift), and vice versa (§ 4.2), in both K -band and the optical/UV. We use this to predict the underlying birthrate of spheroids/quasars with a given final mass/peak luminosity, and compare this with the observed merger mass functions (§ 4.3). Likewise, we use this to predict the distribution of star formation rates in mergers, independently from the observed quasar and merger luminosity functions, and compare with the observed star formation rate functions (§ 4.4). In § 5, we use the observed evolution in the quasar luminosity function to predict the evolution of the merging galaxy luminosity function and star formation rate function, as well as integrated quantities such as the luminosity, mass, and star formation rate densities in mergers, at redshifts $z = 0-6$. In § 6 we consider the relation between the MGLF and HGLF, predicting the quasar host galaxy luminosity function, the joint distribution of observed quasar and quasar host galaxy luminosities, and their co-evolution. Finally, in § 7, we summarize our results and discuss their implications for the merger hypothesis, various theoretical models, and future observations.

Our methodology and calculations are described in detail in § 2 and § 3, but readers interested in the main results may wish to skip to § 4, which compares and tests the relation between various stages and measures of merger-induced activity, and § 5, which uses these relations to predict evolution of these measures with redshift.

Throughout, we adopt a $\Omega_M = 0.3$, $\Omega_\Lambda = 0.7$, $H_0 = 70 \text{ km s}^{-1} \text{ Mpc}^{-1}$ cosmology. All magnitudes are Vega magnitudes, unless otherwise stated.

2. THE SIMULATIONS

Our merger simulations were performed with the parallel TreeSPH code GADGET-2 (Springel 2005). GADGET-2 is based on a fully conservative formulation (Springel & Hernquist 2002) of smoothed particle hydrodynamics (SPH), which conserves energy and entropy simultaneously even when smoothing lengths evolve adaptively (see e.g., Hernquist 1993b, O’Shea et al. 2005). Our simulations account for radiative cooling, heating by a UV

background (as in Katz et al. 1996, Davé et al. 1999), and incorporate a sub-resolution model of a multiphase interstellar medium (ISM) to describe star formation and supernova feedback (Springel & Hernquist 2003a). Feedback from supernovae is captured in this sub-resolution model through an effective equation of state for star-forming gas, enabling us to stably evolve disks with arbitrary gas fractions (see, e.g. Springel et al. 2005b; Springel & Hernquist 2005; Robertson et al. 2004, 2005a).

Supermassive black holes (BHs) are represented by “sink” particles that accrete gas at a rate \dot{M} estimated from the local gas density and sound speed using an Eddington-limited prescription based on Bondi-Hoyle-Lyttleton accretion theory. The bolometric luminosity of the black hole is taken to be $L_{\text{bol}} = \epsilon_r \dot{M} c^2$, where $\epsilon_r = 0.1$ is the radiative efficiency. We assume that a small fraction (typical $\approx 5\%$) of L_{bol} couples dynamically to the surrounding gas, and that this feedback is injected into the gas as thermal energy, weighted by the SPH smoothing kernel. This fraction is a free parameter, which we determine as in Di Matteo et al. (2005) by matching the observed $M_{\text{BH}} - \sigma$ relation. For now, we do not resolve the small-scale dynamics of the gas in the immediate vicinity of the black hole, but assume that the time-averaged accretion rate can be estimated from the gas properties on the scale of our spatial resolution (roughly ≈ 20 pc, in the best cases).

The construction of progenitor galaxy models is described in Springel et al. (2005b), and we review their properties here. For each simulation, we generate two stable, isolated disk galaxies, each with an extended dark matter halo with a Hernquist (1990) profile, motivated by cosmological simulations (e.g. Navarro et al. 1996; Busha et al. 2004), an exponential disk of gas and stars, and (optionally) a bulge. The galaxies have masses $M_{\text{vir}} = V_{\text{vir}}^3 / (10GH_0)$ for $z = 0$, with the baryonic disk having a mass fraction $m_{\text{d}} = 0.041$, the bulge (when present) has $m_{\text{b}} = 0.0136$, and the rest of the mass is in dark matter, with a concentration parameter scaled as in Robertson et al. (2005b) appropriately for the galaxy mass and redshift following Bullock et al. (2001). The disk scale-length is computed based on an assumed spin parameter $\lambda = 0.033$, chosen to be near the mode in the λ distribution measured in simulations (Vitvitska et al. 2002), and the scale-length of the bulge is set to 0.2 times the resulting value.

Typically, each galaxy initially consists of 168000 dark matter halo particles, 8000 bulge particles (when present), 40000 gas and 40000 stellar disk particles, and one BH particle. We vary the numerical resolution, with many of our simulations using instead twice as many particles in each galaxy, and a subset of simulations with up to 128 times as many particles. We vary the initial seed mass of the black hole to identify any systematic dependence of our results on this choice. In most cases, we choose the seed mass either in accord with the observed $M_{\text{BH}} - \sigma$ relation or to be sufficiently small that its presence will not have an immediate dynamical effect. Given the particle numbers employed, the dark matter, gas, and star particles are all of roughly equal mass, and central cusps in the dark matter and bulge profiles are reasonably well resolved (see Figure 2 in Springel et al. 2005b). The galaxies are then set to collide from a zero energy orbit. The majority of our simulations employ parabolic orbits, but we vary the inclinations of the disks and the pericenter separation.

The form of our fitted quasar lifetimes and galaxy scaling relations are based on a series of several hundred simulations of colliding galaxies, described in detail in Robertson et al.

(2005b,c) and Hopkins et al. (2005e). We vary the numerical resolution, the orbit of the encounter, the masses and structural properties of the merging galaxies, initial gas fractions, halo concentrations, the parameters describing star formation and feedback from supernovae and black hole growth, and initial black hole masses. In particular, the impact of feedback from supernovae is described through the parameter q_{EOS} , which ranges from $q_{\text{EOS}} = 0$ for an isothermal gas with effective temperature of 10^4 K, to $q_{\text{EOS}} = 1$, which describes our full multiphase model for the ISM which yields an effective temperature close to 10^5 K.

Progenitor galaxies in our merger simulations have virial velocities $V_{\text{vir}} = 80, 113, 160, 226, 320,$ and 500 km s^{-1} , and redshifts $z = 0, 2, 3,$ and 6 , and our simulations span a range in final black hole mass $M_{\text{BH}} \sim 10^5 - 10^{10} M_{\odot}$. This large set of simulations allows us to investigate merger evolution for a wide range of galaxy properties and to identify any systematic dependence of our modeling. Further, the extensive range of conditions probed gives us a large dynamic range in our simulations, with final spheroid masses spanning $M_* \sim 10^8 - 10^{13} M_{\odot}$, covering essentially the entire range of the observations we consider, from the least massive (faintest) galaxies to the most massive (brightest) galaxies at all redshifts. Of particular interest in this work, we consider initial disk gas fractions (by mass) of $f_{\text{gas}} = 0.2, 0.4, 0.8,$ and 1.0 for several variations of virial velocities, redshifts, and ISM gas equations of state. Most of our simulations are equal-mass mergers, but we have varied the mass ratio to include 2:1, 3:1, 5:1, and 10:1 mergers.

3. LUMINOSITIES, COLORS, AND STAR FORMATION RATES OF MERGERS

Given our large suite of simulations, we wish to calculate a number of expected galaxy properties in mergers, as a function of e.g. the galaxy masses and other conditions. We can then use these throughout to interpret and relate various observations of merging galaxies.

3.1. Host Galaxy Luminosities

3.1.1. K-band Luminosities

To de-convolve the observed pair or merging galaxy luminosity function (MGLF) and infer a merger rate as a function of e.g. galaxy stellar mass, we must first describe the host galaxy lightcurve in the observed band. In the simulations, star formation is tracked self-consistently, so that stellar ages are known and stellar metallicities are determined from the star-forming gas, which itself is enriched by star formation. For pre-existing stars (i.e. initial bulge or disk stars when the gas fraction is less than unity), we generally assume a constant prior on the star formation history (up to the simulation redshift), with metal enrichment calculated self-consistently from initial primordial gas. We have compared this with e.g. exponentially declining star formation rates (“ τ -models”) and late-type star formation histories fitted from observations (e.g., Kauffmann et al. 2003b; Hammer et al. 2005), and find it makes little difference, as new stars formed during the simulation dominate the observed luminosity. From the properties of the stars in our simulations, we use the stellar population synthesis models of Bruzual & Charlot (2003) assuming a Salpeter (1955) initial mass function, to measure the luminosity in a given band.

We first consider the simple case of the K-band galaxy luminosity in mergers. Because the K-band mass to light ratio M/L_K is only weakly dependent on time, a constant

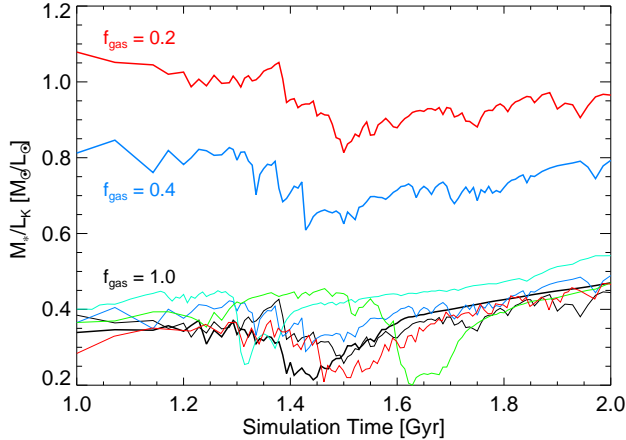


FIG. 1.— Ratio of total stellar mass to total K -band luminosity as a function of time in three representative simulations with gas fractions $f_{\text{gas}} = 0.2, 0.4, 1.0$ as labeled (thick lines). For $f_{\text{gas}} = 1.0$, several simulations with $V_{\text{vir}} = 80\text{--}320\text{ km s}^{-1}$ and $q_{\text{EOS}} = 0.25\text{--}1$ are shown (thin lines). The K -band mass-to-light ratio depends weakly on gas fraction in a simple systematic manner, but not on other varied merger properties.

$M/L_K \approx 1.4$ is usually assumed (e.g., Cole et al. 2001). Figure 1 shows the result of calculating this directly from our simulations for several representative cases, with identical virial velocities $V_{\text{vir}} = 160\text{ km s}^{-1}$ and $q_{\text{EOS}} = 1.0$, $z_{\text{gal}} = 0$, but with a varying gas fraction $f_{\text{gas}} = 0.2, 0.4, 1.0$ (thick lines). In each simulation, we calculate the total K -band luminosity as described above and plot the total stellar mass divided by total K -band luminosity as a function of time during the final merger phase in the simulations. The K -band total mass-to-light ratio is relatively constant with time, even in mergers with a 100% gas disk, reflecting the weak evolution in M/L_K with age, and implying that using a constant M/L_K for merging systems is accurate to $\sim 10\text{--}20\%$.

Figure 1 also explicitly compares systems with different virial velocity and ISM gas equations of state, but similar gas fractions $f_{\text{gas}} = 1.0$. The thin lines show simulations with $f_{\text{gas}} = 1.0$ but $V_{\text{vir}} = 80$ (black), 113 (blue), 160 (cyan), 226 (green), and 320 km s^{-1} (red). These use $q_{\text{EOS}} = 1.0$ as well, except for the thin cyan curve which has $q_{\text{EOS}} = 0.25$ (the only difference between this simulation and that of the thick black curve). It is clear that there is no significant systematic difference in M/L_K at fixed gas fraction. However, there is a systematic difference between systems of different gas fractions, so that M/L_K is significantly lower for high- f_{gas} systems which are dominated by younger stellar populations.

We can estimate the average mass-to-light ratio in a merger as a function of f_{gas} with a simple model, in which a galaxy of total final stellar mass $M_{*,\text{tot}}$ forms a fraction f_{gas} of its mass in a single burst in the merger (i.e. assuming the limit of efficient conversion of gas to stars) with mass-to-light ratio $(M/L_K)_{\text{new}}$, and the remaining mass comes from an older population with $(M/L_K)_{\text{old}}$. This gives

$$\frac{M}{L_K} = \frac{(M/L_K)_{\text{new}}}{f_{\text{gas}} + (1 - f_{\text{gas}}) \frac{(M/L_K)_{\text{new}}}{(M/L_K)_{\text{old}}}}. \quad (1)$$

Fitting to the mean M/L_K in our mergers as a function of f_{gas} gives $(M/L_K)_{\text{new}} \approx 0.4$ and $(M/L_K)_{\text{old}} \approx 1.4$, corresponding to stellar populations with mean ages ~ 0.5 and 5 Gyr, respec-

tively, reasonable values for the stellar populations observed in a merger. This equation gives the mean M/L_K accurate to $\sim 10\text{--}20\%$, i.e. comparable to the scatter in M/L_K in a given merger and across mergers with varied parameters (but similar gas fractions). As demonstrated in Figure 1, there is no clear systematic dependence of the mean K -band mass-to-light ratio on other quantities such as the virial velocity or ISM equation of state (we have also compared against e.g. initial black hole masses, the presence or absence of initial bulges, and the orbital parameters of the merging galaxies). Furthermore, although Equation (1) depends on the gas fraction of the merging galaxies, this dependence is relatively weak, as a factor of 2 change in gas fraction (e.g. $f_{\text{gas}} = 0.1 \rightarrow 0.2$ or $f_{\text{gas}} = 0.2 \rightarrow 0.4$) results in only a $\sim 20\%$ change in M/L_K , which is generally smaller than the relevant observational uncertainties and much smaller than the resulting change in, e.g. the UV luminosity for the same difference in gas fraction.

3.1.2. 280 nm Luminosities

We next consider a synthetic UV band centered at 280 nm, with a 40 nm width, for direct comparison with the results of Wolf et al. (2005) from the GEMS and GOODS surveys. This band is normalized to the solar luminosity in the 280/40 passband, which is $M_{\odot,280} = 6.66$ in Vega units or $L_{\odot,280} = 2.56 \times 10^{10}\text{ W/Hz}$. Here, we use the Starburst99 population synthesis models (Leitherer et al. 1999) to calculate the UV spectra of the stellar particles in our simulations and the corresponding magnitude M_{280} . Attenuation is important in mergers at these wavelengths, and we include this in the manner described in Hopkins et al. (2005a,e).

Briefly, we calculate the column density along ~ 1000 lines-of-sight to each simulation stellar particle at each time during the merger, using the SPH formalism and multiphase ISM equation of state model of the simulations (Springel & Hernquist 2003a) to determine the density, metallicity, and ionization state of gas in the “warm/hot” ISM through which the majority of sightlines will pass (i.e. neglecting mass collapsed in cold clouds). We adopt a gas-to-dust ratio scaled by metallicity (e.g., Bouchet et al. 1985) and normalized to that of the Milky Way, $A_B/N_{\text{HI}} = 8.47(Z/0.02) \times 10^{-22}\text{ cm}^2$, and a Small Magellanic Cloud-like reddening curve (as suggested by observations for the host galaxies of quasars, e.g. Hopkins et al. 2004, Ellison et al. 2005, although the 280 nm cross-section is decreased by only 6% if we instead assume a Milky Way-like reddening curve) with the form from Pei (1992), to attenuate the intrinsic spectrum of each stellar particle. We do not perform a full radiative transfer calculation, and therefore do not model scattering or re-processing of radiation by dust in the infrared. However, we compare the column densities to quasars calculated by variations of this method in Hopkins et al. (2005b) (see their Figures 1, 5, & 6) and find that typical uncertainties are a factor $\sim 2\text{--}3$ in N_{HI} , generally smaller than the variation across different simulations and viewing angles. Furthermore, we find below that our results for the visible (attenuated) luminosities agree well with those expected from the calculations in Jonsson et al. (2005) which employ a complete Monte Carlo radiative transfer model.

Figure 2 shows the result of this calculation for three representative simulations, with $f_{\text{gas}} = 1.0$, $z_{\text{gal}} = 0$, $q_{\text{EOS}} = 1.0$, and $V_{\text{vir}} = 80, 160,$ and 320 km s^{-1} (red, blue, and black, respectively). The median observed M_{280} as a function of time during the merger is shown for each simulation (left panel).

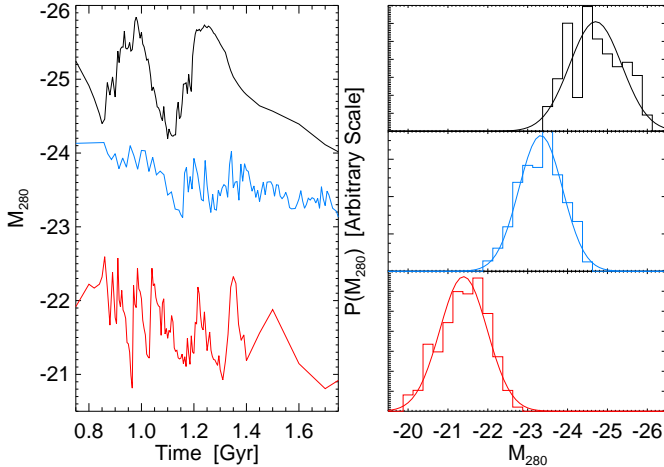


FIG. 2.— Left: Median observed (attenuated) magnitude at 280 nm as a function of time during the peak merger stages from three representative simulations with $V_{\text{vir}} = 80, 160,$ and 320 km s^{-1} (red, blue, and black, respectively). Right: Distribution of observed magnitudes (each weighted by the amount of time across all sightlines that the galaxy is observed at a given M_{280}) for each simulation (histograms of corresponding colors), with best-fit Gaussians (smooth curves). The distribution of optical/UV luminosities is relatively constant throughout the merger, with enhanced star formation and obscuration offsetting one another, and well-fitted by a Gaussian PDF.

As seen in Hopkins et al. (2005e) and Jonsson et al. (2005), the increased densities in the merger give rise to both enhanced star formation but also enhanced obscuration, resulting in a flat observed host galaxy luminosity during these times. Generally, the host galaxy luminosity varies within a factor $\lesssim 2$, i.e. within 1 magnitude, throughout the merger, even though the *intrinsic* (un-attenuated) UV luminosity can rise by more than an order of magnitude as the star formation rate peaks during the merger (see e.g., Springel & Hernquist 2003a; Jonsson et al. 2005).

In the right panel of Figure 2, we show the probability of observing a given M_{280} , i.e. the total time a given M_{280} is visible, integrated over all sightlines and over the duration of the merger. The results are shown as histograms of the corresponding color for each merger in the left panel. In each case, the histograms have a well-defined peak corresponding to the mean observed M_{280} , and a narrow width in M_{280} , emphasizing that the simulation light curves are quite flat with time. The probability distribution in each case is well-fitted by a Gaussian, and the best-fit Gaussian for each is shown (smooth curves of corresponding color). The peak of each distribution gives the mean M_{280} , i.e. the approximately constant observed luminosity, and the width is ≈ 0.6 mag for each (i.e. ≈ 0.2 dex in luminosity). Because the distribution of observed M_{280} in each simulation is well-fitted by a Gaussian, and approximately flat with time, we can characterize the lightcurves of our simulations with a mean M_{280} and rms dispersion about this mean, σ_{280} .

In Figure 3, we quantify the dependence of the mean observed 280 nm luminosity on host galaxy properties. We calculate the complete observed 280 nm galaxy lightcurve along ~ 1000 sightlines for each of a subset of our simulations. We consider simulations with $f_{\text{gas}} = 1.0$ (black points), 0.8 (blue), 0.4 (green), and 0.2 (red), and for each, $V_{\text{vir}} = 113, 160,$ and 320 km s^{-1} and $q_{\text{EOS}} = 1.0$. For $f_{\text{gas}} = 1.0$, we also calculate the results for $V_{\text{vir}} = 80, 226 \text{ km s}^{-1}$, $q_{\text{EOS}} = 1.0$ and for $V_{\text{vir}} = 160 \text{ km s}^{-1}$, $q_{\text{EOS}} = 0.25$, to demonstrate that

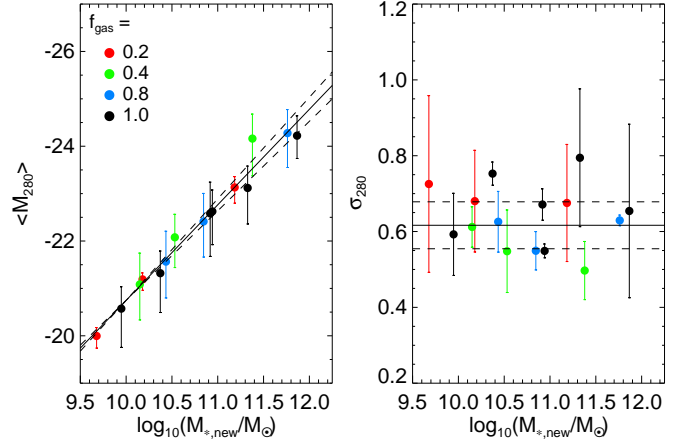


FIG. 3.— Left: Mean observed 280 nm magnitude over the course of a merger for simulations with $V_{\text{vir}} = 80\text{--}320 \text{ km s}^{-1}$ and gas fractions as labeled (circles), as a function of the mass of stars formed during the merger, $M_{*,\text{new}}$. Vertical errors show the range allowing for a factor of 3 uncertainty in the calculated column density. Solid line shows the best-fit power law, dashed lines the 1σ range of this fit. Right: Dispersion in 280 nm magnitude over the course of a merger, for the same simulations (symbols as in left panel). Solid line shows the best-fit constant σ_{280} and dashed lines the 1σ range. The PDF for observing a merger at a given luminosity has a constant shape and width, with the mean optical/UV luminosity scaling with the mass of stars forming in the merger.

these variations do not affect our conclusions. We then use the observed lightcurves along each sightline to calculate the distribution of M_{280} as in Figure 2.

In the left panel of Figure 3, we plot the mean M_{280} for each simulation following this calculation (circles), with vertical error bars showing the range resulting from a factor of 3 systematic increase or decrease in our estimated column densities (roughly parameterizing the maximal uncertainty for our calculation of N_{H} in Hopkins et al. 2005b). This is generally comparable to the rms dispersion σ_{280} about the mean M_{280} for a given lightcurve, which we calculate explicitly for each simulation in the right panel of the figure. Again, the vertical error bars represent the range of results allowing for a factor of 3 difference in our calculated column densities. We expect that the UV luminosity will be dominated by young stars, and therefore show the mean M_{280} as a function of the mass of new stars formed during the merger, $M_{*,\text{new}}$. Unsurprisingly, the two are well correlated, and the scaling does not depend on gas fraction, virial velocity, or ISM gas equation of state. Fitting a relation of the form

$$M_{280} = M_{280,0} + \alpha \log_{10} \left(\frac{M_{*,\text{new}}}{10^{10} M_{\odot}} \right) \quad (2)$$

gives a best fit $M_{280,0} = -20.7 \pm 0.1$, $\alpha = -2.01 \pm 0.13$, which we show as a solid black line with dashed lines showing the 1σ fit range.

In the right panel of Figure 3, we show the dispersion in M_{280} , σ_{280} (symbols as in the left panel), again as a function of the total stellar mass formed in the simulation, and find that it is approximately constant across all simulations, with no significant dependence on stellar mass or gas fraction. We find an identical result if we plot σ_{280} as a function of e.g. total stellar or black hole mass, or other host galaxy properties. The solid line (dashed lines) shows the best fit ($\pm 1\sigma$) constant $\sigma_{280} = 0.62 \pm 0.06$.

The scaling of M_{280} with host galaxy properties can be un-

derstood in terms of a simple model assuming efficient conversion of gas to stars. The best-fit $\sigma_{280} = 0.62 \pm 0.06$, i.e. a dispersion of 0.25 ± 0.02 dex (a factor of 1.7–1.9) in L_{280} reflects the nearly constant UV luminosity during a merger, as a consequence of enhanced densities giving both increased column densities and star formation. The scaling of the mean M_{280} with the mass of new stars formed is also expected, as the young stellar populations formed during the merger dominate the UV luminosity. In terms of L_{280} , we can express our fitted Equation (2) above as

$$L_{280} = L_{280,0} \left(\frac{M_{*,\text{new}}}{10^{10} M_{\odot}} \right)^{0.80 \pm 0.05}, \quad (3)$$

where $L_{280,0} = 5.06 \pm 0.45 \times 10^{10} L_{\odot, 280}$. If the star formation rate as a function of time is qualitatively similar in different mergers (regardless of the total number of new stars formed), as is seen in our simulations (see, e.g., Springel & Hernquist 2003a; Springel 2005), we expect the intrinsic (un-attenuated) UV luminosity (henceforth L_{int}) to scale proportionally with the mass of new stars formed, $L_{\text{int}} = \langle M/L_{280} \rangle^{-1} M_{*,\text{new}}$, where here $\langle M/L_{280} \rangle$ is an effective mass-to-light ratio (which depends only on the shape of the star formation rate vs. time, not its normalization). The timescale of \sim Gyr during which the galaxies will be visible as a merger, or alternatively the fit to the K -band mass-to-light ratios in Equation (1) above, suggests a $\langle M/L_{280} \rangle \approx 0.08 M_{\odot}/L_{\odot, 280}$, corresponding to a population with an age of 0.5 Gyr.

However, the observed luminosity does not scale as steeply as $L_{\text{int}} \propto M_{*,\text{new}}$, owing to the effects of increasing attenuation with increasing gas mass. Jonsson et al. (2005) consider lightcurves of merging galaxies in detail using a smaller set of simulations (without black holes), but with a full Monte Carlo radiative transfer code, and demonstrate that it is reasonable to assume that the newly-formed stars and star-forming gas (which produces most of the obscuration) are uniformly mixed, giving an observed luminosity $L_{280} = L_{\text{int}} \tau^{-1} (1 - e^{-\tau})$ (e.g., Calzetti et al. 1994), where L_{int} is the intrinsic luminosity in the waveband and τ is an effective mean optical depth. From their fits to the attenuation in bolometric, SDSS u -band, and GALEX NUV luminosities we can estimate $\tau \approx \tau_0 (M_g/10^{11} M_{\odot})^{0.16}$, where $\tau_0 \approx 2-3$ and $M_g \approx M_{*,\text{new}}$ is the gas mass, a scaling which they show can be roughly understood in terms of a simple model of uniform density and the scalings of star formation rate and obscuration with that density. We do not consider the more detailed scaling of attenuation with star formation rate and instantaneous luminosity calculated in Jonsson et al. (2005), as we are explicitly attempting to avoid introducing the uncertainties of modeling the much more time-variable intrinsic (un-attenuated) UV luminosity and instead focus on only the mean attenuation over the course of a merger. Given $\tau \gtrsim 1$, the formula for L_{280} above becomes $L_{280} \propto \tau^{-1}$, and we can combine the scalings to obtain the expected relation

$$L_{280} \approx 5.8 - 8.7 \times 10^{10} L_{\odot, 280} \left(\frac{M_{*,\text{new}}}{10^{10} M_{\odot}} \right)^{0.84}, \quad (4)$$

in good agreement with the scaling of L_{280} measured directly in the simulations. That these scalings agree emphasizes that contributions to the observed L_{280} from older stellar populations are relatively small ($\lesssim 30\%$). Furthermore, this suggests that our results using just the calculated column densities (i.e. ignoring scattering processes) would not be significantly changed by a more sophisticated treatment of radiative transfer.

Finally, as suggested from our fit to the K -band mass to light ratios above, we find in our simulations that the conversion of gas to stars in mergers is efficient, i.e. $M_{*,\text{new}} \approx f_{\text{gas}} M_{*,\text{tot}}$. This can also be seen in e.g. Figure 2 of Robertson et al. (2005b), which demonstrates that the final, total stellar mass is nearly independent of gas fraction. The simulations shown in Figure 1 and 3 give a similar result, with final stellar mass changing by $\lesssim 10\%$ over the range of $f_{\text{gas}} = 0.2 - 1.0$ for fixed virial velocity, and with no systematic trend with f_{gas} in that range. Therefore, we can reasonably adopt $M_{*,\text{new}} = f_{\text{gas}} M_{*,\text{tot}} = f_{\text{gas}} M_*$, where for simplicity we subsequently denote the final, total stellar spheroid mass as $M_* = M_{*,\text{tot}}$. We have then determined the observed K -band and 280 nm luminosity of merging galaxies (both mean luminosity and dispersion about that mean during a merger), as a function of host galaxy properties, namely gas fraction f_{gas} and final stellar mass M_* , with no systematic dependence (when quantified in this manner) on the other parameters we have varied in our simulations.

3.1.3. Other Optical and Near-IR Luminosities

For future reference, we perform this set of calculations on our simulations in several different wavebands (280 nm, U, B, V, R, I, J, H, K, and SDSS u, g, r, i, z), calculating for each the equivalent of Equation (2), i.e. the best-fit relation between the median magnitude in the given band (M_{BAND}) and total stellar mass formed in the merger ($M_{*,\text{new}}$), as well as the dispersion in a given merger about the expected median magnitude (σ_{BAND}). The results are shown in Table 1. We also consider fits to M_{BAND} as a function of final black hole mass M_{BH} or total final stellar mass $M_{*,\text{tot}}$ instead of $M_{*,\text{new}}$. For each, we show the resulting χ^2/ν , which quantifies the goodness-of-fit. Note that a small χ^2/ν implies small scatter about the fitted relation, but does not imply that there is no systematic dependence on certain external variables. For example, in the optical/UV, the correlation between M_{BAND} and $M_{*,\text{new}}$ or $M_{*,\text{tot}}$ is comparable, but as demonstrated above, there is a systematic dependence on f_{gas} if M_{BAND} is quantified as a function of $M_{*,\text{tot}}$ (brighter optical/UV at higher gas fractions). Note that σ_{BAND} also quantifies the degree to which it is a good approximation to assume that the luminosity in the given band over the course of the merger is constant (a poor approximation to the bolometric luminosity, but a surprisingly good approximation in the bands we measure). These fits enable future observations of the merger luminosity function in various bands to easily convert the observations into a merger mass function in terms of either the total stellar mass, stellar mass formed in the merger, or final black hole mass / peak quasar luminosity, and correspondingly inform the contribution to the remnant spheroid and quasar populations and the star formation rate density of the Universe at the observed redshift.

3.2. Colors and Color-Magnitude Relations

We examine the color-magnitude relations predicted for merging galaxies from our simulations, both to test whether we are modeling star formation and dust extinction properly, and to estimate the relative importance of dust reddening, metallicity, and the distribution of stellar ages in observed samples. In Figure 4, we plot the $(U - V)$ vs. M_V color-magnitude relation for each of several representative simulations with different virial velocities $V_{\text{vir}} = 116, 160, 320 \text{ km s}^{-1}$ (diamonds, squares, and circles, respectively) and gas fractions $f_{\text{gas}} = 0.2, 0.4, 0.8, 1.0$ (black, blue,

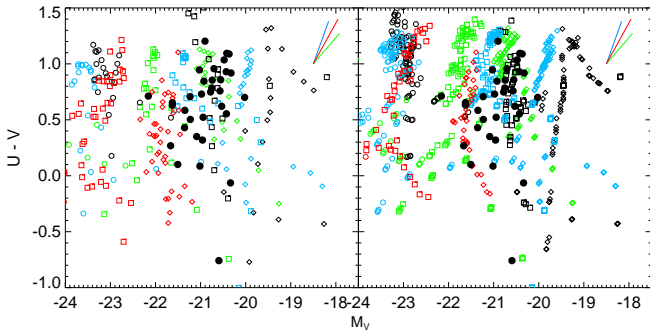


FIG. 4.— Color-magnitude relation at ~ 100 random times and sightlines during each of several merger simulations with $V_{\text{vir}} = 116, 160, 320 \text{ km s}^{-1}$ (diamonds, squares, and open circles, respectively), $f_{\text{gas}} = 0.2, 0.4, 0.8, 1.0$ (black, blue, green, and red, respectively), $z_{\text{gal}} = 0$, $q_{\text{EOS}} = 1.0$. The left panel neglects dust attenuation, the right panel includes its effects. In each, solid lines show the effects of increasing metallicity (from $0.1 Z_{\odot} - Z_{\odot}$; blue), age (from $0.5 - 1 \text{ Gyr}$; green), and column density (from $N_{\text{H}} = 0 - 10^{21} \text{ cm}^{-2}$; red). Filled black circles show local ULIRGs from Surace et al. (2000) and Arribas et al. (2004), K-corrected following Bell et al. (2005a). The color-magnitude distribution of the simulations is similar to that observed, with roughly equal contributions from stellar population effects and variations in column densities.

green, and red, respectively), with $z_{\text{gal}} = 0$ and $q_{\text{EOS}} = 1.0$. For each simulation, we consider ~ 100 randomly selected points in time at which the merger is “observed” during the $\sim 2 \text{ Gyr}$ during which the system shows evidence of merging, and at each point in time consider a random sightline (uniformly sampling the unit sphere). In the left panel of the figure, we neglect the effects of dust attenuation (i.e. consider all stars to be unobscured), and in the right panel we include these effects.

The wide scatter in $(U - V)$ colors in the left panel demonstrates that the effects of different mean stellar ages and metallicities contribute strongly to the scatter in the color-magnitude relation. This is unsurprising, as e.g. the difference between observing a single starburst population $\sim 100 \text{ Myr}$ after forming as opposed to $\sim 500 \text{ Myr}$ after forming corresponds to a difference $\sim 1 \text{ mag}$ in $(U - V)$. The evolution in colors is difficult to disentangle. Generally, later in the merger, the mean age of the stellar populations is larger, giving redder colors. However, the final merger is associated with a starburst which briefly reduces the mean (luminosity-weighted) stellar population age. Metal enrichment through star formation over the course of the merger also pushes remnants to redder colors. Differential extinction will redden the observed colors, as is seen in the right panel of the figure, where the typical reddest colors of mergers are increased by $\sim 0.2 - 0.5 \text{ mag}$. However, in terms of relative evolution, the effect is complicated, as the gas density generally decreases later in the merger, producing less obscuration (as opposed to steadily increasing metallicity and mean ages), and during the starburst, the joint increase in obscuration and the star formation rate has the net effect of yielding little change in the observed optical/UV luminosity (§ 3.1.2).

We illustrate the age/metallicity/obscuration degeneracy in Figure 4 with the solid lines in the upper right of each panel, which demonstrate how a point in the $(U - V)$ vs. M_V color-magnitude space is moved (from the point of origin of the three lines) with increasing mean stellar age ($0.5 - 1 \text{ Gyr}$; green), metallicity ($0.1 Z_{\odot} - Z_{\odot}$; blue), and column density ($N_{\text{H}} = 0 - 10^{21} \text{ cm}^{-2}$; red). Clearly, at least in the $(U - V)$ vs.

M_V space, these effects are highly degenerate.

Even with these complicating effects, several inferences can be drawn from the predicted color-magnitude diagram in Figure 4. We plot for comparison (filled circles) the locations of local ULIRGs from Surace et al. (2000) and Arribas et al. (2004) following Bell et al. (2005a). This is also similar to the observed color-magnitude distribution of the $z \approx 0.7$ interacting sample of Bell et al. (2005a) and Wolf et al. (2005), and the morphologically irregular starburst sample of de Mello et al. (2005), as well as the GEMS AGN host galaxy sample of Sánchez et al. (2004) (see e.g. Figure 7 of Bell et al. 2005a). The agreement with our predictions suggests that our star formation, metal enrichment, and column density calculations are at least reasonable in characterizing certain relevant statistical properties and the considerable scatter of the observed populations.

The large scatter in the left hand panel where dust reddening is not included and the fact that it is comparable to the scatter in the right panel suggests that the scatter in colors of merging galaxies or ULIRGs may be dominated by stellar population evolution (both evolution of mean ages and buildup of metallicity) in mergers. This implies that it may not be accurate (at the $\lesssim 1 \text{ mag}$ level) to model such populations as a single burst viewed recently ($\lesssim 100 \text{ Myr}$) after the event, although this may be true shortly after the peak starburst (when the young population is most dominant) and an upper limit of $\sim 1 \text{ Gyr}$ to the mean age is reasonable. Modeling such populations with a single metallicity over the course of a merger can be similarly inaccurate, although by the end of the merger the rapid star formation has typically enriched galaxies to solar abundances (e.g., Hopkins et al. 2005f; Cox et al. 2005), and this is reflected in the wide range of metallicities observed in interacting systems (e.g., Rothberg & Joseph 2005).

Although the scatter in $(U - V)$ may derive largely from stellar population effects, this does not imply that extinction is unimportant. A comparison of the left and right panels of Figure 4 gives a mean extinction $\sim 0.2 - 0.5$ magnitudes (i.e. typical $N_{\text{H}} \sim 10^{21}$), and during the peak starburst phase the flat optical/UV lightcurves observed (§ 3.1.2) imply large ($\gtrsim 1 - 2 \text{ mag}$) extinction (with much greater extinction towards the innermost regions of the galaxy). Adding extinction also has an important qualitative effect in moving objects out of the bright blue ($M_V \lesssim -21$, $(U - V) \lesssim 0$) region of the color-magnitude diagram, as the brightest objects tend to have the largest gas densities powering rapid starburst activity and correspondingly large attenuation. The faint red ($M_V \gtrsim 19$, $(U - V) \gtrsim 0$) portion of the color-magnitude diagram also appears intrinsically (neglecting dust reddening) under-populated, and this is preserved even when dust reddening is included, reflecting the fact that faint systems tend to have lower densities, powering weaker starbursts and weaker attenuation. This is important for observational studies of the merging galaxy population in optically or UV-selected samples, especially at high redshift, which may not be sensitive to faint red mergers (see e.g. Bell et al. 2005a; Wolf et al. 2005, for further discussion). Finally, although these two general trends (lack of both bright blue and faint red objects) appear reasonably robust in Figure 4 and in examination of our suite of mergers varying other host galaxy properties, we emphasize that there is no real color-magnitude relation in the sense of any tight correlation between $(U - V)$ color and M_V magnitude, and thus any physical inferences from the observed color-magnitude distribution should be considered with caution.

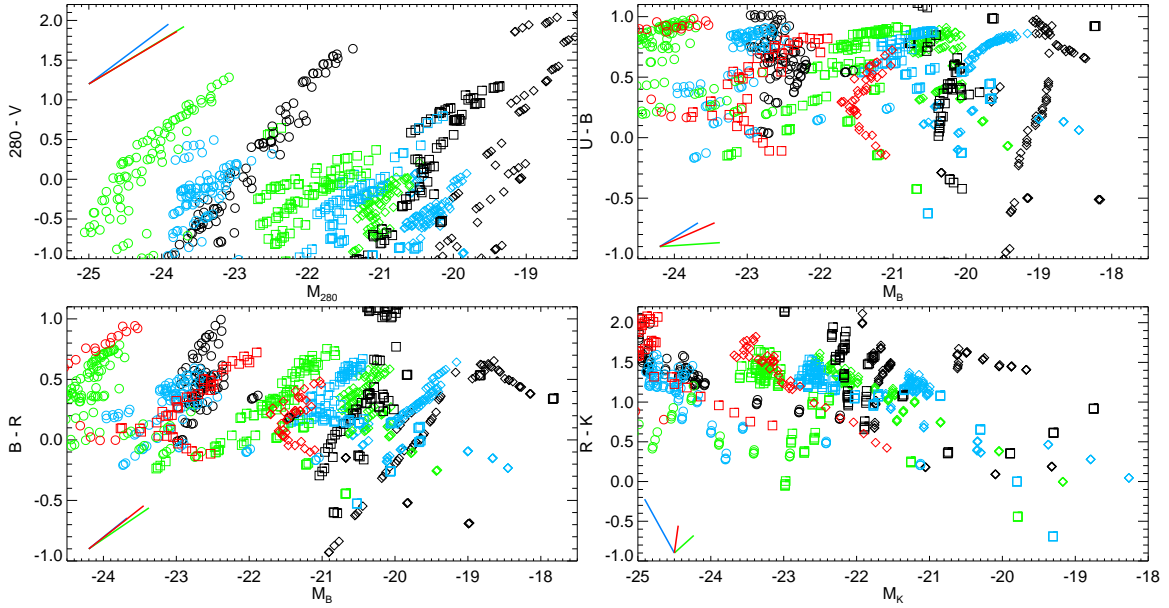


FIG. 5.— Color-magnitude relations in several different bands, in the style of Figure 4. Again, no strong trend of colors with magnitude is evident, but the simulations occupy a locus similar to observed mergers (Wolf et al. 2005; Bell et al. 2005a), and brightest, most rapidly star-forming mergers tend to be red owing to enhanced dust obscuration.

We compare color-magnitude distributions from our simulations in different bands in Figure 5, where we plot a random sampling of the same simulations shown in Figure 4, with points and colors representing different initial virial velocities and gas fractions in the same manner. Solid lines show the effect of increasing mean stellar age (green), metallicity (blue), and column densities (red), also as in Figure 4. We show results for four different color-magnitude combinations, $(M_{280} - V)$ vs. M_{280} (upper left), $(U - B)$ vs. M_B (upper right), $(B - R)$ vs. M_B (lower left), and $(R - K)$ vs. M_K (lower right). The predicted $(M_{280} - V)$ vs. M_{280} distribution can be compared to e.g. the observations in Wolf et al. (2005) at $z = 0.7$, and the agreement between the two is reasonable, which is not surprising given the match between the $(U - V)$ vs. M_V distribution in Figure 4 and that observed by Bell et al. (2005a), but it is nevertheless reassuring given the complex dependence of colors on our modeling of star formation rates, metal enrichment, and obscuration. Note that these effects are degenerate in each of the optical/UV color-magnitude relations, moving points in similar directions (and with similar strengths) in the color-magnitude plane, especially for $(M_{280} - V)$ vs. M_{280} and $(B - R)$ vs. B . The degeneracies, however, are partly broken by considering $(R - K)$ vs. M_K , as the effects of obscuration and stellar ages are relatively small but metallicity effects can be significant.

For each optical/UV color-magnitude distribution, we again find that there is no proper color-magnitude relation in the sense of any strong correlation between the two. However, for both $(U - B)$ vs. M_B and $(B - R)$ vs. M_B , we find similar qualitative trends as for the $(U - V)$ vs. M_V distribution, namely a lack of bright, very blue objects (as such objects with the highest star formation rates tend to have the largest obscuration) and a similar deficit of faint, very red objects, although this end of the distribution will be increasingly populated if low to moderate mass objects are included in stages relaxing and reddening after the merger. At the shortest wavelengths we consider, $(M_{280} - V)$ vs. M_{280} , there are no highly

reddened objects with bright M_{280} because large extinction precludes being bright at these wavelengths, where the optical depth is large. Finally, for the optical-near IR color magnitude relation we plot, $(R - K)$ vs. M_K , there is a general trend of bluer colors at fainter M_K , although still with considerable $\sim 0.5 - 1$ mag scatter. This primarily reflects the trends of increasing typical optical obscuration (e.g., Hopkins et al. 2005e,f; Jonsson et al. 2005) and metallicity (Cox et al., in preparation) with increasing stellar mass or luminosity, as observed in star-forming galaxies by e.g. Burstein et al. (1988); Worthey et al. (1992); Faber et al. (1995); Jørgensen (1997); Kuntschner (2000).

3.3. The Star Formation Rate Distribution in Individual Mergers

We now examine the distribution of star formation rates in our simulations, as a function of initial and/or final conditions, in order to determine the distribution of star formation rates in merging, quasar-producing galaxies; i.e. the star formation rate function (SFRF) in mergers. Because the star formation rate is far from flat during the merger, sharply peaking during the starburst phase and falling off exponentially after, with smaller peaks in earlier stages, a given merger will not necessarily be observed near a single characteristic SFR (as with e.g. the luminosities calculated above). We can, however, apply the identical formalism of Hopkins et al. (2005e), considering the time a given simulation spends in a given interval in SFR (i.e. the SFR-dependent “lifetime” of the merger) instead of the time spent at a given quasar luminosity (accretion rate). We find, as in the case of the black hole luminosity, that the detailed dependence of the SFR \dot{M}_* on time is somewhat chaotic, with e.g. the exact time of the starburst being quite sensitive to initial conditions, and the strength of the starburst and quiescent star formation systematically dependent on e.g. virial velocity, ISM gas equation of state, galaxy gas fractions, and merging galaxy mass ratio. However, when rescaled in terms of the *total* mass of new stars formed dur-

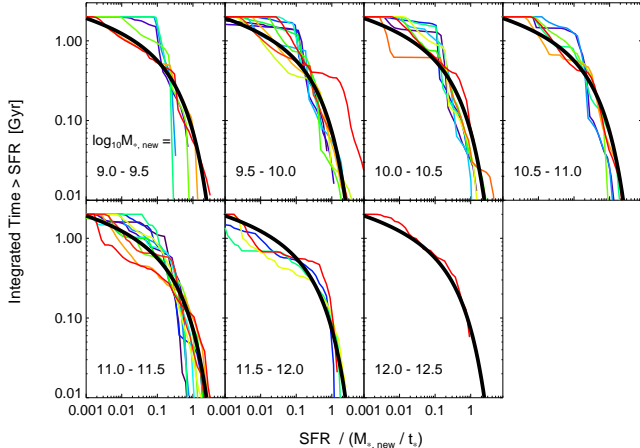


FIG. 6.— Integrated time above a given rescaled star formation rate $\dot{M}_*/(M_{*,\text{new}}/t_*)$, where $M_{*,\text{new}}$ is the mass of new stars formed during the merger and $t_* = 0.3$ Gyr is fitted. Results are shown for ~ 100 simulations, in bins of $M_{*,\text{new}}$ as labeled. Different colors show simulations with different values of V_{vir} , f_{gas} , q_{EOS} , z_{gal} . The thick black line in each interval shows the fitted analytical approximation of Equation (5). Quantified in this manner, the PDF for observing a given merger at some instantaneous SFR is well-determined and independent of systematic effects from varied quantities in the simulations.

ing the merger, $M_{*,\text{new}}$, the critical statistical property of the SFR distribution, namely the time spent by a given simulation in a given interval in \dot{M}_* , is essentially scale invariant, independent of systematic effects from the varied quantities in our simulations.

In Figure 6, we determine the integrated time spent by each of ~ 100 simulations above a given SFR (from $\dot{M}_* \sim 10^{-4} - 10^3 M_{\odot} \text{yr}^{-1}$), as a function of that SFR \dot{M}_* . We then rescale the SFR by dividing out a characteristic SFR $M_{*,\text{new}}/t_*$, i.e. the total new stellar mass formed during the merger divided by some characteristic starburst timescale. For now, t_* is arbitrary (we choose $t_* = 0.3$ Gyr, for reasons demonstrated below). We then plot, for each simulation, the time spent in the simulation with a dimensionless SFR ($\dot{M}_*/(M_{*,\text{new}}/t_*)$) larger than some given dimensionless SFR. We show this for the simulations in bins of $\log(M_{*,\text{new}})$ from $M_{*,\text{new}} \sim 10^9 - 10^{13}$. In each bin, different colored lines correspond to different initial conditions in the simulations, where we have considered various combination of $V_{\text{vir}} = 80 - 500 \text{ km s}^{-1}$, $q_{\text{EOS}} = 0, 1, z_{\text{gal}} = 0, 2, 3, 6$, and $f_{\text{gas}} = 0.2, 0.4, 0.8, 1.0$. Although there is significant scatter in the time spent above some SFR between different simulations, we find that once rescaled in this manner, there is no systematic dependence on the final new stellar mass or any of the varied quantities.

We fit the “lifetime” at a given SFR in Figure 6 to a simple analytical function following Hopkins et al. (2005e),

$$\frac{dt}{d \log \dot{M}_*} = t_* \ln(10) \exp\left(-\frac{\dot{M}_*}{M_{*,\text{new}}/t_*}\right), \quad (5)$$

where $M_{*,\text{new}}$ is the total stellar mass formed in the merger, t_* is a characteristic timescale, and the normalization $t_* \ln(10)$ is determined by the integral constraint

$$\int \dot{M}_* dt = \int \dot{M}_* \frac{dt}{d \log \dot{M}_*} d \log(\dot{M}_*) = M_{*,\text{new}}. \quad (6)$$

This gives a simple one-parameter function to describe the statistical properties of the SFR distribution in mergers.

Fitting to the simulations, we find a best-fit $t_* \approx 0.3 \pm 0.1$ Gyr, with no evidence for a strong dependence of t_* on $M_{*,\text{new}}$ or other varied parameters. This is similar to the star formation timescale ~ 0.1 Gyr implied by observations of starburst galaxies (Kennicutt 1998), and the selection of galaxies in the peak of their starbursts explains the slightly shorter timescale. We show the prediction of this fit as the thick black lines in each panel of Figure 6, where it is clear that this functional form provides a reasonable description of the SFR distribution in each merger, independent of the merger initial/final conditions. The scale-invariant functional form of Equation (5) suggests a sharply peaked SFR in the peak starburst phase, with an exponential transition (i.e. exponentially increasing or decreasing SFR) into and out of that phase. However, too much detail should not be read into the precise SFR as a function of time from these fits, as they are both rough and do not capture a systematic dependence such as e.g. the tendency of higher-mass systems to form a larger fraction of their stars prior to the final merger, as discussed in Robertson et al. (2005c).

Although this functional form is similar to that of the quasar lifetime fitted in Hopkins et al. (2005e), there are two critical differences: in Hopkins et al. (2005f) we show that a Schechter function with $\alpha \sim 0.5$ is more appropriate for the quasar lifetime at faint luminosities (suggesting a $\sim t^{-2}$ power-law decay of quasar luminosity at late times, as opposed to the exponential decay in SFR indicated at late times by the fit in Equation [5]), and in both Hopkins et al. (2005e) and Hopkins et al. (2005f) we find a weak dependence of α or the normalization of the quasar lifetime as a function of luminosity on the peak luminosity, breaking the scale invariance and reflecting the increased importance of black hole feedback in more massive systems.

As an aside, we expect a similar functional form should qualitatively describe quiescent star formation in disk galaxies, which tend to have exponentially declining star formation rates with characteristic timescales (for stable disks) $\sim 4 - 8$ Gyr (of order the star formation timescale, e.g., Li et al. 2005a,b). However, the SFR distribution for a disk galaxy should be characterized by a much lower characteristic SFR ($\sim f_{\text{gas}} M_{\text{disk}}/10 \text{ Gyr}$) and higher normalization $\sim (4 - 8) \ln 10 = 10 - 20 \text{ Gyr}$ (i.e. more than an order of magnitude lower typical star formation rates and longer timescales).

4. COMPARING THE MERGING GALAXY, QUASAR, AND STAR FORMATION RATE DISTRIBUTIONS

4.1. Converting Between Merger, Quasar, and SFR Distributions

From the distribution of observed luminosities during a merger for host galaxies of a given final stellar spheroid mass M_* and gas fraction f_{gas} described in § 3.1, we can use the scaling of black hole and galaxy properties to relate the merging galaxy and quasar luminosity functions (MGLF and QLF). This is similar to the approach used by Hopkins et al. (2005f) to relate the QLF to the red galaxy population, i.e. the remnants that hosted quasars during the mergers that formed them, as opposed to the population of galaxies undergoing mergers at a particular time, which we consider now.

The scalings between black hole mass and host galaxy velocity dispersion or stellar spheroid mass in our simulations are described in Di Matteo et al. (2005); Robertson et al. (2005b); Hopkins et al. (2005f), but what we require here is the relation between final (post-merger) black hole mass and

final total stellar mass,

$$M_{\text{BH}} \approx 0.001 M_*, \quad (7)$$

(Robertson et al. 2005b; Hopkins et al. 2005f). This is similar to observational estimates from e.g. Marconi & Hunt (2003) (accounting for the difference between virial and stellar mass), and our results below are essentially identical whether we use the relationship fitted from the simulations or observations. The scatter about this relation is approximately 0.3 dex (with an approximately lognormal distribution about the mean relation), again similar to that seen observationally.

We have studied the properties of quasars in our simulations in detail in Hopkins et al. (2005a-g), giving, for example, a conversion between final black hole mass M_{BH} and quasar peak luminosity L_{peak} ,

$$\begin{aligned} L_{\text{peak}} &\approx 0.67 L_{\text{Edd}}(M_{\text{BH}}) \left(\frac{M_{\text{BH}}}{10^8 M_{\odot}} \right)^{0.12} \\ &= 2.2 \times 10^{12} L_{\odot} \left(\frac{M_{\text{BH}}}{10^8 M_{\odot}} \right)^{1.12} \end{aligned} \quad (8)$$

(see Equation [10] of Hopkins et al. 2005e; note that this equation is limited by $L_{\text{peak}} \leq L_{\text{Edd}}(M_{\text{BH}})$, but this only significant at $M_{\text{BH}} \gtrsim 10^{10} M_{\odot}$). For a given quasar peak luminosity, our determination of the quasar lifetime and obscuration in Hopkins et al. (2005e,g) allows us to estimate the total time a black hole spends at a given observed luminosity in a given waveband during a merger.

Combining these, it is possible to convert between the observed MGLF and QLF. If the observed MGLF in a band ν is given by $\phi_{\text{gal}}(L_{\nu}) \equiv d\Phi/d\log(L_{\nu})$, then

$$\phi_{\text{gal}}(L_{\nu}) = \int \frac{dt}{d\log(L_{\nu})} \dot{n}(M_*) d\log M_*, \quad (9)$$

where $\dot{n}(M_*) = dn dt^{-1} d\log(M_*)^{-1}$ is the merger rate as a function of final stellar mass, and $dt/d\log(L_{\nu})$ is the time the merging galaxy is visible in a logarithmic interval in L_{ν} . Because, as shown in § 3.1, the merging galaxy luminosity is quite flat in time, and the timescale over which merging galaxies are identifiable as such (~ 2 Gyr) does not depend strongly on the galaxy masses over the range of interest, we can use $dt/d\log(L_{\nu}) = P(L_{\nu} | M_*) t_{\text{merge}}$, where $P(L_{\nu} | M_*)$ is the probability of being observed in a logarithmic interval in L_{ν} over the merger timescale (t_{merge}). We have determined $P(L_{\nu} | M_*)$ in the K -band and at 280 nm in § 3.1, and find it is well approximated by a narrowly peaked Gaussian, which allows us to de-convolve Equation (9) and determine $\dot{n}(M_*)$, modulo the normalization t_{merge} . The de-convolution of the MGLF $\phi(L_{\nu})$ with the PDF for observing a merger at a given luminosity $P(L_{\nu} | M_*)$ directly yields the merger mass function for a given luminosity function, and we can invert this procedure as well to test our modeling of the characteristic luminosities of mergers.

Knowing $M_{\text{BH}}(M_*)$ and $L_{\text{peak}}(M_{\text{BH}})$, we can convert $\dot{n}(M_*)$ (including the appropriate Jacobian factors) to obtain $\dot{n}(L_{\text{peak}})$, the birthrate of quasars of a given peak luminosity in galaxy mergers. This is simply given by the inversion of (noting that M_{BH} and L_{peak} are equivalent)

$$\dot{n}(M_{\text{BH}}) = \int P(M_{\text{BH}} | M_*) \dot{n}(M_*) d\log M_*. \quad (10)$$

We can then express the observed QLF in terms of $\dot{n}(L_{\text{peak}})$ and the quasar lifetime as a function of luminosity (see Equation [11]), identical to the expression in Equation (9) but with M_* replaced by L_{peak} .

Given a model for the quasar lightcurve or lifetime, then, the QLF is determined. We first consider a simple “feast or famine” or “light-bulb” model for the quasar lifetime, following what has generally been adopted in previous works (e.g., Small & Blandford 1992; Kauffmann & Haehnelt 2000; Haiman & Menou 2000; Wyithe & Loeb 2003; Volonteri et al. 2003; Haiman, Quataert, & Bower 2004). In one typical scenario of this type, the quasar turns on in a merger, accretes at constant Eddington ratio \dot{m} , and then either “turns off” or exponentially decays in luminosity (Haiman & Loeb 1998). In this case, the lightcurve is a simple exponential, $L \propto \exp(\pm t/t_Q)$, with a peak at $L = L_{\text{peak}}$, where t_Q is a free parameter. The quantity \dot{m} for growth at constant Eddington ratio is essentially the same free parameter since $t_Q = t_S/\dot{m}$, where $t_S = 4.2 \times 10^7$ yr is the Salpeter time, the e -folding time for $\dot{m} = 1$ with radiative efficiency $\epsilon_r = 0.1$. The quasar lifetime as a function of luminosity is then trivial, $dt/d\log(L) = \ln 10 t_Q = \text{constant}$ (for $L < L_{\text{peak}}$).

We note also, as demonstrated explicitly in Hopkins et al. (2005c), that assuming an even simpler description of quasar activity, in which quasars “turn on” at fixed luminosity $L = L_{\text{peak}}$ for a fixed t_Q , produces nearly identical results to this somewhat more physical exponential growth/decay model. In either case, the peak luminosity is $L_{\text{peak}} = \dot{m} L_{\text{Edd}}(M_{\text{BH}})$. Generally, t_Q is either adopted from observations (with the loose constraint $t_Q \sim 10^6 - 10^8$ yr; see Martini 2004 for a review) or assumed to be the Salpeter time, but we allow it to vary to provide the best fit to the observed QLF.

In Hopkins et al. (2005a-h), we compare these idealized scenarios to a model of quasar lifetimes derived from our simulated galaxy mergers and find that they provide a poor representation of the lifetime from our simulations at any luminosity. The simulated lightcurves are complex, generally having periods of rapid accretion after “first passage” of the galaxies, followed by an extended quiescent period, then a transition to a peak, highly luminous quasar phase, and then a dimming as self-regulated mechanisms expel gas from the remnant center after the black hole reaches a critical mass (Di Matteo et al. 2005). But, even with these complexities, the statistical nature of the lightcurve can be described by simple forms (Hopkins et al. 2005b,e). The key feature of the quasar lifetime not captured by more idealized models is that it *increases* with decreasing luminosity; i.e. a given quasar spends more time at luminosities below its peak than at its peak luminosity.

In Hopkins et al. (2005e,f) we use the set of several hundred simulations from Robertson et al. (2005b,c) described in § 2 to determine the quasar lifetime as a function of instantaneous and peak quasar luminosity. The differential quasar lifetime, i.e. the time spent in a given logarithmic luminosity interval, is well fitted by a Schechter function,

$$\frac{dt}{d\log(L)} = t_Q \left(\frac{L}{L_Q^*} \right)^{-\alpha} \exp[-L/L_Q^*]. \quad (11)$$

Here, L_Q^* is proportional to the *peak* quasar luminosity L_{peak} , t_Q is a fixed constant ($t_Q = \frac{\ln 10}{\eta} t_S$ for $L_Q^* = \eta L_{\text{peak}}$), and $\alpha \sim 0.5$ is weakly dependent on peak luminosity and is determined by the nearly scale-invariant “blowout” of gas as the exponentially growing feedback from black hole growth heats the gas rapidly and it can no longer cool efficiently in a dynamical time (Hopkins et al. 2005g). The lifetime in Equation (11) is entirely determined by our simulations, and when quantified as a function of L_{peak} in this manner, the quasar lifetime shows

no systematic dependence on host galaxy properties, merger parameters, initial black hole masses, ISM and gas equations of state and star formation models, or other varied parameters. Combined with the MGLF, this provides a prediction of the QLF without requiring any cosmological priors on these properties.

We can also perform exactly the same procedure, but in the opposite order, first using the QLF and our modeling of quasar lifetimes to determine $\dot{n}(L_{\text{peak}})$, as is done in Hopkins et al. (2005a-h) to study the properties of the quasar population, then converting this to a merger rate $\dot{n}(M_*)$ (as in Hopkins et al. 2005f). Given $\dot{n}(M_*)$ and using our modeling of the host galaxy luminosity during mergers from § 3.1, we then determine the observed MGLF in a given band.

We have also quantified the time spent by a merger in a given interval in SFR, $t(\dot{M}_*|M_*)$ in § 3.3. We can therefore follow the identical procedure described above, convolving the $\dot{n}(L_{\text{peak}})$ or $\dot{n}(M_*)$ distribution implied by the QLF or MGLF with the calculated $t(\dot{M}_*|M_*)$ to determine the star formation rate function, $\phi(\dot{M}_*)$. Again, we can invert this as well, and predict the QLF or MGLF from the SFRF.

This method would be entirely independent of additional cosmological assumptions about the properties of merging galaxies, if $P(L_\nu|M_*)$ depended on only M_* , as e.g. the quasar lifetime as a function of luminosity in our modeling depends on only peak luminosity (Hopkins et al. 2005e). However, we have shown in § 3.1 that this quantity can depend systematically on the gas fraction of the merging galaxies. Still, in the K -band, this dependence is weak, implying that a comparison of the K -band MGLF and QLF can test our modeling of merger-induced quasar activity almost independent of gas fraction or other cosmological priors. Furthermore, the gas fraction controls only the effective final stellar mass to light ratio during the merger, i.e. it influences the normalization of the stellar masses (and therefore black hole masses and, correspondingly, quasar peak luminosities) inferred from observed merging galaxies of a given luminosity. Therefore, it is only the relative horizontal offset (offset in luminosity) of the QLF and MGLF which is affected by the typical gas fractions of merging galaxies; comparison of the *shape* of the two luminosity functions provides a test and means to constrain the quasar lifetime model independent of the distribution of host galaxy properties.

4.2. The Observed MGLF and QLF

4.2.1. The K -Band Merger Luminosity Function

We examine first the observed K -band pair luminosity function of Xu et al. (2004), at low redshift $z \lesssim 0.1$. The pair luminosity function is determined from the matched 2MASS-2dFGRS 45,289-galaxy sample of Cole et al. (2001), and agrees well with previous estimates of the local pair fraction (e.g., Zepf & Koo 1989; Burkley et al. 1994; Carlberg et al. 1994; Yee & Ellington 1995; Patton et al. 1997, 2000) and the B -band luminosity function of paired galaxies (e.g., Xu & Sulentic 1991; Sulentic & Rabaca 1994; Keel & Wu 1995; Soares et al. 1995; Toledo et al. 1999; Conselice et al. 2003), but accounts for effective pair volume corrections instead of treating each member singly with its own V_{max} (since both objects must be identified in a pair to be included in such a sample). Pairs are defined within a projected separation $\leq 20h^{-1}$ kpc, with velocity difference (where both redshifts are measured) $< 500 \text{ km s}^{-1}$. Further, the sample is restricted to major mergers, with K -band magnitude differ-

ences less than 1 mag (i.e. within a factor ~ 3 in mass), corresponding well to our models and to those mergers which are most likely to trigger starburst and quasar activity and to be visible as peculiar/interacting galaxies for comparison with morphologically selected MGLFs (Mihos & Hernquist 1994a; Walker et al. 1996; Conselice et al. 2003). We consider both their binned data and best-fit Schechter function, with slope $\alpha = 0.30 \pm 0.56$, turnover $M_{K,*} = -23.32 \pm 0.25$, and normalization $\log \phi_* = -3.92 \pm 0.13$ (we have used $h = 0.7$ here).

Because this is a low redshift sample, the already small K -band uncertainty owing to the host galaxy gas fraction is further minimized: with the gas fractions of the merging galaxies most likely not above $f_{\text{gas}} \sim 0.1 - 0.2$, this implies only a $\sim 20\%$ uncertainty in $P(L_K|M_*)$, much smaller than the observational uncertainties in the MGLF. For now, we adopt $f_{\text{gas}} = 0.15$, giving an effective mass-to-light ratio $M/L_K \approx 1.0$, but choosing instead $f_{\text{gas}} = 0.1$ and 0.2 give $M/L_K = 1.1$ and 0.9 , respectively. Because the K -band luminosity of the mergers is nearly constant with $L_K \approx \langle M/L_K \rangle^{-1} M_*$, the inferred merger rate as a function of mass has identical shape and normalization to the observed MGLF, divided by the timescale t_{merge} over which the merger will be identified. The critical point here is that there is a well-defined *turnover* in this quantity, and it decreases or flattens to lower luminosity (smaller galaxy stellar masses), with $dn/d\log(M_*) \propto M_*^{\alpha+1}$.

We take the characteristic timescale of a merger at low redshifts to be $t_{\text{merge}} \approx 2 \text{ Gyr}$, corresponding roughly to the time when the galaxies are within $\sim 50 \text{ kpc}$ of one another in our simulations before merging (appropriate for the maximal projected separation $20h^{-1} \approx 30 \text{ kpc}$ of the observed sample). The actual value of t_{merge} will depend in detail on observational selection effects, but the error introduced is still relatively small, $\lesssim 50\%$, and furthermore since this controls only the vertical normalization of the predicted luminosity functions, we can constrain the allowed range based on comparison of the luminosity functions. We discuss this and uncertainties owing to selection effects further below.

Figure 7 shows (upper left panel) the predicted QLF from the K -band low redshift MGLF of Xu et al. (2004). Solid circles indicate the observed $z < 0.2$ hard X-ray QLF of Ueda et al. (2003), for comparison. We rescale the hard X-ray QLF to a bolometric QLF for ease of comparison with galaxy properties and quasar peak luminosities, using a model of the intrinsic quasar continuum SED following Marconi et al. (2004), based on optical through hard X-ray observations (e.g., Elvis et al. 1994; George et al. 1998; Vanden Berk et al. 2001; Perola et al. 2002; Telfer et al. 2002; Ueda et al. 2003; Vignali et al. 2003), with a reflection component generated by the PEXRAV model (Magdziarz & Zdziarski 1995). This includes the important qualitative feature of the dependence of the optical to X-ray luminosity ratio on bolometric luminosity (e.g., Wilkes et al. 1994; Green et al. 1995; Vignali et al. 2003; Strateva et al. 2005), also suggested as an intrinsic correlation by comparison of a large sample of quasars selected by both optical and X-ray surveys (Risaliti & Elvis 2005). But even if we adopt a constant bolometric correction, our results are qualitatively unchanged (see e.g. Hopkins et al. 2005d,e for a discussion of the impact of bolometric corrections on our predictions). For simplicity, we consider only the hard X-ray (2-10 keV) QLF, where we can neglect attenuation, but we have demonstrated that the modeling of co-evolution of column densities and quasar luminosities in our simulations naturally reproduces the observed differences in optical, soft

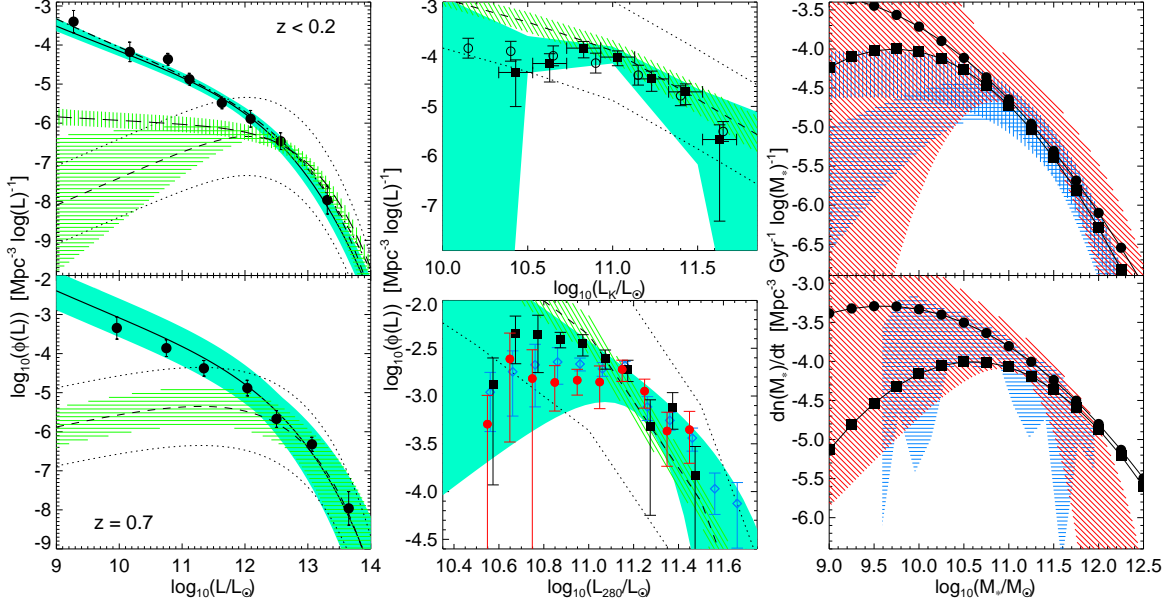


FIG. 7.— *Left*: Predicted QLF from the observed K -band $z < 0.2$ (upper; Xu et al. 2004) and 280 nm $z \approx 0.7$ (lower; Wolf et al. 2005) MGLFs, adopting our full model for quasar lifetimes (solid black line; blue shading shows 1σ range based on errors in the observed MGLF), or a simple “light-bulb” model for the quasar lifetime with t_Q varied to produce the best-fit expected QLF (short dashed; green hatched region shows 1σ range; dotted lines show prediction for t_Q a factor of 10 larger or smaller). Circles show the observed hard X-ray quasar luminosity function of Ueda et al. (2003), rescaled to bolometric luminosity with the corrections from Marconi et al. (2004). The predicted QLF from a constant merger fraction $\sim 6 \pm 3\%$ at $z < 0.2$ is also shown (dot-dashed line uses our full model, long-dashed line a “light-bulb” model). *Middle*: Predicted K -band $z < 0.2$ and 280 nm $z \approx 0.7$ MGLFs from the QLF of Ueda et al. (2003), lines and colors show the same as the left panels. Observations from Xu et al. (2004) from the 2MASS sample are shown as black squares in the upper panel, and a constant merger fraction ($6 \pm 3\%$); given the mass functions of Bell et al. (2003) as circles. In the lower panel, observations from Wolf et al. (2005) are shown as black squares (GOODS), blue diamonds (GEMS), and red circles (GEMS depth on GOODS area). *Right*: Inferred $\dot{n}(M_*)$, the gas-rich merger rate (spheroidal birthrate) with a given stellar mass, from the corresponding (K -band, upper; 280 nm, lower) observed MGLFs (1σ range, blue horizontal hatched; instead using a constant merger fraction shown as blue vertical hatched), and the corresponding QLF at $z < 0.2$, $z \approx 0.7$, respectively (1σ range, red shaded). Lines with circles and squares show the fitted $\dot{n}(M_*)$ from the QLF used in Hopkins et al. (2005e,g), respectively. In all cases, our modeling demonstrates that the observed QLFs and MGLFs are self-consistent and can be used to predict one another, with all mergers producing bright quasars and all bright quasars initially triggered in mergers. Simplified models of the quasar lightcurve give a very misleading relation between MGLF and QLF, predicting a QLF discrepant by $\gtrsim 6\sigma$.

X-ray, and hard X-ray QLFs (Hopkins et al. 2005d,e).

The black solid line in Figure 7 shows the prediction using our full modeling of the quasar lightcurve (described in § 4.1), with the blue shaded region showing the 1σ range allowed based on the 1σ errors in the observed MGLF. The prediction shown is for $f_{\text{gas}} = 0.15$ and $t_{\text{merge}} = 2$ Gyr, but the result is not sensitive to these assumptions. We discuss this point in detail in § 4.5 below, but briefly, if we allow f_{gas} and t_{merge} to vary, a formal best-fit is obtained for $f_{\text{gas}} = 0.25^{+0.21}_{-0.23}$ and $t_{\text{merge}} = 1.7^{+1.2}_{-0.9}$ Gyr. In other words, the quality of the fit is nearly unchanged for the entire reasonable range of f_{gas} and t_{merge} , and the fit for f_{gas} should not be taken too seriously given the wide range of f_{gas} allowed (constraining $t_{\text{merge}} = 2$ Gyr, for example, yields, $f_{\text{gas}} = 0.14^{+0.11}_{-0.12}$). The dashed line shows the prediction adopting the idealized “light-bulb” quasar model described above (§ 4.1), with again the green cross-hatched range showing the 1σ range from the observed MGLF. The prediction shown in this case is the best-fit allowing t_{merge} , f_{gas} , and the quasar lifetime t_Q to vary freely, giving $t_Q \approx 6.3 \times 10^6$ yr for $t_{\text{merge}} = 2$ Gyr (only the ratio t_Q/t_{merge} is constrained) and $f_{\text{gas}} = 0.25$. The dotted lines show the resulting prediction for t_Q larger or smaller by an order of magnitude.

In our model, the faint end of the observed QLF is dominated by quasars with larger peak luminosities in fainter states at various points during and after the mergers in which they form. Therefore, the faint end of the predicted QLF is tightly constrained, as it depends on the MGLF near its turnover, where it is most well-known. With a one-to-one

correspondence between peak and observed quasar luminosity (dashed lines), the faint-end QLF depends directly on the faint-end MGLF, and is thus poorly constrained. The agreement between the observed QLF and our prediction is good, $\chi^2/\nu \approx 3.41/8 = 0.43$ if we fix $t_{\text{merge}} = 2$ Gyr (negligibly improved if we allow t_{merge} to vary), and it requires no fine tuning of any parameters. The horizontal normalization offset is only weakly dependent on gas fraction and gives an essentially identical result for $f_{\text{gas}} \sim 0.05 - 0.5$, including the expected range of gas fractions at $z < 0.2$. The vertical normalization offset is proportional to t_{merge} , but the expected $t_{\text{merge}} \sim 2$ Gyr indeed yields nearly the best fit, and the factor $\sim 2 - 3$ errors in the QLF and MGLF imply that the small corrections to t_{merge} from sample selection effects will not alter our result. However, even allowing both horizontal and vertical normalizations to vary freely, the relative shapes of the quasar and MGLFs rule out a “light bulb” or exponential lightcurve (constant Eddington ratio) model for the quasar lightcurve at greater than 99.9% confidence, with the best-fit $\chi^2/\nu \approx 29.1/7 = 4.15$. Furthermore, even this fit requires a fitted quasar lifetime $t_Q \sim 6 \times 10^6$ yr, at the low extreme of the range indicated by observations (e.g., Martini 2004).

For models where L_{peak} scales with M_{BH} and the observed $M_{\text{BH}} \propto M_*$ is obeyed, $\dot{n}(L_{\text{peak}})$ must have approximately the same shape as the merger rate as a function of M_* , itself given approximately by the merger mass function. This shape is observationally well-defined, with a rapid decline above and flattening or decrease below the break luminos-

ity. In Hopkins et al. (2005c), we argue that this is the shape of $\dot{n}(L_{\text{peak}})$ implied by the combination of our model for quasar lifetimes with the observed QLF. However, with idealized models of the quasar lightcurve, $\dot{n}(L_{\text{peak}})$ must have the same shape as the observed QLF, which cannot be self-consistently resolved with the observed MGLFs. It is true that the faint-end slope of the MGLF is poorly constrained, with $\alpha = 0.30 \pm 0.56$; however, to be compatible with the faint end slope of the QLF in a simple light-bulb model (i.e. to steepen the dashed line to match the solid line in Figure 7) requires a 4σ change in α , which is unlikely especially given the large quoted error which includes possible systematic effects.

We can also invert this comparison, using the observed QLF to estimate the MGLF. Figure 7 (upper middle panel) shows this, using the $z < 0.2$ hard X-ray Ueda et al. (2003) QLF shown in the upper left panel to determine $\dot{n}(L_{\text{peak}})$, and correspondingly $\dot{n}(M_*)$ and $\phi_{\text{gal}}(L_K)$, the K -band $z < 0.2$ MGLF. Again, the blue range shows the prediction and 1σ range (from errors in the observed QLF) using our full model of quasar lifetimes, with $f_{\text{gas}} = 0.15$, $t_{\text{merge}} = 2$ Gyr. Dashed line and green hatched range shows the same for the “light-bulb” quasar lifetime model, allowing f_{gas} , t_{merge} , t_Q to be fit as in the upper left panel (producing identical fits), and the dotted lines show the prediction for an order of magnitude larger or smaller t_Q . These can be compared to the black squares, which show the binned MGLF from Xu et al. (2004). As expected from the upper left panel, the agreement using our full model of quasar lifetimes is good ($\chi^2/\nu = 0.35$), and the agreement with a simplified model of the quasar lifetime is poor ($\chi^2/\nu = 3.82$).

It is clear that the constraints from the observed QLF on the MGLF are significantly weaker than the constraints on the QLF from the observed MGLF. This is not because the QLF is poorly constrained relative to the MGLF (in fact, the opposite is true). Rather it is because a given interval in observed quasar luminosity has significant contributions from quasars with a wide range of peak luminosities $L_{\text{peak}} \gtrsim L$ (and a correspondingly wide range in host galaxy stellar mass), in various stages of evolution. Thus, there are significant degeneracies in predicting the relative contributions from different peak luminosities (black hole or host galaxy stellar masses) to the observed QLF based only on its observed shape. This is increasingly true at fainter merger luminosities, as the observed faint-end QLF is increasingly dominated by larger- L_{peak} sources, and therefore can place only weak constraints on the faint-end $\dot{n}(L_{\text{peak}})$ distribution (as discussed in e.g. Lidz et al. 2005). The weak constraints at the high- L_K end, however, owe to larger errors in the QLF. The wide range in the allowed faint- L_K end of the MGLF is reassuring, in the sense that at low luminosities, selection effects become important in efforts to identify a sample of merging galaxies, but these will not significantly change our result.

As an intermediate stage in these calculations, we have derived the implied $\dot{n}(M_*)$; i.e. the merger or birthrate of spheroids with stellar mass, directly related to the black hole activation rate (e.g. as a function of peak luminosity $\dot{n}(L_{\text{peak}})$). We show these $\dot{n}(M_*)$ distributions in Figure 7 (upper right panel), where the blue shaded range shows the 1σ range implied by the observed MGLF of Xu et al. (2004), and the red range shows the 1σ range implied by the observed QLF of Ueda et al. (2003) at $z < 0.2$. As noted above, it is clear that the QLF provides poor constraints on the low-mass behavior of $\dot{n}(M_*)$. For comparison, we plot the fitted $\dot{n}(M_*)$ distributions of Hopkins et al.

(2005e) and Hopkins et al. (2005g) (circles and squares, respectively), which were fitted to the combination of optical, soft X-ray, and hard X-ray QLFs (Miyaji et al. 2001; Ueda et al. 2003; Croom et al. 2004; Richards et al. 2005; Hasinger, Miyaji, & Schmidt 2005; La Franca et al. 2005). These may rise to lower masses before turning over than is implied by the MGLF, but as we have emphasized above (and shown in e.g. Hopkins et al. 2005e) this produces an essentially identical prediction for the properties of the quasar and remnant red galaxy populations.

It is worth noting that the distinction between the observed merger mass function of Xu et al. (2004) and a constant merger fraction is only marginally significant. Moreover, a number of studies simply measure the merger fraction, lacking the statistics to consider a full merger mass or luminosity function. Therefore, it is worth considering the effect on our predictions if the merger fraction were constant as a function of mass, with the observed low-redshift value $\sim 6 \pm 3\%$ (e.g., Xu et al. 2004; Bundy et al. 2005a,b; Lotz et al. 2006). We take the merger mass function to be this fraction of the observed local galaxy mass function from Bell et al. (2003). The results are shown in the upper panels of Figure 7. In the upper left, the predicted QLF from our full modeling is shown as the dot-dashed line; the difference between the prediction from the Xu et al. (2004) K -band MGLF and the constant merger fraction is negligible. The long dashed line shows the prediction assuming a simple “light bulb” model for the quasar lightcurve (with vertical green shading showing the $\sim 1\sigma$ range). Although the faint-end slope is marginally closer to that of the observed QLF, the two are still inconsistent at $> 6\sigma$. In the upper middle panel, open black circles show the implied merger mass function from a constant merger fraction, which differs from that of Xu et al. (2004) only marginally at low mass, and is within our 1σ prediction at all masses. In the upper right panel, the vertically blue shaded region shows the implied $\dot{n}(M_*)$ from a constant merger fraction, again only differing at low peak luminosity. In all cases, the differences in our predictions and conclusions is small, and this demonstrates the degree to which our predictions are insensitive to the number of low-mass mergers.

4.2.2. The 280 nm Merger Luminosity Function

We now repeat the analysis in § 4.2.1, for the observed 280 nm UV MGLF of Wolf et al. (2005) from the GEMS and GOODS surveys at $z \approx 0.7$. In detail, the galaxies are selected from the overlapping area of COMBO-17 and GEMS, with photometric redshifts $0.65 < z < 0.75$ and a rest-frame U -band selection (observed $R < 24$). The sample consists of visually identified morphologically selected peculiar/interacting galaxies, and as a consequence there is considerable observational uncertainty in the faint end of the MGLF, where tidal features are especially difficult to detect given surface brightness dimming at higher redshifts. However, as we demonstrate above in the case of the K -band MGLF, our modeling of the QLF is not sensitive to this faint-end behavior. We again expect a timescale $t_{\text{merge}} \sim 2$ Gyr over which galaxy mergers will be identified in the observed sample, although the exact value will depend in detail on observational selection effects. As shown in § 3.1, the typical gas fraction of these merging galaxies will generate a systematic horizontal offset in the predicted QLF, as at fixed peak luminosity (i.e. fixed black hole mass and total stellar spheroid mass); a larger gas fraction implies more new stars formed in the merger and

therefore a higher UV luminosity. We can use the relative horizontal normalization of the QLF, then, to constrain the range of allowed host galaxy gas fractions.

Figure 7 shows the result of this analysis in the lower panels, in the same manner as the upper panels which consider the low-redshift K -band MGLF. The lower left panel shows the predicted QLF using our full model for the quasar lightcurve (solid line with 1σ range as blue shaded range), and instead for an idealized “light-bulb” model for the quasar lightcurve (dashed line with green hatched 1σ range; dotted lines show the prediction for a fixed quasar lifetime an order of magnitude larger or smaller). Again, we compare to the observed hard X-ray QLF of Ueda et al. (2003), this time at $z = 0.7$ (black circles). Whether we use the GEMS or GOODS data makes little difference in the prediction of our model, so we show the result using the GOODS luminosity function, which has a larger number of faint merging galaxies, maximizing the ability of the “light bulb” model to fit the data. Again, it is clear that our model provides a good fit, while the “light bulb” model is ruled out, although not as dramatically as in the upper panel, at greater than 90% confidence ($\chi^2/\nu = 0.159, 2.41$ respectively). The shape of the QLF alone provides this qualitative constraint on the quasar lightcurve model, but the normalization implies a best-fit $t_{\text{merge}} = 1 - 3$ Gyr, again spanning the reasonable range and implying that the two normalizations are self-consistent. The relative horizontal offset of the QLF and MGLF provides a much stronger constraint on host galaxy gas fraction than in the K -band case, with $f_{\text{gas}} = 0.2 - 0.4$ implied (which we discuss in detail in § 4.5). As above, t_{merge} , f_{gas} , and t_Q are allowed to vary freely in the “light bulb” model, and although the fit is poor, the best-fit values are $f_{\text{gas}} = 0.3$ and $t_Q = 5.8 \times 10^6$ yr for $t_{\text{merge}} = 2$ Gyr. Again, a $\sim 4\sigma$ change in the faint-end slope of the MGLF would be required for the “light bulb” model to agree with the QLF, even for the maximal estimate of the number of faint mergers in Wolf et al. (2005).

Next, we invert this derivation, and Figure 7 shows (lower middle panel) the 280 nm MGLF inferred from the $z = 0.7$ QLF of Ueda et al. (2003), in the same style as the lower left or upper middle panels. The inferred MGLFs can be compared to those of Wolf et al. (2005) from the GOODS survey (black squares), GEMS survey (blue diamonds), and a combination of GEMS depth on the GOODS area (red circles). The differences in the observed MGLFs at the faint end demonstrate the considerable observational uncertainty here, but it is clear that the QLF is not sensitive to this faint-end behavior, and a wide range of faint-end MGLFs will produce a similar QLF. This is not the case for an idealized “light bulb” model, as demonstrated by the narrow range of the green hatched region even at low luminosities. The same parameters controlling the normalization are allowed to vary, and give essentially identical results as expected. The agreement between our model predictions and the observed MGLF is good ($\chi^2/\nu = 0.31$, compared to $\chi^2/\nu = 2.15$ for the light-bulb model), but as discussed in § 4.2.1, the constraints derived from the QLF on the MGLF are much weaker than those derived in the opposite direction.

Finally, we consider the $n(M_*)$ distribution implied by the MGLF of Wolf et al. (2005), shown in Figure 7 (lower right panel) as the blue shaded range (in the same style as the upper right panel). The range implied by the QLF at $z = 0.7$ is indicated as the red shaded range, with the fits to $n(M_*)$ used in Hopkins et al. (2005e,g) shown as lines with circles and squares, respectively. The implied $n(M_*)$ distributions

at $z = 0.7$ and $z < 0.2$ from 280 nm and K -band observations, respectively, can be compared to infer the evolution of merger rates and quasar birthrates as a function of mass, but we caution against taking this comparison too far. The samples use various selection criteria, are from different surveys, are not in the same wavebands, and have different dependence on gas fraction. Therefore, the potential systematic effects could be quite different between the two. However, with a MGLF selected uniformly from a given sample, in a single rest-frame waveband, the evolution of the galaxy merger rate and birthrate of quasars as a function of peak luminosity and final black hole mass can be studied as a function of redshift using our modeling of the galaxy luminosity in mergers.

4.2.3. Optical and Near-IR Merger Mass Functions

Finally, we repeat this analysis using the morphologically separated mass functions of Bundy et al. (2005a,b) from GOODS and DEEP2. Stellar masses are determined for all objects by fitting to optical spectroscopy and near-IR photometry, and we adopt the mass functions for objects visually classified as mergers (following Brinchmann et al. 1998) with ACS morphologies. This gives a binned merger stellar mass function determined in each of the intervals $z = 0.2 - 0.55$, $z = 0.55 - 0.8$, and $z = 0.8 - 1.4$, spanning $M_* \sim 10^9 - 10^{12} M_\odot$ (see Figure 8 below for a detailed comparison with the $z = 0.55 - 0.8$ mass function). In each case, the observed merger mass function implies a QLF in good agreement with the observations of Ueda et al. (2003) ($\chi^2/\nu \approx 0.85, 0.52, 0.98$ for $z = 0.2 - 0.55, 0.55 - 0.8, 0.8 - 1.4$, respectively), and the implied mass function from the QLF, albeit less well-constrained, is consistent with the observed mass functions. These observations also consistently rule out a “light bulb” or similarly simplified model for the quasar lightcurve at $\gtrsim 10\sigma$.

4.3. Direct Comparison of Merger Mass and Luminosity Functions

Although the agreement between quasar and merger statistics is encouraging, we would like to test our modeling of the MGLF directly. We do so by comparing the observed 280 nm MGLF of Wolf et al. (2005) to the measured merger mass functions of Bundy et al. (2005a,b). We consider the Bundy et al. (2005a) mass functions determined from the GOODS field by fitting optical spectroscopy and near-IR photometry, with redshifts $0.55 < z < 0.8$, similar to the $0.65 < z < 0.75$ range considered in Wolf et al. (2005). In both cases, optical or near-IR morphologies are used to visually select merging systems, so the ambiguity if e.g. t_{merge} is different for the “pair” and “peculiar” phases is minimized.

From our modeling in § 3.1.2 and methodology in § 4.1, we can convert the observed 280 nm MGLF to a merger mass function. Essentially, our simulations determine $P(L_{280} | M_*)$, and we use this to deconvolve $\phi(L_{280})$ and determine $\phi(M_*)$. Figure 8 shows the resulting inferred merger mass function. The observations of Wolf et al. (2005), converted to a mass function, are shown as cyan stars (GOODS), blue diamonds (GEMS), and red circles (GEMS depth on GOODS area). Alternatively, adopting the $\sim 1\sigma$ range in allowed fitted MGLFs from Wolf et al. (2005) and converting this to a merger mass function yields the shaded yellow range. The range shown can also be thought of as a range in gas fraction, with $f_{\text{gas}} \approx 0.15 - 0.30$. The observed merger mass function of Bundy et al. (2005a) is shown as the black squares, with the black dotted line showing the best-fit Schechter function.

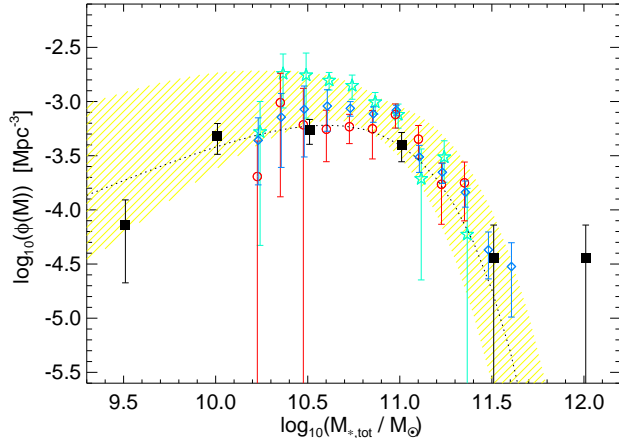


FIG. 8.— Merger mass function at $z \approx 0.7$, predicted from our modeling with the observed 280 nm MGLF of Wolf et al. (2005) (colored), and directly calculated from near-IR and optical observations in Bundy et al. (2005a) (black). Points converted from the 280 nm observations in Figure 7 are shown as cyan stars (GOODS), blue diamonds (GEMS), and red circles (GEMS depth on GOODS area), and the $\sim 1\sigma$ allowed mass function from our modeling as the yellow shaded region. Black squares show the binned mass function from Bundy et al. (2005a), black dotted line shows the best-fit Schechter function. The agreement between the two suggests that our simulations can reliably be used to map between MGLFs and merger stellar or black hole mass functions.

That the merger mass function implied by the MGLF and our modeling agrees well with the directly observed mass function is encouraging, and implies that we are modeling the critical dependence of observed merger properties on e.g. total merger stellar mass reliably. Observations also confirm that the relation between black hole and spheroid mass remains similar at these redshifts (e.g., Peng et al. 2006), which means that our mapping between merger and quasar luminosity functions successfully reproduces the active black hole and host galaxy mass functions.

4.4. The Distribution of Star Formation Rates

In § 4.2 we consider the rate of formation of galaxies with total new stellar mass $M_{*,\text{new}}$ in mergers, as determined from the MGLF or (assuming some characteristic gas fraction) from the QLF. We can convolve these estimates with the time each merger spends in some interval in SFR \dot{M}_* (Equation [5]) to determine the observed SFRF in mergers. The form of this convolution is identical to that used to determine the MGLF and QLF, given in Equation (9), considering \dot{M}_* instead of L_ν as a function of $M_{*,\text{new}}$. Figure 14 shows the results of this convolution, where we have used the determination of the rate of formation of galaxies as a function of $M_{*,\text{new}}$ from the 280 nm observed peculiar/interacting luminosity function of Wolf et al. (2005) at $z = 0.7$ from GEMS and GOODS (circles). We compare this to the observed SFRF of the same merging galaxy sample, determined in Bell et al. (2005a). We note that while Bell et al. (2005a) determine the SFRF and relative number density as a function of morphology, they do not determine the absolute SFRF normalization (i.e. proper effective volume correction), and so we adopt that inferred by Le Floch et al. (2005) at $z = 0.6 - 0.8$ from Spitzer in the Chandra Deep Field South. Red points are the observations, with no correction for the expected incompleteness below $\dot{M}_* \sim 10 M_\odot \text{yr}^{-1}$, and black points have been corrected for incompleteness at low SFR based on the comparison of GEMS

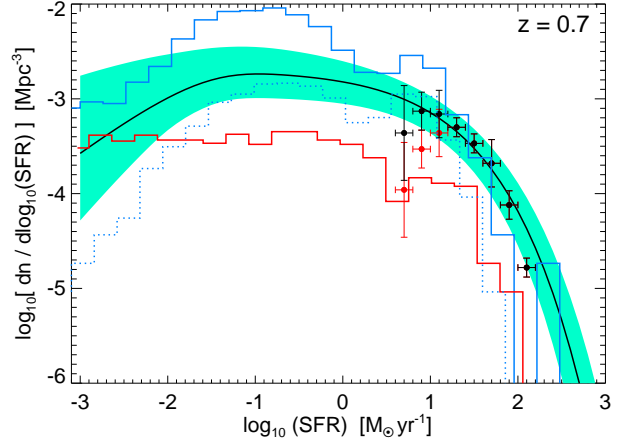


FIG. 9.— Distribution of star formation rates in mergers at $z = 0.7$, inferred from our modeling and the $z = 0.7$, 280 nm MGLF of Wolf et al. (2005) (solid line). Shaded range shows 1σ range based on observational errors in the MGLF. Circles show the observed SFRF of Bell et al. (2005a) at the same redshift (black, corrected for completeness; red, uncorrected), normalized with the observed IR luminosity functions of Le Floch et al. (2005). Red line shows the predicted SFRF owing to major mergers from the semi-analytic models of Somerville et al. (2001), blue lines include minor mergers. Solid lines adopt $t_{\text{merge}} \sim 10 t_{\text{dyn}} \sim \text{Gyr}$, dotted lines $t_{\text{merge}} \sim 10^8 \text{yr}$ as the maximum time since the last merger-tree merger. Again, the agreement suggests that our modeling can be reliably used to predict the merger-induced SFR distribution from a given MGLF or QLF. Note the increasing importance of the contribution from minor mergers at low SFR.

and GOODS luminosity functions from Wolf et al. (2005).

The agreement between the predictions from the 280 nm luminosity function and the observed SFRF is good, which implies that we are properly modeling the relation between the optical/UV luminosity of mergers and at least the statistics of the induced star formation as a function of time. Like the quasar luminosity discussed previously, there is no simple one-to-one correspondence between the 280 nm luminosity and SFR, as the optical/UV luminosity remains approximately constant during the merger, while the SFR evolves dramatically, characteristically spanning ~ 3 orders of magnitude (Figure 6). We also note that, because both the 280 nm magnitude and SFR distributions are functions of $M_{*,\text{new}}$ (as opposed to $M_{*,\text{tot}}$), the relation between the two is independent of $M_{*,\text{tot}}$ and f_{gas} .

It is also of interest to compare the distribution of mergers and SFRFs predicted by our modeling to that from semi-analytic models. In general, this is difficult, as the mergers of interest are not mergers of dark matter halos, but involve the luminous galaxies themselves, and where the galaxies are of comparable mass and have a large supply of cold (rotationally supported) gas. Furthermore, the exact requirements for triggering starbursts and AGN depend on, for example, the pressurization of ISM gas, star formation recipes, and the distribution of orbital parameters in the mergers (e.g., Hernquist & Mihos 1995). We have specifically chosen to quantify the properties of mergers in terms of e.g. L_{peak} , $M_{*,\text{tot}}$, and $M_{*,\text{new}}$, in a manner which suppresses these dependencies, in order to relate merger, starburst, and quasar populations independent of these detailed (and difficult to model) cosmological distributions. It is therefore outside the scope of this paper to consider a detailed comparison of merger rates as a function of these conditions as implied by e.g. our semi-empirical modeling, semi-analytic models, and cosmological

simulations. However, we can briefly consider a comparison between our predicted merger-driven SFRF and that predicted by semi-analytic models in Figure 9.

We show as the red solid line the SFRF predicted owing to major mergers (mass ratios less than $\sim 3:1$), and as the blue solid line the SFRF owing to “minor” mergers (generally, mass ratios greater than $\sim 10:1$), calculated at $z = 0.7$ from the semi-analytic models of Somerville et al. (2001, 2004a). In detail, we consider a galaxy to be “merging” if it has undergone a merger tree-defined merger within a time $\sim 10t_{\text{dyn}} \sim \text{Gyr}$. For comparison, if we consider a merger timescale $\sim t_{\text{dyn}} \sim 10^8 \text{ yr}$, the resulting SFRF is shown as the blue dotted line (for minor mergers). The agreement between the semi-analytic prediction and that of our modeling is encouraging, and suggests that the rate of gas-rich mergers in the standard CDM cosmology is appropriate to that implied by our modeling and the observations. Of particular interest, it is only with the inclusion of some “minor” mergers that the semi-analytic model predictions match the observations and our predictions from the QLF and MGLF, suggesting that our implied merger rates as a function of final, total stellar mass are contributed to by a wide range of mass ratios $\sim 10:1$ to $1:1$ (which we implicitly account for by expressing the merger rate in terms of the final mass and peak quasar luminosity), increasingly dominated by major mergers at the high-mass end. Any a priori theoretical modeling of merger rates and their associated quasar and starburst phases in cosmological simulations or semi-analytic models must then account for such mergers, and specifically for the sensitivity of these relatively low mass-ratio mergers to the initial conditions.

4.5. Systematic Uncertainties: Calibrating Gas Fractions and Merger Timescales/Selection Effects

Although the shapes of the MGLF and QLF by themselves constrain models of quasar lifetimes, the vertical and horizontal offsets of the luminosity functions depend on two parameters which are not well determined. Specifically, the vertical offset (i.e. ratio of the number of observed quasars to number of observed mergers) scales with t_{merge} , the time during which a galaxy would be identified as a merger in an observed sample. In principle, our simulations can be used to determine this quantity from first principles for a given observational sample, convolving the predicted galaxy images with the appropriate observational response (including e.g. surface brightness dimming) and selection criteria, to calculate the probability along each sightline that the object will be identified in the observational sample.

Such an investigation is beyond the scope of this paper, although it is important for a detailed calculation of merger rates as a function of mass and redshift for a uniformly selected merging galaxy sample at different redshifts. Some preliminary results can be obtained by tracking the path of one of our simulated mergers in Gini-M20 space, a non-parametric morphological classification scheme in which spirals, ellipticals, and mergers occupy distinct regions (Lotz et al. 2004). This quantitative analysis implies that the galaxy interaction may be classified as a merger somewhere between $\sim 0.5 - 3.0 \text{ Gyr}$, depending on the viewing angle, the merging orbit, the progenitor disk orientation, and the dark matter halo concentration. The median merger time is $\approx 2.0 \text{ Gyr}$ and it is worth noting that a similar estimate obtains from dynamical time considerations and observations (Patton et al. 2000). Improved observations of merger mass or luminosity functions which will enable more detailed comparison with quasar

statistics will demand a more detailed calculation of t_{merge} , specifically determining the effective t_{merge} appropriate for the given selection method. Morphological selection and pair selection, for example, identify different phases of merger activity, which can have different durations. Although for the “typical” pair separation of Xu et al. (2004) with which we compare ($\lesssim 50 \text{ kpc}$), the two timescales are comparable, this will obviously change with the definition of the pair or morphologically-selected sample. Such comparison can also calibrate further uncertainties, such as the fraction of missed light owing to low surface brightness extended features, as a function of merger stage.

The horizontal offset (i.e. the characteristic luminosity of a merger with a given $M_{*,\text{tot}}$ or peak quasar luminosity L_{peak}) scales with f_{gas} , at least for optical/UV samples. However, our approach is not embedded in a full cosmological model: we do not calculate the distribution of host galaxy properties a priori, but rather model individual mergers in order to attain the resolution necessary to model processes such as star formation, black hole accretion, and feedback from both. As shown in § 3.1, by quantifying our scalings in terms of e.g. L_{peak} and $M_{*,\text{tot}}$, we formulate our methodology independent of the vast majority of host galaxy properties (these differences manifest in e.g. different final stellar or black hole masses, but do not change any scalings expressed in terms of stellar or black hole mass). Consequently, our deconvolution of the QLF does not directly constrain these properties. However, for a given black hole mass and corresponding total stellar mass, a larger gas fraction implies that more new stars form during the merger, yielding a larger optical/UV luminosity, giving a different horizontal (luminosity) offset between the MGLF and QLF.

Having identified these dependencies and shown that the MGLF and QLF shapes are self-consistent given our modeling of quasar activity in mergers, we can use the combination of the observed luminosity functions to constrain both t_{merge} and f_{gas} . Figure 10 shows probability contours (at 10, 25, 50, 75, 90% as labeled) in t_{merge} and f_{gas} , from comparison of the MGLFs of Xu et al. (2004) in K -band at $z < 0.2$ (left) and Wolf et al. (2005) at 280 nm at $z = 0.7$ (center) to the corresponding Ueda et al. (2003) QLFs. The weak dependence of the K -band MGLF on f_{gas} is clear through the weak constraint it places on the gas fraction, but as a result the K -band MGLFs do constrain t_{merge} reasonably well, giving $t_{\text{merge}} \sim 1 - 2 \text{ Gyr}$ as we expect from our simulations. The 280 nm MGLF, on the other hand, has a much stronger dependence on f_{gas} , and thus places tight constraints on gas fraction while being nearly independent of t_{merge} . In either case, the degeneracy between f_{gas} and t_{merge} is well-defined, and this highlights the importance of determining t_{merge} in order to reliably constrain f_{gas} from the observations and testing whether the relative number of quasars and mergers are consistent to high precision.

In future samples which determine the merging galaxy luminosity function by uniform, automated selection criteria (see, e.g., Lotz et al. 2006), this comparison can be made more accurate by inferring t_{merge} a priori from the simulations. A key point from the above, however, is that our theoretical factor ~ 2 uncertainty in t_{merge} (which stems from not modeling the full sample selection function and e.g. cosmological orbit distributions) is not important for our conclusions, as any value of t_{merge} in this range still produces a good fit to observed QLFs (i.e. gives a self-consistent mapping between QLF and MGLF). This theoretical uncertainty does limit our compari-

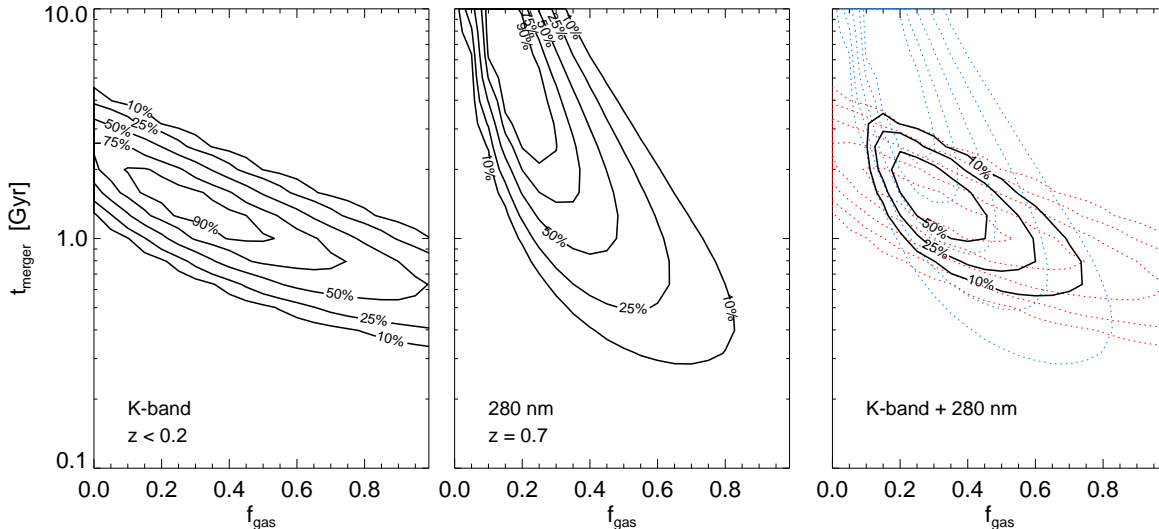


FIG. 10.— Probability contours in host galaxy gas fraction f_{gas} and time the merger is visible in the observed sample t_{merge} for the MGLF in K -band at $z < 0.2$ (left; Xu et al. 2004) and at 280 nm at $z = 0.7$ (middle; Wolf et al. 2005). Contours are shown at 10, 25, 50, 75, 90% as labeled. Right panel shows the previous two contour sets (dotted) and the joint (combined) probability contours of both luminosity functions (solid). Allowing these to vary freely yields physically reasonable values, and comparison of the two demonstrates that the dominant systematic uncertainties are different in near-IR and optical/UV MGLFs.

son of more subtle effects, but in any case we do not have a set of luminosity functions in the same rest frame wavelength at different redshifts where such detailed modeling of the selection criteria is important for comparison. Therefore, we adopt our theoretical estimate $t_{\text{merge}} \sim 2$ Gyr, and find that although this prior places no significant constraint on the $z < 0.2$ gas fractions determined from the K -band MGLF, it constrains the $z = 0.7$ gas fractions determined from the 280 nm MGLF to $f_{\text{gas}} = 0.28 \pm 0.09$, a relatively tight limit. Given the small relative errors, a sample with a uniform selection of rest frame optical/UV merging galaxies at different redshifts could be used to determine the evolution in gas fraction with redshift, so long as it was deep enough to resolve the break at each redshift. Even if potential systematic errors in e.g. our modeling of star formation or dust reddening yield some bias, the trend with redshift should be robust. Furthermore, this calculation uses the MGLF of Wolf et al. (2005), which is poorly constrained at moderate luminosities - improving the constraints on any given MGLF will improve the constraints on the implied $f_{\text{gas}}(z)$.

We can also use a comparison with the K -band MGLF to constrain t_{merge} and obtain, as a consequence, tighter constraints on f_{gas} . In the right panel of Figure 10 we show the constraints from both the K -band (red dotted; Xu et al. 2004) and 280 nm (blue dotted; Wolf et al. 2005) MGLFs, and the joint probability contours (black solid lines). It is clear here that the degeneracies in the $t_{\text{merge}} - f_{\text{gas}}$ fit plane from the IR and optical/UV MGLFs are nearly orthogonal, allowing this combination to much more strongly constrain host galaxy gas fractions. This results in a best-fit allowed $t_{\text{merge}} \sim 1 - 2$ Gyr, as expected (and as must be true if quasar and merging galaxy number counts are self consistent), with $f_{\text{gas}} \sim 0.2 - 0.4$. We primarily show this combination as a qualitative illustration, however, and caution against taking these numbers too seriously as the luminosity functions are determined at different redshifts, from various observed samples, with different selection criteria. It is therefore not clear that the time a merger will spend in the observed sample t_{merge} is the same in both cases, beyond the simple constraint $t_{\text{merge}} \sim 1 - 2$ Gyr demanded by

the evolution of morphologies in our simulations.

The effects of cosmic variance are also likely to overwhelm the systematic normalization issues above for the small areas probed in the observations of merging galaxy statistics. We discuss this further in § 5.2.2 below, but for now it is important to note that observations with the deep imaging required to identify merging systems have generally been limited to small fields. Somerville et al. (2004b) and Wolf et al. (2005) consider this in greater detail, and estimate that cosmic variance introduces a systematic factor of $\sim 1.5 - 2$ in the normalization of the merger luminosity functions. Therefore, it is not necessarily useful to apply a more detailed model of t_{merge} in our modeling, which considers the relation between e.g. the MGLF and QLF, if these are measured in different fields and either (more seriously the MGLF) is significantly affected by cosmic variance.

Furthermore, in detail we expect that the distribution of gas fractions will be drawn from some PDF, which can e.g. broaden the MGLF for a given merger total stellar mass function or QLF. However, this would primarily affect the implied faint-end slope, rather than ϕ_* or M_* which the QLF constrains. Essentially, the mean $\langle f_{\text{gas}} \rangle$ enters nearly linearly in the optical/UV luminosity (see Table 1), simplifying this comparison. Moreover, it is likely that the typical f_{gas} will have some dependence on galaxy mass. We have not modeled this, primarily because it introduces additional parameters which are loosely constrained and because it is unclear the extent to which this correlation is driven by heavier systems having undergone major mergers (i.e. their gas fractions pre-merger may have been uniform). However, the effect is less important than one might expect, for two reasons. First, the scaling with mass is not steep (i.e. a factor $\sim 10^2 - 10^3$ in M_* yields a factor $\sim 2 - 3$ in f_{gas} , still comparable to the existing uncertainty). Second, our modeling and the observations of Xu et al. (2004); Wolf et al. (2005); Bundy et al. (2005a) imply that the merger mass and luminosity functions do not have steep low mass/faint-end slopes, meaning that the typical f_{gas} near the MGLF “break” dominates the relative horizontal offset between merger mass and optical/UV luminos-

ity functions. In detail, we have considered our calculations adopting the f_{gas} as a function of late-type galaxy mass from Roberts & Haynes (1994), and find it makes little difference to our predictions (generally modifying them within existing $\sim 1\sigma$ uncertainties). Of course, to the extent that f_{gas} may evolve with redshift (discussed below), this consideration is important in disentangling how much of that evolution owes to a change in the characteristic masses of merging galaxies or to depleting gas supplies in quiescent star formation.

In general, it is always preferable to determine t_{merge} on purely theoretical grounds (by calibrating the sample selection criteria using a similar set of simulations), rather than allowing for the degeneracies in fitting it. It is also important to note that t_{merge} can vary depending on the mass of the progenitors, the mass ratio of the merger, and the orbital parameters, with e.g. the widest orbits ($R_{\text{peri}} \sim 0.3 R_{\text{vir}}$) taking ~ 5 Gyr to merge and the most radial ($R_{\text{peri}} \sim R_{\text{disk}}$) taking ~ 1 Gyr (Robertson et al. 2005a). Although these fits do not alter the qualitative conclusions, as e.g. even a factor ~ 2 revision in t_{merge} does not result in conflict between the observations of quasars and merging galaxies, they do alter the quantitative constraints on f_{gas} . However, at least to a factor ~ 2 accuracy in absolute f_{gas} values (and greater accuracy in the relative f_{gas} as a function of redshift), this implies that IR and optical/UV MGLFs at the same redshift (ideally determined using similar selection criteria) can be combined to more tightly constrain f_{gas} without the detailed model dependencies of calculating e.g. morphological selection probabilities throughout a merger.

5. THE EVOLUTION OF MERGER LUMINOSITY FUNCTIONS AND STAR FORMATION RATE DISTRIBUTIONS

5.1. Merger Luminosity Functions

Having predicted the MGLF from the QLF at low and intermediate redshifts in Figure 7, we can extend these predictions to other redshifts where the QLF is known. As is clear in Figure 7, however, the fact that the faint end of the observed QLF is dominated by sources with much larger peak luminosities means that the constraints on the faint end of the MGLF from the QLF are weak. If we assume that the MGLF is well-fitted by a Schechter function,

$$\phi(M) = \phi_* 10^{-0.4(M-M_*)(\alpha+1)} \exp\{-10^{-0.4(M-M_*)}\}, \quad (12)$$

this means that the QLF has almost no power to empirically constrain α . However, if we assume a specific value of α , we can then easily fit the observed QLF to determine the allowed range of ϕ_* and M_* .

Figure 11 shows this determination of ϕ_* and M_* , assuming a constant $\alpha = 0.5$, for both the K -band $z < 0.2$ and 280 nm $z = 0.7$ MGLFs, compared to the observations of Xu et al. (2004) and Wolf et al. (2005), respectively. The observed MGLF ϕ_* and M_* have been re-fit assuming the same $\alpha = 0.5$. Note that because a constant α is assumed, this can equivalently be considered a prediction of the total number and luminosity density of mergers, $\Phi = \phi_* \Gamma(\alpha + 1)$ and $\rho_L = \phi_* L_* \Gamma(\alpha + 2)$. For each wavelength, we show the contours enclosing the 1σ range of ϕ_* , M_* for a given gas fraction and t_{merge} . Points with error bars show the measurements at the corresponding frequency and redshift of Xu et al. (2004) and Wolf et al. (2005), respectively. We show the prediction assuming both $t_{\text{merge}} = 2$ Gyr (solid lines) and $t_{\text{merge}} = 1$ Gyr (dashed lines). As we discuss above, a more detailed comparison of trends with redshift should determine t_{merge} directly by testing the selection efficiency using simulated mergers, but for now our results are insensitive to the reasonable range of $t_{\text{merge}} \sim 1 - 2$ Gyr during which mergers

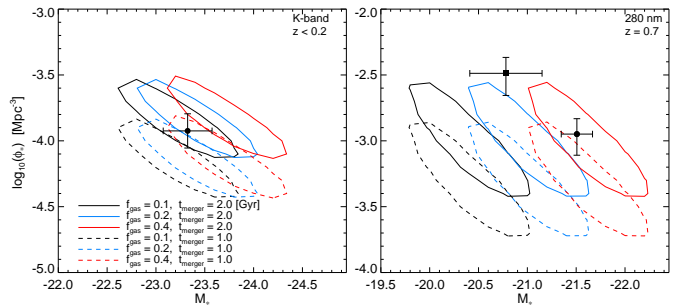


FIG. 11.— Contours of the 1σ allowed Schechter function parameters M_* , ϕ_* (assuming $\alpha = 0.5$) for the MGLF in K -band at $z < 0.2$ (left) and at 280 nm at $z = 0.7$ (right), assuming different values for the gas fraction f_{gas} and selection efficiency (time during which the merger will be identified as such) t_{merge} , as labeled. Points with error bars show the measurements at the corresponding frequency and redshift of Xu et al. (2004) from the 2MASS-2dFGRS survey in K -band and Wolf et al. (2005) from GOODS (square) and GEMS (circle) at 280 nm (observations rescaled assuming $\alpha = 0.5$). The QLF can significantly constrain the allowed MGLF parameters ϕ_* and M_* , modulo systematic uncertainty in the merger timescale t_{merge} (i.e. sample selection effects) and typical merging galaxy gas fraction f_{gas} .

will be identified, as the normalization ϕ_* is inversely proportional to t_{merge} , with observed errors a factor ~ 2 . We also show the prediction assuming different gas fractions $f_{\text{gas}} = 0.1$ (black), 0.2 (blue), 0.4 (red).

Increasing the gas fraction of merging galaxies naturally increases M_* , as galaxies with larger gas fraction form more new stars in a merger and are therefore brighter. The change is much stronger at 280 nm, as expected given that the optical/UV luminosity is more sensitive to the contribution from young stellar populations. The two parameters t_{merge} and f_{gas} then independently control the prediction of ϕ_* and M_* , respectively, and if there were no error in observations of the relevant luminosity functions, comparison of M_* alone (i.e. that predicted from the QLF vs. the measured MGLF) could be used to determine f_{gas} . However, even small errors in the observed luminosity functions make ϕ_* and M_* strongly degenerate parameters, as can be seen in the shape and overlap of the 1σ contours shown, and therefore makes it important to consider both quantities simultaneously.

The predictions agree well with the observations, for reasonable values of t_{merge} and f_{gas} , but this is expected from the more detailed comparison above in § 4.2 (Figure 7 and 10). However, the constraints on the MGLF from the QLF are not strong, and require a prior on α . We have assumed $\alpha = 0.5$, and scaled both our predictions and the observations to this α ; this introduces another, albeit well-known, degeneracy in ϕ_* and M_* . It is also clear in Figure 11 that the K -band MGLF is quite insensitive to the gas fraction, and the observations are consistent with a wide range of values, whereas observations in the optical/UV can distinguish between different gas fractions, demonstrating the distinction seen in Figure 10.

We can extend this prediction of ϕ_* and M_* to different redshifts, and probe the evolution of the MGLF and galaxy gas fractions. Most of the observational estimates of the merger fraction and luminosity density have been in the rest-frame B -band, so we consider the prediction in both K -band and B -band. The B -band (440 nm) calculation of host galaxy luminosities is identical to our calculation at 280 nm, and we refer to the full calculation of the B -band host galaxy luminosities in Hopkins et al. (2005e) (see also Jonsson et al. 2005). As expected, the resulting luminosities and their scaling with

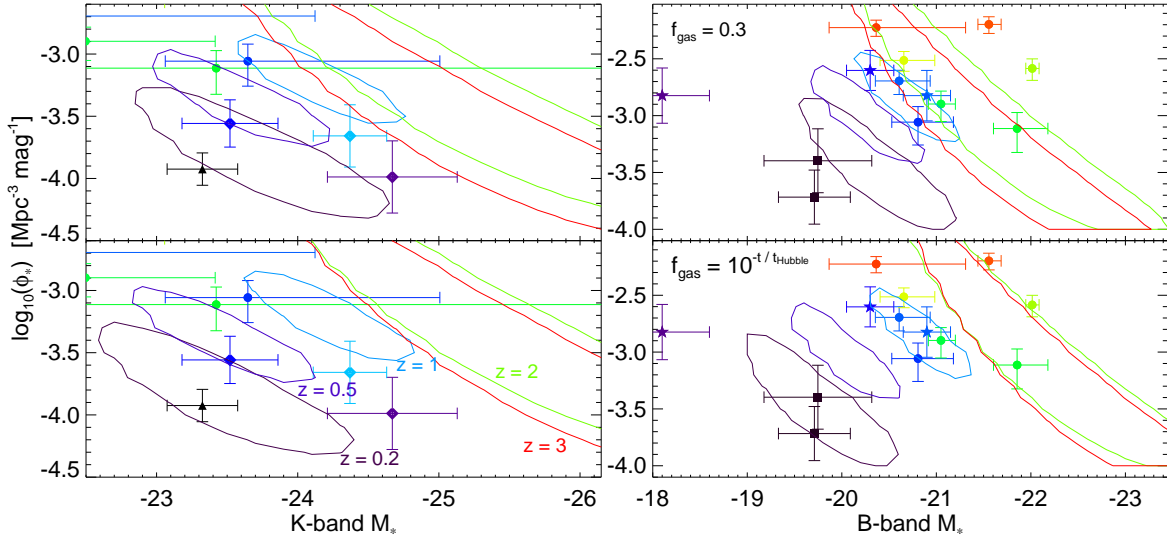


FIG. 12.— Predicted 1σ contours in ϕ_* and M_* for the MGLF in K -band (left) and B -band (right) determined from our model and the QLF of Ueda et al. (2003), at different redshifts as labeled. Observations (color-coded to match the appropriate redshift, from black at $z = 0$ to red at $z = 3$) are shown from Xu et al. (2004) (triangle), Bundy et al. (2005a,b) (diamonds), Conselice et al. (2003, 2005) (circles), Toledo et al. (1999) (squares), and Brinchmann et al. (1998) (stars). Upper panels assume a constant gas fraction $f_{\text{gas}} = 0.3$ at all z , lower panels assume an exponentially declining $f_{\text{gas}} = 10^{-t/t_{\text{Hubble}}}$. Observational uncertainties and degeneracies between the best-fit parameters make direct comparison difficult, but the data do favor an evolving gas fraction with $\sim 2\sigma$ confidence.

L_{peak} are nearly identical at the two frequencies, modulo a nearly mass-independent $M_B - M_{280} \approx 0.9$ (this reflects the dominant $\sim 0.1 - 0.5$ Gyr young blue stellar population in the optical/UV). Figure 12 shows the 1σ contours in the fitted MGLF ϕ_* and M_* for the K -band (left) and B -band (right) MGLF at different redshifts, as determined from the hard X-ray QLF of Ueda et al. (2003) at each redshift. We assume $t_{\text{merge}} = 2$ Gyr for each, but as shown in Figure 11 above, this controls only the vertical normalization and does not change our results within the reasonable range. We show the predicted ϕ_* , M_* at $z = 0.2, 0.5, 1, 2, 3$, as labeled.

We also show several observational estimates at different redshifts. In K -band, the black triangle is the $z < 0.2$ measurement of Xu et al. (2004), and circles show the estimates from the merger IR luminosity density and mass density of Conselice et al. (2005) at mean redshift $z = 0.88$ (blue) and $z = 1.68$ (green). Diamonds show the estimates from the peculiar/interacting galaxy mass functions of Bundy et al. (2005a,b) at $z = 0.2 - 0.55$ (purple), $z = 0.55 - 0.8$ (blue), and $z = 0.8 - 1.4$ (cyan). In the B -band, black squares show the $z < 0.1$ estimate from the optical pair luminosity function of Toledo et al. (1999); stars show the estimate from B -band peculiar galaxy luminosity and number density measures of Brinchmann et al. (1998) at $z = 0.2 - 0.5$ (purple), $z = 0.5 - 0.75$ (dark blue), and $z = 0.75 - 1.0$ (blue); and circles show the results from the morphologically identified B -band peculiar luminosity density estimates of Conselice et al. (2003, 2005) at mean redshifts $z = 0.88$ (blue), $z = 1.68$ (green), $z = 2.22$ (yellow), and $z = 2.71$ (red) from the HDF-N and HDF-S. In each case, we have re-fit the observations assuming the same $\alpha = 0.5$ as our predictions. Several of the observations do not measure a luminosity function, but a number density (or merger fraction) and luminosity density - in these cases we estimate ϕ_* , M_* also assuming a MGLF with $\alpha = 0.5$. Although assuming different values of α will not change the agreement of our predictions with the observations at any redshift, it will change the absolute values of the predictions by a significant amount, and therefore we caution that any comparison should

account for this difference.

In order to predict M_* at each redshift from the QLF, we must assume some typical gas fraction f_{gas} of the merging galaxies. In the upper panels of Figure 12, we adopt a constant $f_{\text{gas}} = 0.3$, where the value of f_{gas} is chosen because it provides a best fit to the cumulative observations plotted. In the lower panel, we assume an exponentially declining gas fraction with cosmic time, $f_{\text{gas}} = 10^{-t/t_{\text{H}}}$ where t_{H} is the Hubble time, such that $f_{\text{gas}} = 1$ at early times and $f_{\text{gas}} = 0.1$, similar to the Milky Way, at present. This gives an e -folding time for f_{gas} of $t_{\text{H}}/\ln(10) \approx 6$ Gyr, similar to that expected for quiescent spirals following a Schmidt-type star formation law (Kennicutt 1998; Rownd & Young 1999; Martin & Kennicutt 2001; Springel & Hernquist 2003a; Li et al. 2005a,b). We have also compared with the evolution of the distribution of cold (rotationally supported) gas mass fractions in galaxy mergers (with total baryonic mass above $10^{10} M_{\odot}$) predicted by the semi-analytic models of Somerville et al. (2004a), and find that these cosmological models predict a similar evolution in the mean gas fraction.

Although it is clear that the observations do not strongly distinguish between the two cases, and we caution that we have assumed a constant selection efficiency t_{merge} despite different observed sample selection criteria and different redshifts, there is a significantly better fit in the case of the exponentially declining gas fraction ($\chi^2/\nu = 0.4$ compared to $\chi^2/\nu = 2.1$). This distinction is derived from the B -band data; as discussed above, the K -band is relatively insensitive to the gas fraction and does not significantly constrain this evolution. That the exponential decline in gas fraction is preferred by the data is expected, and the observations are not accurate enough to significantly constrain the timescale or detailed functional form of the decrease in gas fraction with time, but this demonstrates the key qualitative behavior, that merging galaxies were more gas rich in the past and that these measurements can constrain that evolution through the evolution in $M_*(z)$. Essentially, resolving whether $\lesssim 0.5$ or ~ 2 magnitudes of evolution takes place in $M_*(z)$, is, combined with

our modeling of the QLF, sufficient to constrain the history of merging, quasar-producing galaxy gas fractions. The agreement with the K -band observations is good in either case, but with the exception of the Xu et al. (2004) observations at low redshift, the data are not well enough constrained to be a strong test of the model.

The well-known degeneracy between ϕ_* and M_* in fitting or predicting any luminosity function does mean that our predictions of either quantity individually are loosely constrained. However, the combination of the two, namely the total luminosity density, is a well-constrained quantity in our modeling. The full luminosity density, $\rho_L = \phi_* L_* \Gamma(\alpha + 2)$, technically includes the order unity correction from the integrated faint-end contribution, $\Gamma(\alpha + 2)$, which our modeling has little power to constrain from the observed QLF. However, the quantity $\phi_* L_*$ is well-determined, and in Figure 13 we show our predictions for this combination (i.e. neglecting the $\Gamma(\alpha + 2)$ correction, or equivalently assuming $\alpha = -1$ or $\alpha = 0$, although the corrections from α are small for the reasonable range $-1.5 \leq \alpha \leq 1.0$). We show the predicted luminosity density in K -band (left) and B -band (right), as a function of redshift from $z = 0 - 6$, based on the Ueda et al. (2003) QLF. The solid line assumes a gas fraction $f_{\text{gas}} = 10^{-t/t_H}$, and the dotted line assumes a constant $f_{\text{gas}} = 0.3$ at all z . The yellow shaded range shows the 1σ allowed range inferred from the QLF, for the evolving f_{gas} case. For clarity, we do not show the errors for the constant f_{gas} case, but they are similar at all redshifts.

We compare these predictions to observations from Xu et al. (2004) (red triangle), Bundy et al. (2005a,b) (blue diamonds), Conselice et al. (2003, 2005) (circles; HDF-N in cyan, HDF-S in green), Toledo et al. (1999) (red squares), and Brinchmann et al. (1998) (blue stars). It is clear from the figure that our predictions for the luminosity density are narrowly constrained, generally within a factor ~ 2 at all redshifts, with the errors dominated by uncertainties in the observed QLF (and thus potentially improved by future, high redshift complete samples which can constrain the QLF break luminosity at a range of redshifts) instead of by fitting degeneracies. The variation owing to different gas fractions is small in K -band, as expected, but enters approximately linearly into the B -band luminosity densities. Improved constraints on the K -band MGLF measurements and extension of B -band MGLF measurements to higher redshifts can provide a strong test of whether the consistent relation between merger and quasar populations this modeling demonstrates at $z \lesssim 3$ remains true at high redshifts.

5.2. Star Formation Rates in Mergers

5.2.1. The Star Formation Rate Distribution

Instead of the observed MGLF, we can use the QLF to determine the merger rate as a function of stellar mass, and calculate the resulting SFRF, in analogy to our calculation of the MGLF from the QLF in § 4.2.2. Figure 14 shows the results of this calculation at several redshifts $z = 0 - 3$ (as labeled). In each panel, the solid line shows the prediction and shaded range the 1σ allowed range based on errors in the observed QLF and uncertainty in our fitting to it. The dashed line shows the prediction from the MGLF at $z = 0.7$ from Figure 9 for comparison in each panel. Points in the $z = 0.7$ panel show the observations from Bell et al. (2005a); Le Floch et al. (2005) also as in Figure 9. The dashed line and solid line at $z = 0.7$ are slightly different because the former is predicted from the

observed merger luminosity function at that redshift, the latter from the observed QLF, but they agree within the larger uncertainties in the prediction from the QLF. Because the observed QLF constrains the distribution of mergers in terms of $M_{*,\text{tot}}$ but the SFRF, by definition, depends on $M_{*,\text{new}}$, we must adopt a gas fraction, as in our determinations of the MGLF in § 5.1, and so we take $f_{\text{gas}} = 10^{-t/t_H} \approx \exp(-t/6\text{Gyr})$, following our calculations in § 5.1 (although we show the effects of different assumptions for f_{gas} in Figure 15 below).

The character of the inferred SFRF is similar at each redshift. The peak and break evolve to larger SFR at higher redshift, driven by two effects. First, the dominant effect is a reflection of the luminosity evolution of the QLF with redshift, as the break in the QLF evolves towards larger luminosities by close to two orders of magnitude over this range, meaning typical quasar peak luminosities and corresponding black hole and host galaxy masses (and therefore the mass of new stars formed) must evolve similarly. Second, as we have assumed $f_{\text{gas}} = 10^{-t/t_H}$, the typical gas fraction rises with redshift, increasing the SFR for a given total (final) mass. This results in a further factor ~ 3 increase in $M_{*,\text{new}}$ from $z = 0.2 - 2$.

The uncertainty in the predicted SFRF is sizable at low SFR, but this is many orders of magnitude below the peak SFR in mergers and below typically measured SFRs (see the observations in the $z = 0.7$ panel). Furthermore, comparison with the lower middle panel of Figure 7 shows that the uncertainty, even at the faint end of the SFRF, is considerably smaller than the uncertainty in the MGLF and the corresponding rate of formation of spheroids in mergers as inferred from the QLF. This is because both the SFRF and QLF are the result of a convolution of the time spent at a given SFR/quasar luminosity with the rate of formation of objects in mergers, and the time per unit SFR/quasar luminosity have similar functional forms. Thus, in a similar manner to the QLF, the dependence on the faint end of the MGLF is suppressed, as many objects observed with low SFRs are mergers with a much larger peak SFR, viewed in stages of the merger before or after this peak.

Finally, although this calculation suggests a form for e.g. the ULIRG and LIRG IR luminosity functions, we caution that we are not in a position to predict the IR luminosity function at various wavelengths. This is because we do not model re-radiation of absorbed light by dust. However, a rough calculation shows that we expect counts of ULIRGs to be consistent with our modeling (Hopkins et al. 2005e). We defer a more thorough calculation of the IR spectrum, including the effects of dust heating, re-radiation and line emission, to future work.

5.2.2. The Star Formation Rate Density of the Universe

We can integrate the SFRF at each redshift to determine the SFR density in mergers as a function of redshift. Figure 15 shows the results of this integration, where we have determined the SFRF from the QLF in the manner of Figure 14 at each redshift. The solid black line shows our prediction from the best-fit to the QLF, assuming $f_{\text{gas}} = 10^{-t/t_H} \approx \exp(-t/6\text{Gyr})$ as estimated in § 5.1. The shaded area shows the 1σ range allowed, based on the errors in the observed QLF and more important, degeneracies in fitting to the observed QLF. We also show the prediction assuming a constant $f_{\text{gas}} = 1.0$ (dot-dashed line) or $f_{\text{gas}} = 0.1$ (dashed line) at all redshifts. For clarity, we do not show the errors for each of these predictions, but they are identical in form to those about the solid line. Clearly, the

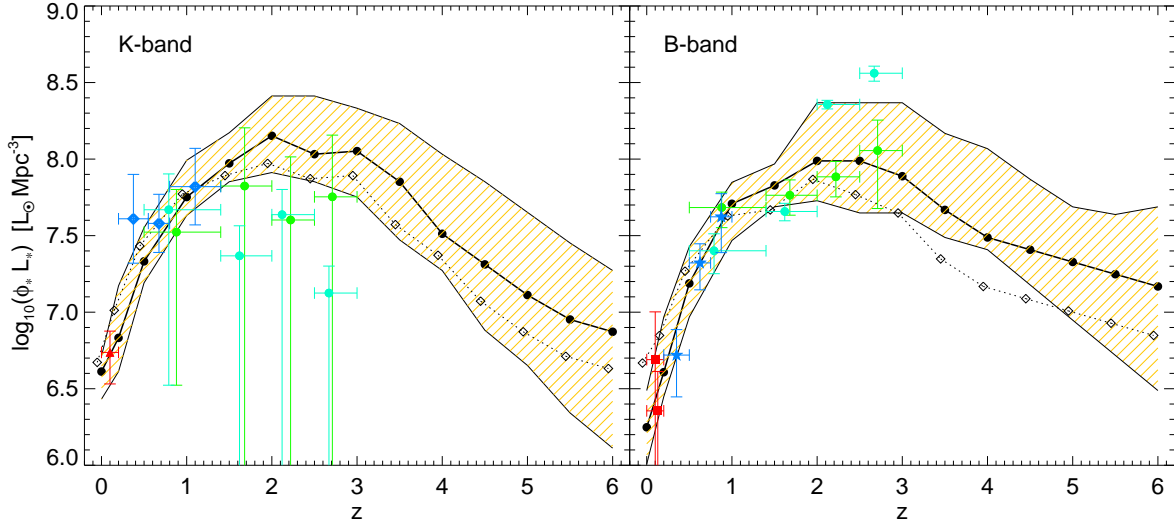


FIG. 13.— Predicted luminosity density contributed by merging galaxies in K -band (left) and B -band (right), as a function of redshift. Solid line assumes a gas fraction $f_{\text{gas}} = 10^{-1/tH}$, dotted line assumes a constant $f_{\text{gas}} = 0.3$ at all z . Yellow shaded range shows the 1σ allowed range inferred from the QLF, for the evolving f_{gas} case (errors are similar for constant f_{gas}). Observations are shown from Xu et al. (2004) (red triangle), Bundy et al. (2005a,b) (blue diamonds), Conselice et al. (2003, 2005) (circles; HDF-N in cyan, HDF-S in green), Toledo et al. (1999) (red squares), and Brinchmann et al. (1998) (blue stars). The observed mass/luminosity density in mergers and its evolution is consistent with that required if all bright quasars are triggered in mergers *and* the converse, that all mergers trigger bright quasars. The quasar luminosity function and our modeling can be used to predict the merger mass and luminosity density at all redshifts where the QLF break is reasonably constrained.

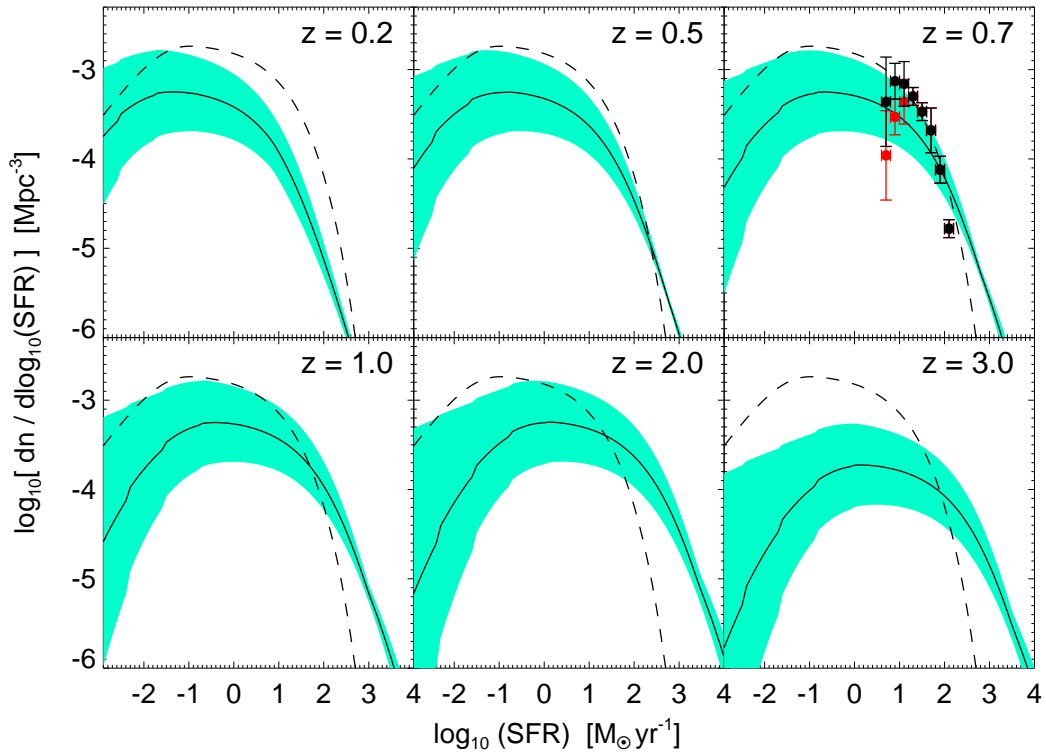


FIG. 14.— Inferred SFRF in mergers from the QLF as a function of redshift (black lines) at the redshifts shown. The shaded area shows the 1σ range from errors in the observed QLF and uncertainties in fitting to it. Observations of Bell et al. (2005a); Le Floch et al. (2005) are shown at $z = 0.7$ in the manner of Figure 9, and the dashed line and solid line at $z = 0.7$ are slightly different because the former is predicted from the observed merger luminosity function at that redshift, the latter from the observed QLF. The QLF alone allows us to reasonably constrain the distribution of star formation rates in mergers, over a wide range of redshifts where direct observations are not available.

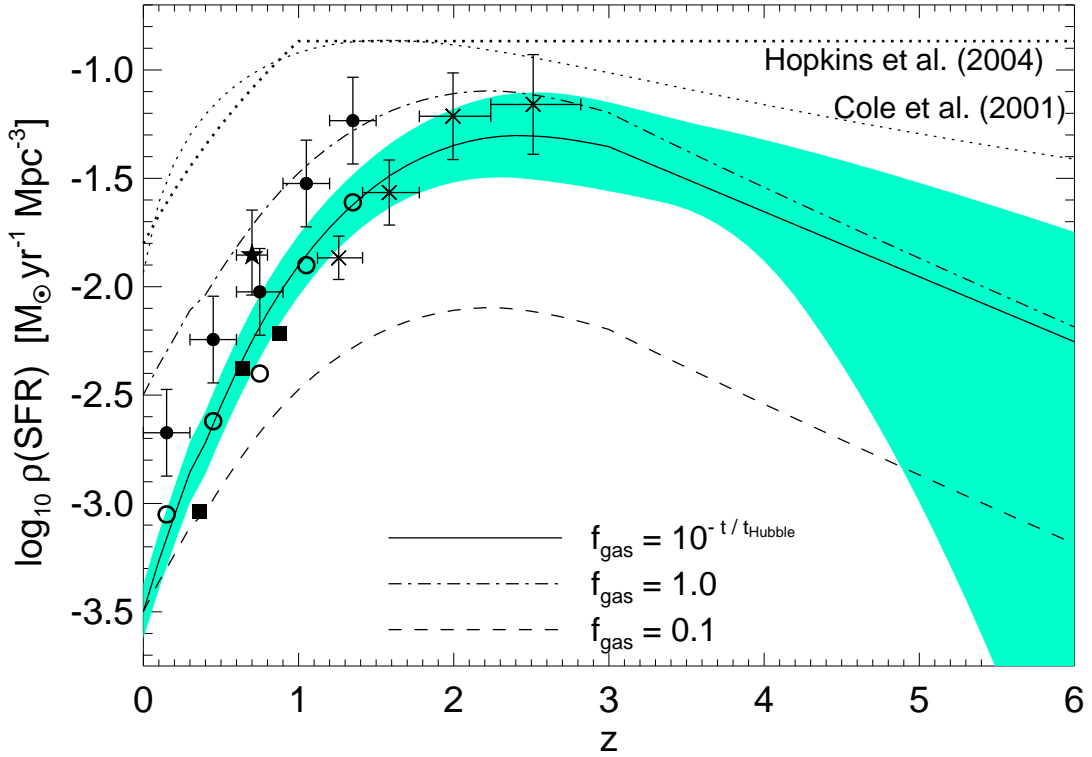


FIG. 15.— Star formation rate density in mergers, inferred from the quasar luminosity function assuming an average gas fraction $f_{\text{gas}} = 10^{-t/t_{\text{Hubble}}} = \exp(-t/6\text{Gyr})$ (solid line). The shaded area shows the 1σ range allowed (owing to degeneracies in fitting to the observed QLF). Note that adopting the steeper faint-end slope estimates from the deeper GOODS subsample of Wolf et al. (2005); Bundy et al. (2005a) systematically increases our prediction by a factor ~ 2 (at the upper range of the 1σ uncertainty). The dot-dashed line and dashed lines show the result assuming a constant gas fraction $f_{\text{gas}} = 1.0$ and $f_{\text{gas}} = 0.1$, respectively (for clarity, errors are not shown, but they have identical form). Dotted lines show the estimated total (extinction-corrected) star formation rate density from Cole et al. (2001) and Hopkins (2004). Observations of the SFR density in mergers at various redshifts are shown from Bell et al. (2005a) (star), Brinchmann et al. (1998) (squares), Pérez-González et al. (2005) (\times 's; from the estimate of the ULIRG contribution to the SFR density), and Menanteau et al. (2001, 2005) (filled circles, open circles show the same but renormalized to match the integrated stellar density from mergers inferred by Brinchmann et al. (1998); Conzelmann et al. (2003); Bell et al. (2005a)). The $f_{\text{gas}} = 1$ line can also be thought of as the total rate at which stellar mass is “moved” or “generated” onto the red sequence by quasar-producing gas-rich mergers. The QLF alone can be used as an independent constraint the merger-induced SFR density of the universe; the SFR density in mergers must rise from $\lesssim 1\%$ of the total SFR density at $z=0$ to $\sim 10\text{--}20\%$ at $z=1$ and $\sim 25\text{--}50\%$ at $z=2$.

solid line effectively interpolates between a high-gas fraction era at $z \gtrsim 2$ to present characteristic low gas fractions $f_{\text{gas}} \sim 0.1$ at $z = 0$. For comparison, we show the total (integrated over all morphological types), extinction-corrected SFR density estimated in Cole et al. (2001) and Hopkins (2004) as the dotted lines (thin and thick, respectively). Both, and in particular the estimate from the compilation of Hopkins (2004), agree favorably with other recent estimates from e.g. IR observations (Pérez-González et al. 2005) and cosmological simulations (e.g., Springel & Hernquist 2003b; Hernquist & Springel 2003).

Observations of the SFR density in merging/peculiar systems are also plotted, from Bell et al. (2005a) (star), Brinchmann et al. (1998) (squares, where we have corrected the densities to the cosmology we adopt), and Menanteau et al. (2001, 2005) (circles). The filled circles, which show the measurements of Menanteau et al. (2001, 2005), are systematically higher than the other measurements, a point discussed by the authors, and so we consider also their observations re-normalized to produce the same integrated $0 < z < 1$ stellar density formed in mergers as that estimated by Brinchmann et al. (1998); Conselice et al. (2003); Bell et al. (2005a) (open circles). The estimate of the SFR density in ULIRGs from Pérez-González et al. (2005) is also shown (\times 's), but we caution that although these bright IR objects are usually associated with mergers at low redshift, dusty, more concentrated disks at high redshift may make up a significant fraction of this population and result in an overestimate of the contribution of mergers to the SFR density.

In Hopkins et al. (2005e,f), we fit the birthrate of quasars as a function of peak luminosity from the QLF to a lognormal distribution. Because L_{peak} is related to M_{BH} (Equation [8]), this gives a rate of creation/activation as a function of final black hole mass

$$\dot{n}(M_{\text{BH}}) = \frac{\dot{n}_{\text{BH}}(z)}{\sigma_{\text{BH}} \sqrt{2\pi}} \exp\left(-\frac{\log^2\{M_{\text{BH}}/M_{\text{BH},0}(z)\}}{2\sigma_{\text{BH}}^2}\right), \quad (13)$$

where $\dot{n}_{\text{BH}}(z)$ is the total number density of black holes being created/activated at z , σ_{BH} is the width of the lognormal (characterizing the slope of the bright end of the luminosity function), and $M_{\text{BH},0}(z)$ is the characteristic black hole mass being activated, corresponding to the break in the observed QLF approximately by $L_{\text{break}} \sim L_{\text{Edd}}[M_{\text{BH},0}(z)]$. If we adopt this simple fit, then, assuming also that deviations about the $M_{\text{BH}} = \mu M_{*,\text{tot}}$ (black hole-stellar mass) relation are distributed in a lognormal fashion with dispersion $\sigma_{M_{\text{BH}}-M_*}$ and using $M_{*,\text{new}} \approx f_{\text{gas}} M_{*,\text{tot}}$, we arrive at a particularly simple expression for the SFR density

$$\rho_{\text{SFR}} = \dot{n}_{\text{BH}} \left(\frac{1}{\mu} f_{\text{gas}} M_{\text{BH},0} \right) e^{\frac{1}{2} \ln^2 10 (\sigma_{\text{BH}}^2 - \sigma_{M_{\text{BH}}-M_*}^2)}. \quad (14)$$

Although we do not restrict ourselves to this lognormal fit in our predictions in Figure 15 (rather allowing $\dot{n}(M_{\text{BH}})$ to vary freely and constraining the range as in Figure 7), this simple calculation allows us to illustrate the key qualitative points of the derivation.

In our fits to the QLF, \dot{n}_{BH} is constant at least to $z \sim 2-3$, while M_{BH} evolves by $\sim 1-2$ orders of magnitude, reflecting the approximate pure luminosity evolution in the break of the QLF. Therefore at $z \lesssim 3$, the evolution in ρ_{SFR} corresponds to the evolution in the QLF, as the characteristic final stellar mass, black hole mass, and quasar peak luminosity produced in mergers rises with redshift (approximately as $L_{\text{peak}} \propto \exp(6\tau)$, where τ is the fractional lookback time, or

$L_{\text{peak}} \propto z - 0.2z^2$; Boyle et al. 2000, Hopkins et al. 2005e). If the characteristic gas fraction increases with redshift, this will also contribute to increasing ρ_{SFR} , as for a given black hole and total stellar mass, a larger fraction of the stars are formed during the merger, and for example our assumption of $f_{\text{gas}} = 10^{-t/t_H}$ gives an additional factor of $\sim 7-8$ increase in ρ_{SFR} from $z = 0$ to $z = 3$. Above $z \sim 2-3$, the normalization of the quasar luminosity function decreases, and the predicted ρ_{SFR} evolution is dominated by e.g. density evolution as $\dot{n}_{\text{BH}} \propto 10^{-0.48(z-2)}$ (Fan et al. 2001). Above $z \sim 4$, the constraints on the SFR density from the QLF become poor, as the QLF is weakly constrained and, in particular, the break in the observed QLF is no longer well-determined. Finally, we note that the correction for the convolution of the formation rate as a function of black hole mass and the black hole-stellar mass relation ($\sigma_{M_{\text{BH}}-M_*}$) is small, $\sim 20\%$, for the observationally determined $\sigma_{M_{\text{BH}}-M_*} \sim 0.3$ or intrinsic $\sigma_{M_{\text{BH}}-M_*} \sim 0.2$ from our simulations (Di Matteo et al. 2005; Robertson et al. 2005b), and is thus unimportant compared to the uncertainties in fitting the observed QLF.

The agreement between the observations of the SFR density in merging galaxies as a function of redshift from Brinchmann et al. (1998) and Bell et al. (2005a) and the predictions from the observed QLF and our modeling is good, implying that the QLF can in fact be used as an independent, albeit indirect constraint on the star formation history in mergers and the contribution of merger-induced starbursts to present stellar populations. Of course, the agreement with Bell et al. (2005a) is unsurprising, given the agreement between their detailed SFRF and that we predict in Figure 14. The observations of Menanteau et al. (2001, 2005) are systematically high compared to those of Brinchmann et al. (1998), a point which the authors themselves discuss. However, as they note, the absolute calibration is the most uncertain element of their calculation, and the trend with redshift they observe agrees well with that observed by Brinchmann et al. (1998) and predicted in Figure 15. This is clear from the open circles, which show the Menanteau et al. (2001, 2005) observations renormalized to produce the same integrated $0 < z < 1$ stellar density produced in mergers as that inferred by Brinchmann et al. (1998) and Conselice et al. (2003); i.e. a uniform factor ≈ 2 lower ρ_{SFR} . In addition to possible systematic errors in the measurements of Menanteau et al. (2001, 2005), it is worth noting that their measurement is for the peculiar/irregular-selected subsample, and therefore if the contribution of irregular late-type galaxies in this sample is large (as opposed to the $\sim 25-30\%$ estimated by Bell et al. 2005a), it may explain the discrepancy. Even if the higher ρ_{SFR} measurements of Menanteau et al. (2001, 2005) are correct, they are still consistent with our predictions for $f_{\text{gas}} \sim 0.5-1$, implying that quasar-producing mergers at low to moderate redshifts may be characteristically still quite gas-rich, and that e.g. the MGLF and SFRF measurements of Brinchmann et al. (1998) may be somewhat incomplete (perhaps owing to extinction in the highest SFR systems).

More important, the effects of cosmic variance are likely to overwhelm the systematic normalization issues above for the small areas probed in the observations shown. The difficulty of identifying mergers without deep imaging has naturally limited the effective volume of many of such measurements. Somerville et al. (2004b) and Wolf et al. (2005) discuss this for several of the fields from which we have considered measurements (e.g., GOODS, GEMS, HDF), and for the

specific application to different morphological classifications. They estimate this could be a significant source of uncertainty, a factor of $\sim 1.5-2$ in their estimates from GOODS. Lacking a sufficiently large volume to suppress the effects of cosmic variance, we should ideally compare measurements from the same fields. In other words, regardless of cosmic variance in a particular field, the observed QLF in the field should be consistent with observed MGLFs and merging galaxy SFRFs in the field. In fact, if we limit our comparisons in this manner, we find very good agreement between the observations and our predictions (see e.g. § 4). In general, our predictions from the QLF may be more representative of the cosmic mean, in that they agree with the observed QLFs from large volume surveys such as the SDSS (e.g., Richards et al. 2005, 2006).

Despite this systematic uncertainty in characteristic gas fractions, we predict the trend in SFR density with redshift accurately and can make several comparisons between the SFR density in mergers and the total SFR density estimated by Cole et al. (2001); Hopkins (2004); Pérez-González et al. (2005) in a robust manner. In fact, uncertainties in the direct comparison are dominated by the factor $\sim 2-3$ scatter in observational estimates of the total SFR density, rather than the uncertainties in our predictions. Regardless, we confirm the results of various direct observational estimates of merger fractions and their evolution with redshift (Le Fèvre et al. 2000; Patton et al. 2002; Conselice et al. 2003; Lin et al. 2004; Bundy et al. 2004; Conselice et al. 2005; Bell et al. 2005a; Wolf et al. 2005), namely that at $z \lesssim 1$, star formation triggered in mergers contributes only a small fraction to the SFR density of the Universe, but that this increases near the era of peak merger and quasar activity at $z \gtrsim 2$. Specifically, from Figure 15 we predict that only $\sim 1\%$ of the SFR density at $z = 0$ owes to mergers, and even assuming a maximal $f_{\text{gas}} = 1.0$ in all mergers only increases this to $\sim 10\%$ (setting a strong upper limit). The predicted contribution from mergers rises to $\sim 10-20\%$ by $z = 1$, with an upper limit $\sim 30\%$ ($f_{\text{gas}} = 1$). At $z = 2$, the contribution from mergers rises to $30_{-10}^{+15}\%$ of the cumulative SFR density, and $35_{-10}^{+20}\%$ at $z = 3$. Above these redshifts, the best-fit prediction approximately preserves these ratios, but the uncertainties in our prediction (as well as the determination of Cole et al. 2001) become large. Thus, at low redshifts $z \lesssim 1$, merger-induced star formation represents a small $\lesssim 10\%$ fraction of the SFR density, growing to a substantial but not dominant $\sim 25-50\%$ contribution at $z \gtrsim 2$.

Note that the above predictions do depend systematically on the faint-end slope of the MGLF, or equivalently the low-mass slope of the merger mass function, which the observed QLF only weakly constrains even where it is very well-constrained (see Figure 7). This systematic uncertainty dominates the shaded error range shown in Figure 15, a factor ~ 2 uncertainty at most redshifts where the QLF is well-measured. A more detailed constraint is possible with the measurements of the merger mass or luminosity functions, but the observations are still highly uncertain. For example, the MGLFs of Xu et al. (2004), Bundy et al. (2005a) at $z > 0.55$ (where incompleteness may be severe at the lowest masses), and Wolf et al. (2005) from GEMS yield faint-end slopes $\alpha \gtrsim 0.5$, implying a SFR density quite similar to our median prediction. However, if we consider the observations of Wolf et al. (2005) from the deeper GOODS subsample, from Bundy et al. (2005a) at $z < 0.55$, or simply a constant merger fraction with mass, this yields a steeper $\alpha \lesssim 0$. This

is, in all cases, within the $\sim 1\sigma$ range shown in Figure 15, but systematically increases the prediction by a factor ~ 2 . If this is indeed the “true” slope (and other observations are affected by incompleteness at low mass or luminosity), this implies a contribution to the total SFR density of $\sim 30\%$ at $z = 1$ and $\sim 60\%$ at $z = 2$.

We have demonstrated that feedback from black hole growth in mergers efficiently terminates star formation after the merger and regulates it thereafter, leaving red, elliptical remnants (Springel et al. 2005a; Hopkins et al. 2005f), and therefore expect an even smaller contribution to the SFR density at each z from the elliptical population (as is observed by e.g. Menanteau et al. 2005; Wolf et al. 2005). Thus, the dominant contribution to the star formation rate density of the Universe is from spiral galaxies (and possibly irregular galaxies, especially at high redshift, e.g. Cross et al. (2004); Daddi et al. (2004); Somerville et al. (2004a)), even assuming the most optimistic $f_{\text{gas}} = 1.0$ pure gaseous mergers, and this is true even at high redshift where there is at most a comparable $\sim 25-50\%$ contribution from star formation in mergers.

By convolving our predicted rate of formation of spheroids as a function of redshift with the characteristic gas fraction as a function of redshift, we can estimate a “mean” f_{gas} for spheroids of a given $z = 0$ mass. This f_{gas} represents the typical gas fractions of the mergers that made spheroids of that mass, and gives e.g. the fraction of stars formed in the spheroid-producing starburst (as opposed to in quiescent disks before the merger). We detail the rate of formation of spheroids as a function of redshift in Hopkins et al. (2005e), but it is essentially given by the merger rates as a function of total, final mass at each redshift. For example, the $f_{\text{gas}} = 1$ line in Figure 15 can also be thought of as the total rate at which stellar mass is “moved” from the blue sequence to the red sequence or “generated” in the red sequence by quasar-producing gas-rich mergers. Because our predicted spheroid population is old, with most forming at $z \gtrsim 2$ corresponding to the peak of quasar activity, assuming $f_{\text{gas}} = 10^{-t/t_H}$ gives a nearly constant characteristic mean gas fraction $\sim 60\%$ for essentially all spheroid masses of interest ($M_* \gtrsim 10^8 M_\odot$). Obviously a constant f_{gas} at all redshifts implies the same f_{gas} for all spheroid-producing mergers. In other words, the old ages of spheroids coupled with the expected increase in disk gas fractions at high redshift means that it is indeed a good approximation to assume that most spheroids are formed in quite gas-rich mergers. This is also directly supported by observations, as e.g. Hoekstra et al. (2005) find from stellar population analysis that elliptical galaxies must have formed most of their stars in the elliptical-producing event (i.e. a large fraction of the final stellar content coming from older, pre-existing stars in the elliptical progenitors is ruled out). This does not, of course, prohibit subsequent spheroid-spheroid mergers, which will not trigger star formation or quasar activity.

Finally, although the characteristic gas fraction in quasar-producing mergers is somewhat uncertain, and in detail will most likely follow a distribution rather than having a characteristic value at a given redshift, it is simple to adjust our predictions to any f_{gas} distribution. This is because f_{gas} enters linearly in the predicted SFR density at z in Equation (14), even though this is not strictly true for different formation rates as a function of final black hole mass. Thus, as observational and theoretical estimates of the typical f_{gas} of systems at these redshifts improve, this can be simply used to rescale

Equation (14) and Figure 15.

5.2.3. Specific Star Formation Rates and their Evolution

We now investigate the distributions of specific star formation rates (SSFRs; \dot{M}_*/M_*) in mergers, and their evolution with redshift. From Equation (5), we expect a characteristic $\text{SFR} \sim M_{*,\text{new}}/t_*$ in mergers with a given total stellar mass $M_{*,\text{new}}$ formed during the merger. While there is a broad distribution of SFRs over the course of an individual merger, it scales similarly about this characteristic rate, which depends on the *final* new stellar mass created in the merger, and not on the instantaneous stellar mass. From the evolution in the QLF or MGLF break luminosity with redshift, the characteristic stellar mass of quasar-producing mergers must increase with redshift, as must the characteristic gas fraction of these mergers. Therefore, the characteristic SFR observed in mergers must increase with redshift, regardless of the instantaneous stellar mass of the typical merging galaxies observed.

Figure 16 shows the specific star formation rates in our simulations, as a function of the instantaneous stellar mass M_* . We consider simulations with $f_{\text{gas}} = 1$, as this is probably more appropriate for the high-redshift comparisons shown, but changing the gas fraction will simply systematically shift the SSFR by $M_{*,\text{new}}/M_{*,\text{tot}} \approx f_{\text{gas}}$. In the upper left panel, we show the results for a range of simulations with $z = 0 - 6$, $M_* = 10^8 - 10^{12} M_\odot$, $q_{\text{EOS}} = 0.25 - 1$. Each simulation is color-coded by $M_* \approx M_{*,\text{new}}$, from $10^8 M_\odot$ in black to $10^{12} M_\odot$ in red. The dotted lines correspond to constant SFRs $\dot{M} = 1, 10, 100 M_\odot \text{yr}^{-1}$ (from bottom to top, respectively). The systematic shift to higher characteristic SFR with higher $M_{*,\text{new}}$ expected from § 3.3 is clear.

From the SSFR in Figure 16, a critical distinction is apparent. Although the SSFR systematically increases with total (final) stellar mass formed in the merger, $M_{*,\text{new}}$, as the characteristic SFR scales as $\sim M_{*,\text{new}}/t_*$, the SSFR for a given individual simulation generally *decreases* with the instantaneous stellar mass of the merger. This reflects the fact that the mergers build up a large amount of stellar mass with a SFR varying by generally less than one or two orders of magnitude (also seen in Figure 6 or from integrating Equation [5]). This distinction arises because gas-rich mergers can build up a large amount of their stellar mass over the course of a merger, and therefore (analogous to the distinction between instantaneous and peak quasar luminosity) the instantaneous stellar mass is not necessarily the same quantity as the total stellar mass which will be present after the merger. If the mergers occurring at a given redshift have a characteristic $M_{*,\text{new}}$ (i.e. the distribution of gas-rich merger rates or quasar peak luminosities is peaked), as we expect in our modeling, then the SSFRs of mergers at that redshift will decrease with observed stellar mass as appropriate for that $M_{*,\text{new}}$ in Figure 16. Indeed, several samples have observed that the SSFR appears to decrease with mass at all masses and redshifts (e.g., Bauer et al. 2005; Pérez-González et al. 2005; Feulner et al. 2005b), for all morphological types. In quiescent galaxies, this trend is easy to understand: at low masses, the population is dominated by disks which continue active star formation and have a high SSFR, and at high masses, the population is dominated by ellipticals which have terminated star formation and thus have a low SSFR. Our simulations demonstrate that we expect mergers to follow a similar trend, albeit for different physical reasons.

If we consider the characteristic $M_{*,\text{new}}$ of gas-rich mergers

as a function of redshift, we can predict how the SSFR distribution of mergers should evolve. In Figure 16, we show this prediction for a range of redshifts $z = 0 - 6$ (as labeled). At each redshift, we use the observed QLF of Ueda et al. (2003) (extrapolated to high redshifts following Hopkins et al. 2005e) to determine the distribution of quasar peak luminosities and corresponding masses of merging galaxies, and also assume the exponential evolution in gas fraction suggested in § 5.1, $f_{\text{gas}} = 10^{-t/t_H}$. This defines a characteristic $M_{*,\text{new}}(z)$ at each redshift, and we consider simulations with initial conditions scaled to be appropriate at that redshift and a final $M_{*,\text{new}}$ within a factor ~ 3 of that $M_{*,\text{new}}(z)$. For each such simulation at each redshift, we plot the SSFR at all times as a function of instantaneous stellar mass at that epoch. At each time, we compute the stellar mass-weighted mean stellar population age, and color-code the plotted SSFRs according to $\log_{10}(\text{age})$, with black points corresponding to ages $\lesssim 0.01$ Gyr and red points ages ~ 2.5 Gyr (e.g. dark blue at $\sim 0.05 - 0.1$ Gyr, green at $\sim 0.3 - 0.5$ Gyr, yellow at $\sim 0.8 - 1.2$ Gyr). These can be compared to the mean ages as a function of SSFR in e.g. Feulner et al. (2005a,b), and the age distributions agree well. In each panel, we again show lines of constant $\dot{M} = 1, 10, 100 M_\odot \text{yr}^{-1}$ (dotted lines). We also show the evolution in the mean SSFR, as observed at $0 \leq z \leq 1.5$ (extrapolated to other redshifts) in MUNICS, FORS, and SDSS (solid lines; Bauer et al. 2005), at $0 \leq z \leq 5$ from FORS and GOODS (circles and dashed lines; Feulner et al. 2005b), which also compares favorably with the evolution seen at $0 \leq z \leq 3$ from Spitzer observations of the CDF-S and HDF-N (Pérez-González et al. 2005).

At each redshift, our predictions preserve the general trend of higher SSFRs at lower M_* . However, this is not because lower-mass mergers are “more active” at that redshift, as is the common interpretation for quiescent galaxies, but rather represents the simple scaling of SSFRs with instantaneous stellar mass for mergers at that redshift which have similar total $M_{*,\text{new}}$; i.e. mergers of systems with similar total, final mass observed at various stages. At higher redshifts, gas fractions and the characteristic masses of merging systems increase, driving the characteristic SFR in mergers from e.g. $\sim 10 M_\odot \text{yr}^{-1}$ at $z \sim 1$ to $\sim 100 M_\odot \text{yr}^{-1}$ at $z \sim 3 - 4$ as $M_{*,\text{new}}$ (which defines the characteristic SFR $\sim M_{*,\text{new}}/t_*$) systematically increases. This evolution with redshift agrees well with the observations, despite the fact that these observations are not specific to merging systems (although such systems will be a significant part of these samples especially at the highest SFR). It is interesting that the evolution of SSFRs in disks, presumably driven by increasing concentrations and gas fractions at higher redshifts, may follow a similar trend, but we cannot compare the two in detail without a cosmological model for the distribution of disk properties. However, the SSFR evolution in merging systems, at least, is ultimately another manifestation of the downsizing seen in merging galaxy, quasar, and spheroid evolution.

6. QUASAR HOST GALAXY LUMINOSITY FUNCTIONS

Given the luminosity function of merging galaxies which produce quasars in our modeling, it is relatively simple to convert this into the expected luminosity function of quasar “host galaxies” (HGLF). In order to do this, of course, we must define what we mean by quasar host galaxies. If we consider all objects which have an X-ray AGN of even low luminosity, then we will recover a similar merger luminosity function to that we calculate from the X-ray QLF.

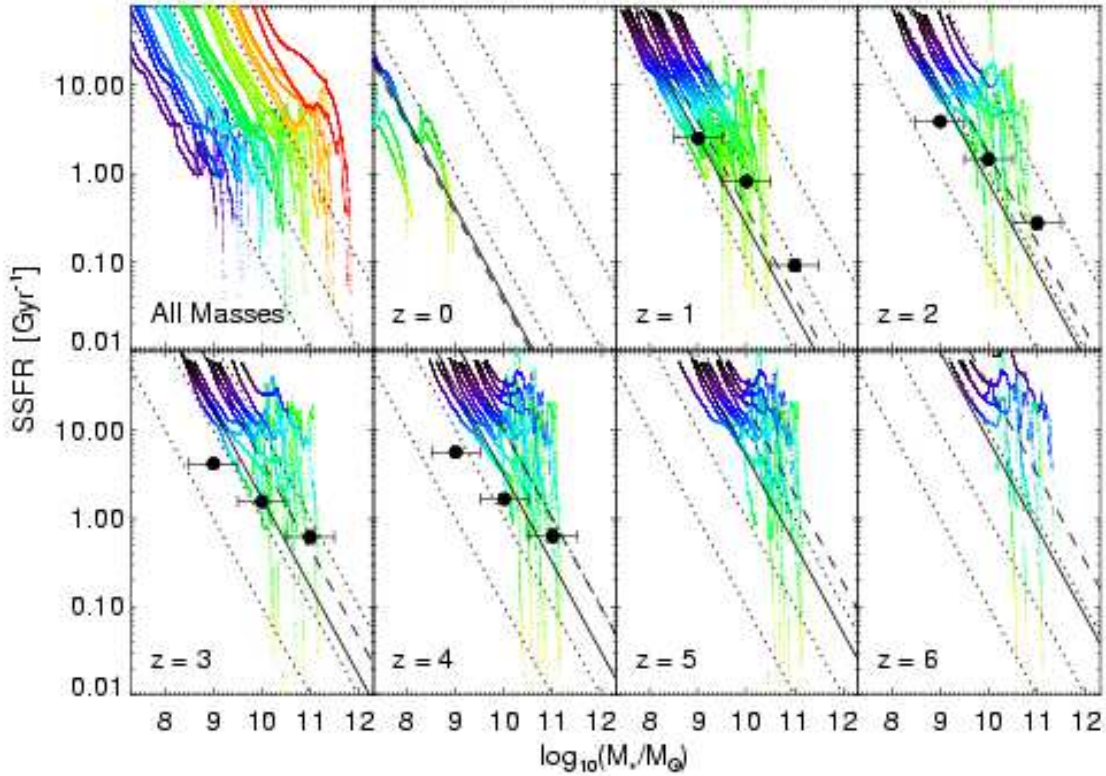


FIG. 16.— Specific star formation rates (\dot{M}_*/M_*) as a function of stellar mass at a given instant in the simulations. Upper left shows results for a range of simulations with $z = 0-6$, $M_* = 10^8 - 10^{12} M_\odot$, $q_{EOS} = 0.25-1$, color-coded by total stellar mass formed during the merger $M_{*,\text{new}}$ (from $10^8 M_\odot$ in black to $10^{12} M_\odot$ in red). In all panels, dotted lines correspond to constant SFRs $\dot{M} = 1, 10, 100 M_\odot \text{yr}^{-1}$ (from bottom to top, respectively). Subsequent panels show the SSFRs from simulations with a M_* characteristic of galaxies merging at that redshift, as implied by the QLF, at redshifts $z = 0-6$ (as labeled). SSFRs are color-coded by the mean (stellar mass-weighted) stellar population ages, from 0.01 Gyr (black) to 2.5 Gyr (red), binned in $\log_{10}(\text{age})$ (compare e.g. Figure 1 of Feulner et al. 2005b). The evolution in the mean SSFR is shown, as observed at $0 \leq z \leq 1.5$ (extrapolated to other redshifts) in MUNICS, FORS, and SDSS (solid; Bauer et al. 2005), at $0 \leq z \leq 5$ from FORS and GOODS (circles and dashed lines; Feulner et al. 2005b), which also compares favorably with the evolution seen at $0 \leq z \leq 3$ from Spitzer observations of the CDF-S and HDF-N (Pérez-González et al. 2005). The observed evolution in SSFRs in mergers is consistent with the evolution of the QLF and MGLF; it reflects the trend of the characteristic gas-rich merger mass increasing with redshift.

However, most previous efforts to measure the distribution of AGN host galaxy luminosities (e.g., Bahcall et al. 1997; McLure et al. 1999; Falomo et al. 2001; Hamilton et al. 2002; Jahnke & Wisotzki 2003; Dunlop et al. 2003; Floyd et al. 2004; Vanden Berk et al. 2005) have considered host galaxies of bright, *optical*, broad-line quasars. In our modeling, this phase of quasar activity is associated with the “blowout,” i.e. the final stages of black hole growth, when the surrounding gas is expelled and heated and the black hole is briefly rendered a bright optical source before accretion shuts down. We study this in Hopkins et al. (2005e), where we use both host galaxy and quasar optical luminosities to determine the relationship between quasar peak luminosity and host galaxy optical luminosity, and the resulting optical quasar luminosity function. Specifically, in Hopkins et al. (2005e) (Equation [26]), we derive the mean relation

$$\frac{L_{\text{B, obs}}^{\text{qso}}}{L_{\text{B, obs}}^{\text{gal}}} = 7.9 \frac{1}{f_{\text{gas}}} \left(\frac{M_{\text{BH}}^f}{10^8 M_\odot} \right)^{0.2} \frac{L}{L_{\text{peak}}}, \quad (15)$$

We can use this modeling to determine the optical luminosity function of quasar hosts by taking our already determined optical/UV merging galaxy luminosity functions and adding the additional selection criteria appropriate to these galaxies being identified as the hosts of bright optical quasars.

We show in § 3.1 and Hopkins et al. (2005e) that the host galaxy optical/UV luminosity is essentially constant in time, correlated with the peak quasar luminosity of the merger. However, in our picture the faint end of the observed QLF is dominated by sources at luminosities well below their peaks. Consequently, the observed quasar luminosity is uncorrelated with the host galaxy luminosity. This is discussed further in Hopkins et al. (2005c,e) in the context of the observed lack of correlation between quasar luminosity and black hole mass (e.g., Ho 2002; Heckman et al. 2004; Hao et al. 2005), but similarly explains the observed lack of a correlation between nuclear and host galaxy optical luminosity (Bahcall et al. 1997; McLure et al. 1999; Jahnke & Wisotzki 2003; Hao et al. 2005; Vanden Berk et al. 2005). At the brightest luminosities above the break in the quasar luminosity function, this is no longer strictly true, as black holes do increasingly tend to be at high Eddington ratio and near peak luminosity, and a correlation between nuclear and host luminosity is expected. These bright luminosities are precisely those for which the host galaxy luminosity is most difficult to measure, and therefore a quantitative observational assessment of this correlation is difficult. However, using our modeling of the quasar and galaxy luminosities during a merger, we can predict the joint distribution in optical quasar and host

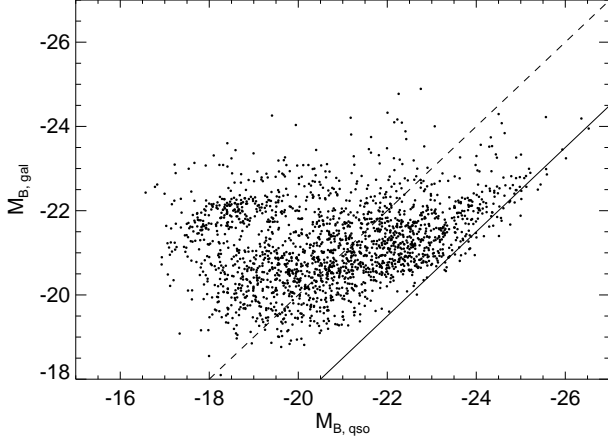


FIG. 17.— Predicted optical B -band quasar and host galaxy magnitudes for a mock sample of ~ 2000 optical “AGN” with $L_{\text{peak}} > 10^9 L_{\odot}$, at redshifts $z = 0.5$. Dashed line shows $L_{B, \text{gal}} = L_{B, \text{qso}}$ ($L_{\text{QSO}} \approx 0.1 L_{\text{Edd}}$), solid line $L_{B, \text{gal}} = 0.1 L_{B, \text{qso}}$ ($L_{\text{QSO}} \approx L_{\text{Edd}}$). Quasar and host luminosities are uncorrelated except at the brightest luminosities where systems are generally near-Eddington, as observed (e.g., Hao et al. 2005).

galaxy luminosity.

In Figure 17, we generate a mock sample of ~ 2000 optical “AGN” and plot their quasar and host galaxy B -band magnitudes. The procedure by which the mock distribution is generated is described in detail in Hopkins et al. (2005e), but briefly, we consider intervals of $\log(L_{\text{peak}})$ from the distribution of peak luminosities $\dot{n}(L_{\text{peak}})$ at $z = 0.5$ with $10^9 L_{\odot} < L_{\text{peak}} < 10^{14} L_{\odot}$. For each, we consider the simulations with the nearest peak luminosity, and calculate the PDF for their being observed as optical AGN (defined here by $M_{B, \text{qso}} < -16$ and an obscuring column density $N_H < 10^{22} \text{cm}^{-2}$) with a given AGN and host galaxy B -band luminosity (both calculated including attenuation using the method described in § 3.1). For a full derivation of the mean relation between quasar and host galaxy B -band luminosity as a function of instantaneous and peak quasar luminosity, see Hopkins et al. (2005e) (Equation [26]). From this distribution, we randomly calculate ~ 2000 points in $M_{B, \text{qso}}, M_{B, \text{gal}}$, which are shown in the figure. We assume $f_{\text{gas}} = 0.2$, but this only changes the normalization of $M_{B, \text{gal}}$ in this distribution. For comparison, the dashed line in the figure shows $L_{B, \text{gal}} = L_{B, \text{qso}}$ and the solid line shows $L_{B, \text{gal}} = 0.1 L_{B, \text{qso}}$. These approximately correspond to Eddington ratios of $L \approx 0.1 L_{\text{Edd}}$ and $L \approx L_{\text{Edd}}$, respectively. The distribution demonstrates the lack of correlation between quasar and host galaxy luminosity, and agrees well with various observational estimates (e.g., Bahcall et al. 1997; McLure et al. 1999; Jahnke & Wisotzki 2003; Sánchez et al. 2004). Specifically, compare Figure 13 of Vanden Berk et al. 2005, who find a nearly identical distribution considering host galaxy-AGN spectral decomposition of SDSS AGN complete to $L_{g, \text{gal}} \approx 0.1 L_{g, \text{qso}}$ (where the SDSS g -band is generally equivalent to B -band for our purposes).

Using the relation between B -band quasar and host galaxy luminosity as a function of instantaneous and peak quasar luminosity, we can infer the quasar HGLF from the MGLF. For a given peak luminosity (or correlated merging galaxy luminosity), we can calculate from Equation (15) and our scaling of the quasar lifetime as a function of instantaneous and peak

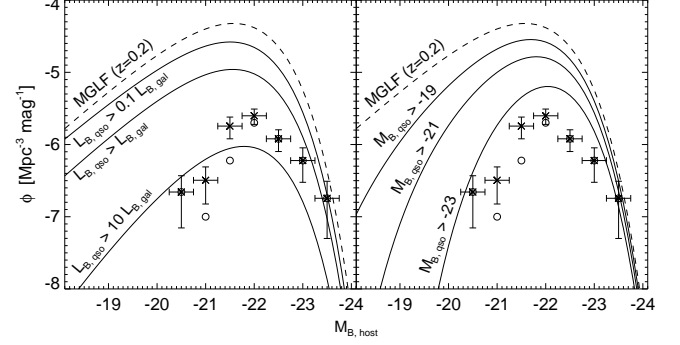


FIG. 18.— Predicted B -band HGLF of optical quasars at $z = 0.2$. Dashed line shows the full best-fit B -band MGLF (assuming $\alpha = 0.5$), solid lines show the HGLF requiring an observed B -band quasar luminosity above a given fraction of the host galaxy luminosity (left panel, as labeled) or requiring an observed B -band quasar magnitude above some fixed limit (right panel, as labeled). Points show the observational estimate of Hamilton et al. (2002) (requiring $M_{V, \text{qso}} < -23$, open circles) at $z \sim 0-0.4$, rescaled to typical B -band host luminosities following Bahcall et al. (1997) and Vanden Berk et al. (2005). Although these quasars are not necessarily predicted to be observed in an obvious merger stage, their host luminosity function is a subset of the MGLF, selected at a different merger stage.

luminosity what the time spent above some observed quasar B -band luminosity limit $L_{B, \text{qso}}$ and/or some limit in the ratio of quasar to host galaxy optical luminosity $L_{B, \text{qso}}/L_{B, \text{gal}}$ will be; i.e. the time during which we can estimate the merging galaxy can be identified as a traditional optical or broad-line AGN host galaxy.

Figure 18 shows the results of this calculation assuming different selection criteria in determining the HGLF. In the left panel, we show the MGLF at $z = 0.2$, determined from the $z = 0.2$ hard X-ray QLF of Ueda et al. (2003) as the dashed line. For clarity, we do not show the uncertainty in this prediction, but adopt the best-fit ϕ_*, M_* assuming $\alpha = 0.5$ and $f_{\text{gas}} = 0.2$; the uncertainty about the plotted MGLF can be seen in the upper and lower middle panels of Figure 7. As solid lines, we then show the HGLF, i.e. the MGLF given some selection criteria for the quasar and host galaxy B -band luminosity, namely $L_{B, \text{qso}} > 0.1 L_{B, \text{gal}}$, $L_{B, \text{qso}} > L_{B, \text{gal}}$, and $L_{B, \text{qso}} > 10 L_{B, \text{gal}}$, as labeled. In the right panel, we show the same, but instead imposing the B -band quasar magnitude limits $M_{B, \text{qso}} < -19$, $M_{B, \text{qso}} < -21$, and $M_{B, \text{qso}} < -23$, as labeled. In each, the observationally estimated optical quasar HGLF of Hamilton et al. (2002) is plotted, which is composed of quasars primarily of optical magnitude $M_B < -23$ (crosses with error bars; open circles show the inferred luminosity function applying a strict $M_V < -23$ magnitude cut). Because the host galaxy luminosities of Hamilton et al. (2002) are in V -band and appear to be systematically higher than those of most other samples (including overlapping samples) (Bahcall et al. 1997; McLure et al. 1999), a point discussed in detail by the authors, we fix the B -band magnitude of the peak of the HGLF to be that observed by e.g. Bahcall et al. (1997) and the much larger sample of Vanden Berk et al. (2005), $M_B \approx -22$.

In any case, the agreement between our predicted HGLF and the observed distribution of host galaxy luminosities, requiring that a bright optical quasar ($M_B < -23$) be observable, is good. There are several uncertainties in this comparison: for example, the normalization and absolute host magnitudes of the observed sample may be biased, our prediction only

loosely estimates the full distribution of dust obscuration as a function of time (see Hopkins et al. 2005e for a discussion, the key point is that by $M_B < -23$, a more accurate prediction from our simulations of the HGLF may be up to a factor ~ 2 lower), and as shown in Figure 7 the uncertainties in the initial MGLF (which propagate linearly into the HGLF) as determined from the QLF are large. For these reasons, the slight discrepancy in normalization between our prediction and the observations is not significant. Also, note that the appearance in Figure 18 that all bright mergers host optical quasars is an artifact of how steeply the Schechter function falls off – even at the brightest luminosities, there can be a factor $\sim 2-10$ difference between the MGLF and $M_B < -23$ HGLF prediction.

However, despite these uncertainties, the key qualitative point is clear – the quasar HGLF can be understood as a subset of the MGLF, with the appropriate though more sophisticated selection criteria applied as only mergers undergoing (or coming out of) the “blowout” phase will be identified. The characteristic magnitude, relative normalization, and narrow width of the HGLF are explained in this modeling, and this demonstrates that this luminosity function is self-consistent with both the QLF and MGLF in our interpretation of quasar fueling and the quasar luminosity function. Direct observations of e.g. the fraction of mergers with optical AGN (e.g., Sánchez et al. 2005), although traditionally more difficult than observations of the fraction of AGN in mergers, also suggest a similar fraction of mergers hosting optical AGN to that we predict for the appropriate luminosity limits in Figure 18. Although we have only shown this at one redshift, where most of the observations have been made, the qualitative result is the same regardless of the redshift (or e.g. value of f_{gas} or α) chosen.

Finally, this does not imply that all quasar host galaxies will necessarily be visible as mergers or interactions, although the low-redshift sample of Bahcall et al. (1997) indeed identifies the vast majority as such. Generally, the “blowout” phase in our simulations follows the final coalescence of the black holes, meaning that tidal tails and other evidence of a recent merger should in principle be evident, but at higher redshift surface brightness dimming will make these features nearly impossible to observe. Moreover, once the blowout begins, star formation is terminated and the host galaxy rapidly begins to redden, and extended tidal features will rapidly fade in ~ 1 Gyr.

The HGLF distribution we predict is also consistent with a wide range of observed properties of lower-luminosity AGN host galaxies. For example, Kauffmann et al. (2003a) study the host galaxies of $\sim 20,000$ SDSS narrow line, relatively low-luminosity AGN at $z < 0.3$ and find that a large fraction of these objects correspond to what we expect and find in our simulations for post-“blowout” objects with rapidly declining accretion rates in relaxing, rapidly reddening systems (see e.g. Hopkins et al. [2005g] for a description of the falloff in AGN luminosity as the merger relaxes). These objects reside in massive spheroids, with properties of “normal” ellipticals except for young stellar populations and evidence of starbursts in the past $\sim 1-2$ Gyr, with a sizable fraction ($\sim 30\%$) of especially the brightest objects showing obvious evidence of interaction and/or recent mergers. Similar results are also found for e.g. the AGN host population in GEMS (Sánchez et al. 2004) and radio loud quasars (Sánchez & González-Serrano 2003), although these may be preferentially at relatively low accretion rates (e.g., Ho 2002).

7. DISCUSSION

We have used simulations of galaxy mergers which account for star formation, metal enrichment, radiative cooling, supernova feedback and pressurization of a multi-phase interstellar medium, and black hole growth and feedback, to relate the distribution of observed quasar properties and its evolution with redshift to the distributions of merging galaxy properties, including their luminosity and mass functions, characteristic gas fractions, and contribution to the star formation rate density of the Universe. Our simulations span a wide range of initial and final conditions, varying virial velocities, initial gas fractions, masses, orbital parameters, initial black hole masses, ISM gas equations of state, redshifts, and galaxy mass ratios. Our modeling allows us to self-consistently map between the merging galaxy and quasar distributions in a physically motivated manner without invoking tunable cosmological distributions and enables predictions of many properties of merging galaxies at different redshifts.

We find that:

- The joint scaling of dust obscuration and star formation with gas density yields quite flat lightcurves in the optical/UV, allowing us to simply quantify the probability for observing a given merger at a given luminosity. To enable future comparison with observations, we provide a number of fits from our simulations to quantify the distribution of observed luminosities in different bands as a function of the stellar mass formed in mergers, total stellar mass, or final black hole mass of the merging systems (Table 1). This also allows us to determine color distributions, with a large and comparable scatter from both stellar population and obscuration effects, and a general lack of bright, blue objects.

- Given these simple lightcurves it is straightforward to transform an observed merger luminosity function into a merger rate as a function of mass. We test this directly, comparing the MGLF of Wolf et al. (2005) to the merger mass functions of Bundy et al. (2005a,b), and find good agreement between the two. Future measurements of these quantities from large galaxy surveys using automated morphological selection criteria can reliably calibrate selection efficiency against the results of our (or similar) simulations, removing the final $\sim 20-50\%$ absolute normalization uncertainty in the merger rate.

- We consider in detail the observed merger luminosity functions of Xu et al. (2004) in K -band at $z < 0.2$ and that of Wolf et al. (2005) at 280 nm at $z = 0.7$, as well as the observed merger mass functions of Bundy et al. (2005a,b) at $z = 0.2-0.55, 0.55-0.8$, and $0.8-1.4$. We use our simulations to map this to a quasar luminosity function at each redshift, and find that the predicted quasar luminosity functions agree with that observed by Ueda et al. (2003). Conversely, we invert this procedure, predicting the merger luminosity function from the observed quasar luminosity function, and again find agreement, although the predictions are significantly less well-constrained in this direction. Both distributions are self-consistent (each predicts the other) and can be used to predict merger rates and the rate of formation of quasars or spheroids as a function of that luminosity, mass and redshift.

Although merger mass functions are not yet well determined above these redshifts, the demonstration in Hopkins et al. (2006) that the characteristic masses of observed mergers, the “quenching” or “transition” mass where elliptical galaxies begin to dominate the total galaxy population, and the characteristic mass of quasars (at the observed

QLF break) all trace one another over the range $0 < z \lesssim 3$ further suggests that the accuracy of this mapping extends to high redshift.

- We compare this relation of merger and quasar distributions to that inferred if quasars turn “on/off” in simple step-function fashion or follow exponential lightcurves, and find that the observations rule out such scenarios at $\gtrsim 99.9\%$ confidence, even if we allow the quasar lifetime to vary freely to produce the best-fit. This can be determined entirely from the observed *shapes* of the QLF and MGLF, independent of selection efficiencies, gas fractions, or other cosmological properties; it would require a $\gtrsim 4-6\sigma$ change in the observed shape to change this conclusion. Any comparison of merger rates or merger distributions and quasar activity must account for complex quasar lightcurves and the non-trivial nature of quasar lifetimes which vary as a function of both instantaneous and peak luminosity.

- Our modeling allows us to directly compare the sensitivity of observations at different wavelengths to e.g. different stellar populations. Thus *K*-band observations provide a direct constraint of the merger rate as a function of final *total* stellar mass, and a test of the consistency of e.g. quasar, merger, and elliptical galaxy formation rates and mass/luminosity distributions. The optical/UV luminosity, on the other hand, depends directly on $M_{*,\text{new}} \approx f_{\text{gas}} M_{*,\text{tot}}$, and thus provides a direct constraint on the evolution of gas fractions in quasar and spheroid-producing mergers and the rate and distribution of total star formation in mergers (as opposed to the *instantaneous* star formation rate distribution, measured in e.g. IR and far UV observations).

- Using the quasar luminosity function, we predict the evolution of the MGLF in the optical/UV and near IR as a function of redshift. Because quasars spend most of their lives at luminosities well below their peak luminosities, and as a result the faint-end of the QLF is dominated by systems with much higher peak luminosities (i.e. mergers in more massive systems than would otherwise be inferred based on the low instantaneous quasar luminosity), the QLF places only weak constraints on the faint-end slope of the MGLF. However, we can predict the number density and characteristic luminosity (or luminosity density), ϕ_* and M_* , at each redshift where the QLF is constrained. Comparing these to a wide range of measurements of mergers rates/fractions and merger luminosity densities at $z = 0-3$, we find good agreement with the predictions from the QLF. This demonstrates that, with proper modeling of quasar activity, the QLF provides a significant independent constraint on merger rates and the mass/luminosity density in mergers as a function of redshift, at many redshifts $z = 0-6$ where complete morphological samples of interacting galaxies are difficult to obtain.

- Using an identical formalism, we consider the distribution of star formation rates in individual mergers and for the merger population. We can convolve these distributions with the observed optical/UV MGLF or QLF, and obtain the SFRF of merging galaxies. Comparing the inferred SFRF from the MGLF of Wolf et al. (2005) at $z = 0.7$ to the SFRF from the same galaxy sample from Bell et al. (2005a), we find good agreement. The trends of specific star formation rate as a function of instantaneous stellar mass and mean stellar ages are reproduced by all simulations as mass builds up during mergers, and the implied evolution of gas-rich mergers to higher masses and gas fractions at high redshifts inferred from the QLF accurately predicts the evolution in SSFRs with redshift.

- We use the QLF to predict the SFRF at various redshifts, and subsequently the SFR density in mergers as a function of redshift from $z = 0-6$. Comparison of these predictions with measurements, which currently exist at $z \lesssim 1$ (Brinchmann et al. 1998; Menanteau et al. 2001, 2005; Bell et al. 2005a), shows good agreement, and suggests that the QLF can provide a new, powerful, and independent probe of the SFR density in the universe driven by mergers. At redshifts $z \lesssim 4$, this allows us to predict the SFR density caused by mergers to a factor ~ 2 accuracy, with the primary systematic uncertainty being weak constraints on typical gas fractions of disks at low redshift $z \lesssim 1$. At $z > 4$, future improvements in constraints on the QLF break luminosity will enable similar predictions, without a large uncertainty in gas fractions, as gas-rich systems are expected at these high redshifts. Thus, quasar measurements can provide strong constraints on the SFR density triggered by mergers at high redshifts and at the end of the reionization epoch, where attempts to measure morphological properties of galaxies and determine this quantity directly are not likely to be possible in the near future. This also provides a prediction of the total rate at which mass is moved from the blue (disk) sequence to the red (spheroid) sequence, independent of gas fraction, as analyzed in detail in Hopkins et al. (2005f).

We find that the SFR density triggered in mergers is small at low redshift: $\sim 1\%$ of the total SFR density at $z \sim 0$, with a maximum of $\sim 10\%$ even if we assume all mergers have $f_{\text{gas}} = 1.0$ instead of a Milky Way-like $f_{\text{gas}} = 0.1$. This fraction of the SFR density rises to a significant, but not dominant $\sim 30\%$ (upper limit 60%) at $z \sim 2-3$, and remains approximately constant at higher redshift (assuming the extrapolation of Cole et al. (2001) is accurate at these redshifts). Given that black hole feedback rapidly terminates (and subsequently regulates) star formation in remnant ellipticals (Springel et al. 2005a; Hopkins et al. 2005e), the dominant contribution to the SFR density at all redshifts (but especially $z \lesssim 2$) must come from late-type spiral or irregular galaxies.

- We predict the joint distribution of quasar and host galaxy luminosities in good agreement with observations (Bahcall et al. 1997; McLure et al. 1999; Vanden Berk et al. 2005). The observation that quasar luminosities appear to be uncorrelated with host galaxy luminosities (especially at low quasar luminosity; Bahcall et al. 1997; McLure et al. 1999; Ho 2002; Jahnke & Wisotzki 2003; Heckman et al. 2004; Hao et al. 2005; Vanden Berk et al. 2005) is a natural consequence of the nearly constant optical/UV merger light curves we discuss above while quasar luminosities change by orders of magnitude during a merger.

We predict the quasar HGLF from either the observed QLF or MGLF at any given redshift. We find that the HGLF has a similar shape to the MGLF in a given band, but becomes increasingly peaked about M_* as the minimum optical quasar luminosity or minimum ratio of optical quasar to optical host galaxy luminosity is increased. For a given minimum quasar optical luminosity, e.g. $M_B < -23$, we find good agreement between the observed HGLF (Bahcall et al. 1997; Hamilton et al. 2002; Vanden Berk et al. 2005) and our prediction from the observed MGLF of Xu et al. (2004) or QLF of Ueda et al. (2003). The observed shape, normalization, and break/turnover luminosity in the quasar HGLF is a natural consequence of its being a subset of the MGLF, with e.g. a break at approximately the same luminosity (so long as the luminosity limit of the quasars in the sample is not so high as to exclude typical $\sim M_*$ hosts). This does not necessar-

ily mean that all quasar hosts will be obvious mergers, as in particular the bright optical phase of quasar activity is associated with the “blowout” phase following the final coalescence, in which rapidly fading tidal features may represent the only morphological merger signature.

We have demonstrated that the statistics and distributions of merging galaxy and quasar populations are self-consistent and can be used to predict one another in the context of the merger hypothesis. Coupled with the analysis of quasar properties in Hopkins et al. (2005a-e,g), remnant red-sequence elliptical galaxies in Hopkins et al. (2005f), and the co-evolution of the “transition” mass and merger and quasar masses in Hopkins et al. (2006), the modeling presented here unifies the populations of multiple relevant merger stages. The number of observed mergers accounts for the bright quasar population as well as the observed buildup in the mass of the elliptical / red-sequence galaxy population, and vice versa. *There is no room for a large fraction of gas-rich mergers which do not produce a bright quasar phase and remnant, reddening elliptical, nor is there room for a large fraction of bright quasars or elliptical galaxies which are not formed in gas-rich mergers.*

This allows us to make a wide range of predictions and provides a critical test of the hypothesis that starbursts, quasars, and elliptical galaxies are linked through the process of gas-rich mergers, a test which is complimentary and equally important to measurements of the individual photometric and kinematic properties and correlations of mergers and merger remnants (e.g., their profiles, metal enrichment, phase space densities, fundamental plane and $M_{\text{BH}} - \sigma$ relations: Lake & Dressler 1986; Doyon et al. 1994; Oliva et al. 1995; Shier & Fischer 1998; James et al. 1999; Genzel et al. 2001; Rothberg & Joseph 2004, 2005) and comparison of these remnants to detailed simulations (e.g., Barnes & Hernquist 1992; Hernquist 1993a; Springel et al. 2005a; Cox et al. 2005; Robertson et al. 2005a,b).

This does not mean, of course, that ellipticals never evolve via dry (gas-poor, spheroid-spheroid) mergers (see, e.g., Bell et al. 2005b; van Dokkum 2005), as such mergers only modify a necessarily pre-existing population of ellipticals (see also Hopkins et al. (2005f) for a calculation of the effects of such processes on observed elliptical distributions). This also does not imply that all AGN activity is associated with gas-rich mergers, as there can be a substantial contribution to low-luminosity AGN from activity triggered in quiescent spirals, as well as the large amount of quiescent, low-level activity in relaxed ellipticals which we predict (and account for) many dynamical times after the spheroid-forming merger as the quasar lightcurve decays (Hopkins et al. 2005e).

Our modeling makes predictions that can be used to test our underlying theory. For example, mergers at high redshifts should involve galaxies that are, on average, more gas-rich than local spirals (our preliminary comparison, for example, favors an exponentially declining f_{gas} over \sim a few Gyr). Preliminary evidence from D. Erb (2005, private communication) indicates that galaxies at redshift $z \approx 2$ do, indeed, have large gas fractions $f_{\text{gas}} \sim 0.5$, with some approaching $f_{\text{gas}} \sim 0.8 - 0.9$; but future observatories such as ALMA should be able to measure these quantities reliably.

The connection between merger induced star formation and quasar activity can also be used to test the correlation between our predicted SFR distributions and quasar peak luminosity. This should be possible with improved observations of quasar hosts in relaxed, post-merger systems which can be used to determine their individual star formation histories (e.g., Kauffmann et al. 2003a), as well as direct measurements of star formation in obscured, lower-luminosity merger phases, possibly associated with IR-bright Type 2 quasar activity (e.g., C. Hao et al. 2005; Kim et al. 2006) and strongly reddened optical quasars (e.g., Urrutia et al. 2005).

Mergers of gas-rich spirals will imprint structure into the remnants that may be difficult to account for otherwise (see e.g., Robertson et al. 2005b; Cox et al. 2005). The starburst population left behind will characteristically modify the central light profiles of merger remnants (e.g. Mihos & Hernquist 1994b), possibly explaining the central excesses of light seen in merging systems (e.g. Rothberg & Joseph 2004, 2005). This can be tested in detail by comparing predictions for metallicity and color gradients with observations. Even more subtle may be the shells, ripples, loops and other fine structures seen around many relaxed ellipticals (see, e.g. Schweizer 1998) that are a natural consequence of major mergers involving disk galaxies (e.g. Hernquist & Spergel 1992), but that do not form in major mergers between hot stellar systems. A measurement of the rate of occurrence of fine structure in red galaxies with redshift would further constrain the importance of mergers involving disk galaxies to the formation of ellipticals (Bell et al. 2005b; van Dokkum 2005).

We use our simulations to develop a formalism to derive the relations between the various populations we have studied in a manner robust against different cosmological distributions which are poorly constrained and often tuned to reproduce observations. However, this also means that we cannot constrain certain cosmological distributions. For example, we find that the distribution of observed luminosities of a merger is robust when expressed as a function of the final stellar mass or total stellar mass formed in the merger. This allows us to map the MGLF to a merger mass function, but does not allow us to consider the relative contribution of mergers with e.g. different initial mass ratios, ISM equations of state, or star formation histories. It will be interesting to see whether cosmological simulations naturally predict a priori the distributions of merger statistics that we have derived from quasar, merger, and elliptical galaxy observations. Coupling such cosmological descriptions with our detailed modeling of the complex star formation and black hole growth histories in mergers enables an a priori theoretical prediction of the wide array of phenomena we have demonstrated are linked through gas-rich galaxy mergers.

This work was supported in part by NSF grants ACI 96-19019, AST 00-71019, AST 02-06299, and AST 03-07690, and NASA ATP grants NAG5-12140, NAG5-13292, and NAG5-13381. The simulations were performed at the Center for Parallel Astrophysical Computing at the Harvard-Smithsonian Center for Astrophysics.

REFERENCES

- Alexander, D. M., et al. 2005a, *Nature*, 434, 738
 Alexander, D. M., Bauer, F. E., Chapman, S. C., Smail, I., Blain, A. W., Brandt, W. N., & Ivison, R. J. 2005b, *ApJ*, in press [astro-ph/0506608]
 Allen, D.A., Roche, P.F. & Norris, R.P. 1985, *MNRAS*, 213, 67p
 Armus, L., Heckman, T.M. & Miley, G. 1987, *AJ*, 94, 831

- Arribas, S., Bushouse, H., Lucas, R. A., Colina, L., & Borne, K. D. 2004, *AJ*, 127, 2522
- Bahcall, J.N., Kirhakos, S. & Schneider, D.P. 1994, *ApJ*, 435, L11
- Bahcall, J.N., Kirhakos, S. & Schneider, D.P. 1995, *ApJ*, 450, 486
- Bahcall, J. N., Kirhakos, S., Saxe, D. H., & Schneider, D. P. 1997, *ApJ*, 479, 642
- Barnes, J.E. 1998, in *Galaxies: Interactions and Induced Star Formation*, eds. D. Friedli, L. Martinet & D. Pfenniger (Springer-Verlag, Berlin), p. 275
- Barnes, J. E. & Hernquist, L. 1992, *ARA&A*, 30, 705
- Bauer, A. E., Drory, N., Hill, G. J., & Feulner, G. 2005, *ApJ*, 621, L89
- Baugh, C. M., Lacey, C. G., Frenk, C. S., Granato, G. L., Silva, L., Bressan, A., Benson, A. J., & Cole, S. 2005, *MNRAS*, 356, 1191
- Bell, E. F., McIntosh, D. H., Katz, N., & Weinberg, M. D. 2003, *ApJS*, 149, 289
- Bell, E. F., et al. 2005a, *ApJ*, 625, 23
- Bell, E. F., et al. 2005b, *ApJ*, in press [astro-ph/0506425]
- Borys, C., Smail, I., Chapman, S. C., Blain, A. W., Alexander, D. M., & Ivison, R. J. 2005, *ApJ*, in press [astro-ph/0507610]
- Bouchet, P., Lequeux, J., Maurice, E., Prevot, L., & Prevot-Burnichon, M. L. 1985, *A&A*, 149, 330
- Boyle, B. J., Shanks, T., Croom, S. M., Smith, R. J., Miller, L., Loaring, N., & Heymans, C. 2000, *MNRAS*, 317, 1014
- Brinchmann, J., et al. 1998, *ApJ*, 499, 112
- Brotherton, M. S., et al. 1999, *ApJ*, 520, L87
- Brotherton, M. S., Grabelsky, M., Canalizo, G., van Breugel, W., Filippenko, A. V., Croom, S., Boyle, B., & Shanks, T. 2002, *PASP*, 114, 593
- Bruzual, G. & Charlot, S. 2003, *MNRAS*, 344, 1000
- Bullock, J. S., Kolatt, T. S., Sigad, Y., Somerville, R. S., Kravtsov, A. V., Klypin, A. A., Primack, J. R., & Dekel, A. 2001, *MNRAS*, 321, 559
- Bundy, K., Fukugita, M., Ellis, R. S., Kodama, T., & Conselice, C. J. 2004, *ApJ*, 601, L123
- Bundy, K., Ellis, R. S., & Conselice, C. J. 2005a, *ApJ*, 625, 621
- Bundy, K., et al. 2005b, *ApJ*, in press [astro-ph/0512465]
- Burkley, J. M., et al. 1994, *ApJ*, 429, L13
- Burstein, D., Davies, R. L., Dressler, A., Faber, S. M., & Lynden-Bell, D. 1988, *ASSL Vol. 141: Towards Understanding Galaxies at Large Redshift*, 17
- Busha, M.T., Evrard, A.E., Adams, F.C. & Wechsler, R.H. 2004, *MNRAS*, submitted [astro-ph/0412161]
- Calzetti, D., Kinney, A. L., & Storchi-Bergmann, T. 1994, *ApJ*, 429, 582
- Canalizo, G., Stockton, A., Brotherton, M. S., & van Breugel, W. 2000, *AJ*, 119, 59
- Canalizo, G. & Stockton, A. 2001, *ApJ*, 555, 719
- Carlberg, R. G. 1986, *ApJ*, 310, 593
- Carlberg, R. G., Pritchet, C. J., & Infante, L. 1994, *ApJ*, 435, 540
- Cen, R., Miralda-Escudé, J., Ostriker, J. P., & Rauch, M. 1994, *ApJ*, 437, L9
- Cole, S., Lacey, C. G., Baugh, C. M., & Frenk, C. S. 2000, *MNRAS*, 319, 168
- Cole, S., et al. 2001, *MNRAS*, 326, 255
- Conselice, C. J., Bershad, M. A., Dickinson, M., & Papovich, C. 2003, *AJ*, 126, 1183
- Conselice, C. J., Blackburne, J. A., & Papovich, C. 2005, *ApJ*, 620, 564
- Cox, T. J., Di Matteo, T., Hernquist, L., Hopkins, P. F., Robertson, B., & Springel, V. 2005, *ApJ*, submitted [astro-ph/0504156]
- Croft, R.A.C., Weinberg, D.H., Katz, N. & Hernquist, L. 1998, *ApJ*, 495, 44
- Croft, R.A.C., Weinberg, D.H., Pettini, M., Hernquist, L. & Katz, N. 1999, *ApJ*, 520, 1
- Croft, R.A.C., Weinberg, D.H., Bolte, M., Burles, S. Hernquist, L., Katz, N., Kirkman, D., & Tytler, D. 2002, *ApJ*, 581, 20
- Croom, S. M., Smith, R. J., Boyle, B. J., Shanks, T., Miller, L., Outram, P. J., & Loaring, N. S. 2004, *MNRAS*, 349, 1397
- Cross, N. J. G., et al. 2004, *AJ*, 128, 1990
- Croton, D. J., et al. 2005, *MNRAS*, in press [astro-ph/0508046]
- Daddi, E., et al. 2004, *ApJ*, 600, L127
- Davé, R., Hernquist, L., Katz, N. & Weinberg, D.H. 1999, *ApJ*, 511, 521
- de Mello, D. F., Wadadekar, Y., Dahlen, T., Casertano, S., & Gardner, J. P. 2005, *AJ*, in press [astro-ph/0510145]
- Di Matteo, T., Springel, V., & Hernquist, L. 2005, *Nature*, 433, 604
- Doyon, R., Wells, M., Wright, G. S., Joseph, R. D., Nadeau, D., & James, P. A. 1994, *ApJ*, 437, L23
- Dunlop, J. S., McLure, R. J., Kukuła, M. J., Baum, S. A., O'Dea, C. P., & Hughes, D. H. 2003, *MNRAS*, 340, 1095
- Ellison, S. L., Hall, P. B., Lira, P. 2005, *AJ*, accepted [astro-ph/0507418]
- Elvis, M., et al. 1994, *ApJS*, 95, 1
- Faber, S. M., Trager, S. C., Gonzalez, J. J., & Worthey, G. 1995, *IAU Symp. 164: Stellar Populations*, 164, 249
- Falomo, R., Kotilainen, J., & Treves, A. 2001, *ApJ*, 547, 124
- Fan, X., et al. 2001, *AJ*, 122, 2833
- Ferrarese, L. & Merritt, D. 2000, *ApJ*, 539, L9
- Feulner, G., Goranova, Y., Drory, N., Hopp, U., & Bender, R. 2005a, *MNRAS*, 358, L1
- Feulner, G., Gabasch, A., Salvato, M., Drory, N., Hopp, U., & Bender, R. 2005b, *ApJ*, 633, L9
- Floyd, D. J. E., Kukuła, M. J., Dunlop, J. S., McLure, R. J., Miller, L., Percival, W. J., Baum, S. A., & O'Dea, C. P. 2004, *MNRAS*, 355, 196
- Franceschini, A. et al. 2006, *A&A*, in press [astro-ph/0601003]
- Gebhardt, K., Bender, R., Bower, G. et al. 2000, *ApJ*, 539, L13
- George, I. M., Turner, T. J., Netzer, H., Nandra, K., Mushotzky, R. F., & Yaqoob, T. 1998, *ApJS*, 114, 73
- Genzel, R., Tacconi, L. J., Rigopoulou, D., Lutz, D., & Tecza, M. 2001, *ApJ*, 563, 527
- Gerssen, J. et al. 2004, *AJ*, 127, 75
- Granato, G. L., De Zotti, G., Silva, L., Bressan, A., & Danese, L. 2004, *ApJ*, 600, 580
- Green, P. J., et al. 1995, *ApJ*, 450, 51
- Gunn, J.E. 1987, in *Nearly Normal Galaxies*, ed. S. Faber (Springer-Verlag: New York), p. 455
- Haiman, Z., & Loeb, A. 1998, *ApJ*, 503, 505
- Haiman, Z., & Menou, K. 2000, *ApJ*, 531, 42
- Haiman, Z., Quataert, E., & Bower, G. C. 2004, *ApJ*, 612, 698
- Hamilton, T. S., Casertano, S., & Turnshek, D. A. 2002, *ApJ*, 576, 61
- Hammer, F., Flores, H., Elbaz, D., Zheng, X. Z., Liang, Y. C., & Cesarsky, C. 2005, *A&A*, 430, 115
- Hao, L., et al. 2005, *AJ*, 129, 1795
- Hao, C. N., Xia, X. Y., Mao, S., Wu, H., & Deng, Z. G. 2005, *ApJ*, 625, 78
- Hasinger, G., Miyaji, T., & Schmidt, M. 2005, *A&A*, in press [astro-ph/0506118]
- Heckman, T. M., Bothun, G. D., Balick, B., & Smith, E. P. 1984, *AJ*, 89, 958
- Heckman, T. M., Kauffmann, G., Brinchmann, J., Charlot, S., Tremonti, C., & White, S. D. M. 2004, *ApJ*, 613, 109
- Hernquist, L. 1990, *ApJ*, 356, 359
- Hernquist, L. 1992, *ApJ*, 400, 460
- Hernquist, L. 1993a, *ApJ*, 409, 548
- Hernquist, L. 1993b, *ApJ*, 404, 717
- Hernquist, L., & Mihos, J. C. 1995, *ApJ*, 448, 41
- Hernquist, L. & Spergel, D.N. 1992, *ApJ*, 399, L117
- Hernquist, L., Spergel, D.N. & Heyl, J.S. 1993, *ApJ*, 416, 415
- Hernquist, L., Katz, N., Weinberg, D. & Miralda-Escudé, J. 1996, *ApJ*, 457, L51
- Hernquist, L., & Springel, V. 2003, *MNRAS*, 341, 1253
- Ho, L. C. 2002, *ApJ*, 564, 120
- Hoekstra, H., Hsieh, B. C., Yee, H. K. C., Lin, H., & Gladders, M. D. 2005, *ApJ*, in press [astro-ph/0510097]
- Hopkins, A. M. 2004, *ApJ*, 615, 209
- Hopkins, P. F., Bundy, K., Hernquist, L., Ellis, R. S., 2006, *ApJ*, submitted, [astro-ph/0601621]
- Hopkins, P. F., Hernquist, L., Martini, P., Cox, T. J., Robertson, B., Di Matteo, T., & Springel, V. 2005a, *ApJ*, 625, L71
- Hopkins, P. F., Hernquist, L., Cox, T. J., Robertson, B., Di Matteo, T., Martini, P., & Springel, V. 2005b, *ApJ*, 630, 705
- Hopkins, P. F., Hernquist, L., Cox, T. J., Robertson, B., Di Matteo, T., & Springel, V. 2005c, *ApJ*, 630, 716
- Hopkins, P. F., Hernquist, L., Cox, T. J., Robertson, B., Di Matteo, T., & Springel, V. 2005d, *ApJ*, 632, 81
- Hopkins, P. F., Hernquist, L., Cox, T. J., Robertson, B., Di Matteo, T., & Springel, V. 2005e, *ApJ*, accepted [astro-ph/0506398]
- Hopkins, P. F., Hernquist, L., Cox, T. J., Robertson, B., & Springel, V. 2005f, *ApJ*, accepted [astro-ph/0508167]
- Hopkins, P. F., Hernquist, L., Cox, T. J., Robertson, B., Di Matteo, T., & Springel, V. 2005g, *ApJ*, accepted [astro-ph/0508299]
- Hopkins, P. F., Hernquist, L., Narayan, R. 2005, *ApJ*, submitted [astro-ph/0510369]
- Hopkins, P. F., Strauss, M. A., Hall, P. B., Richards, G. T., Cooper, A. S., Schneider, D. P., Vanden Berk, D. E., Jester, S., Brinkmann, J., & Szokoly, G. P. 2004, *AJ*, 128, 1112
- Hui, L., Burles, S., Seljak, U., Rutledge, R.E., Magnier, E. & Tytler, D. 2001, *ApJ*, 552, 15
- Hutchings, J. B., & Neff, S. G. 1992, *AJ*, 104, 1
- Jahnke, K., & Wisotzki, L. 2003, *MNRAS*, 346, 304
- James, P., Bate, C., Wells, M., Wright, G., & Doyon, R. 1999, *MNRAS*, 309, 585
- Jogee, S. 2005, in *AGN Physics on All Scales*, LNP Volume, eds. D. Alloin, R. Johnson & P. Lira (Springer: Berlin), Ch. 6, in press [astro-ph/0408383]
- Jonsson, P., Cox, T. J., Primack, J. R., & Somerville, R. S. 2005, *ApJ*, in press [astro-ph/0503135]
- Jørgensen, I. 1997, *MNRAS*, 288, 161

- Joseph, R.D. & Wright, G.S. 1985, MNRAS, 214, 87
- Katz, N., Weinberg, D.H., Hernquist, L. & Miralda-Escudé, J. 1996a, ApJ, 457, L57
- Katz, N., Weinberg, D.H. & Hernquist, L. 1996b, ApJS, 105, 19
- Kauffmann, G., et al. 2003a, MNRAS, 346, 1055
- Kauffmann, G., et al. 2003b, MNRAS, 341, 54
- Kauffmann, G. & Haehnelt, M. 2000, MNRAS, 311, 576
- Keel, W. C., & Wu, W. 1995, AJ, 110, 129
- Kennicutt, R. C. 1998, ApJ, 498, 541
- Kim, M., Ho, L. C., & Im, M. 2006, ApJ, in press [astro-ph/0601316]
- Kleinmann, S.G. et al. 1988, ApJ, 328, 161
- Komossa, S., Burwitz, V., Hasinger, G., Predehl, P., Kaastra, J. S., & Ikebe, Y. 2003, ApJ, 582, L15
- Kormendy, J. & Richstone, D. 1995, ARA&A, 33, 581
- Kormendy, J. & Gebhardt, K. 2001, in AIP Conf. Proc. 586: 20th Texas Symposium on Relativistic Astrophysics, 363
- Kuntschner, H. 2000, MNRAS, 315, 184
- La Franca, F. et al. 2005, ApJ, in press [astro-ph/0509081]
- Lake, G. 1989, AJ, 97, 1312
- Lake, G., & Dressler, A. 1986, ApJ, 310, 605
- Le Fèvre, O., et al. 2000, MNRAS, 311, 565
- Le Floch, E. et al. 2005, ApJ, in press [astro-ph/0506462]
- Leitherer, C., et al. 1999, ApJS, 123, 3
- Li, Y., Mac Low, M.-M., & Klessen, R. S. 2005a, ApJ, 626, 823
- Li, Y., Mac Low, M.-M., & Klessen, R. S. 2005b, ApJ, in press [astro-ph/0508054]
- Lidz, A., Hopkins, P. F., Cox, T. J., Hernquist, L., & Robertson, B. 2005, ApJ, accepted [astro-ph/0507361]
- Lin, L., et al. 2004, ApJ, 617, L9
- Lotz, J. M., Primack, J., & Madau, P. 2004, AJ, 128, 163
- Lotz, J. M., Madau, P., Gialalisco, M., Primack, J., & Ferguson, H. C. 2006, ApJ, 636, 592
- Magdziarz, P., & Zdziarski, A. A. 1995, MNRAS, 273, 837
- Magorrian, J. et al. 1998, AJ, 115, 2285
- Marconi, A., Risaliti, G., Gilli, R., Hunt, L. K., Maiolino, R., & Salvati, M. 2004, MNRAS, 351, 169
- Marconi, A., & Hunt, L.K. 2003, ApJ, 589, L21
- Martin, C. L., & Kennicutt, R. C. 2001, ApJ, 555, 301
- Martini, P. 2004, in Carnegie Obs. Astrophys. Ser. 1, Coevolution of Black Holes and Galaxies, ed. L.C. Ho (Cambridge: Cambridge Univ. Press), 170
- Max, C.E. et al. 2005, ApJ, in press [astro-ph/0411590]
- McDonald, P., Miralda-Escudé, J., Rauch, M., Sargent, W.L., Barlow, T.A., Cen, R. & Ostriker, J.P. 2000, ApJ, 543, 1
- McDonald, P. et al. 2004, ApJ, submitted [astro-ph/0407377]
- McLure, R. J., Kukula, M. J., Dunlop, J. S., Baum, S. A., O'Dea, C. P., & Hughes, D. H. 1999, MNRAS, 308, 377
- Melnick, J. & Mirabel, I.F. 1990, A&A, 231, L9
- Menanteau, F., Abraham, R. G., & Ellis, R. S. 2001, MNRAS, 322, 1
- Menanteau, F., Ford, H. C., Motta, V., Benítez, N., Martel, A. R., Blakeslee, J. P., & Infante, L. 2005, AJ, in press [astro-ph/0509759]
- Mihos, J. C., & Hernquist, L. 1994a, ApJ, 425, L13
- Mihos, J. C., & Hernquist, L. 1994b, ApJ, 437, L47
- Miyaji, T., Hasinger, G., & Schmidt, M. 2001, A&A, 369, 49
- Navarro J. F., Frenk C. S., White S. D. M., 1996, ApJ, 462, 563
- Oliva, E., Origlia, L., Kotilainen, J. K., & Moorwood, A. F. M. 1995, A&A, 301, 55
- O'Shea, B.W., Nagamine, K., Springel, V., Hernquist, L. & Norman, M.L. 2005, ApJ, submitted [astro-ph/0312651]
- Pannella, M., Hopp, U., Saglia, R. P., Bender, R., Drory, N., Salvato, M., Gabasch, A., & Feulner, G. 2006, ApJ, in press [astro-ph/0601338]
- Patton, D. R., et al. 1997, ApJ, 475, 29
- Patton, D. R., et al. 2000, ApJ, 536, 153
- Patton, D. R., et al. 2002, ApJ, 565, 208
- Pei, Y. C. 1992, ApJ, 395, 130
- Peng, C. Y., Impey, C. D., Rix, H.-W., Keeton, C. R., Falco, E. E., Kochanek, C. S., Lehar, J., & McLeod, B. A. 2006, in press [astro-ph/0601391]
- Pérez-González, P. G., et al. 2005, ApJ, 630, 82
- Perola, G. C., Matt, G., Cappi, M., Fiore, F., Guainazzi, M., Maraschi, L., Petrucci, P. O., & Piro, L. 2002, A&A, 389, 802
- Richards, G. T. et al. 2005, in press [astro-ph/0504300]
- Richards, G. T., et al. 2006, in press [astro-ph/0601434]
- Richstone, D. et al. 1998, Nature, 395, A14
- Risaliti, G. & Elvis, M. 2005, ApJ, in press [astro-ph/0507434]
- Roberts, M. S., & Haynes, M. P. 1994, ARA&A, 32, 115
- Robertson, B., Yoshida, N., Springel, V., & Hernquist, L. 2004, ApJ, 606, 32
- Robertson, B., Hernquist, L., Bullock, J.S., Cox, T.J., Di Matteo, T., Springel, V., & Yoshida, N. 2005a, ApJ, submitted [astro-ph/0503369]
- Robertson, B., Hernquist, L., Cox, T. J., Di Matteo, T., Hopkins, P. F., Martini, P., & Springel, V. 2005b, ApJ, accepted [astro-ph/0506038]
- Robertson, B., Cox, T. J., Hernquist, L., Di Matteo, T., Hopkins, P. F., Martini, P., & Springel, V. 2005c, ApJ, accepted [astro-ph/0511053]
- Rothberg, B., & Joseph, R. D. 2004, AJ, 128, 2098
- Rothberg, B., & Joseph, R. D. 2005, AJ, in press [astro-ph/0510019]
- Rownd, B. K., & Young, J. S. 1999, AJ, 118, 670
- Salpeter, E. E. 1955, ApJ, 121, 161
- Sánchez, S. F., Becker, T., Garcia-Lorenzo, B., Benn, C. R., Christensen, L., Kelz, A., Jahnke, K., & Roth, M. M. 2005, A&A, 429, L21
- Sánchez, S. F., et al. 2004, ApJ, 614, 586
- Sánchez, S. F., & González-Serrano, J. I. 2003, A&A, 406, 435
- Sanders, D.B. et al. 1986, ApJ, 305, L45
- Sanders, D.B. et al. 1988a, ApJ, 325, 74
- Sanders, D.B. et al. 1988b, ApJ, 324, L55
- Sanders, D.B. et al. 1988c, ApJ, 328, L35
- Sanders, D. B. & Mirabel, I. F. 1996, ARA&A, 34, 749
- Sargent, A.I. et al. 1987, ApJ, 312, L35
- Sargent, A.I., Sanders, D.B. & Phillips, T.G. 1989, ApJ, 346, L9
- Schweizer, F. 1982, ApJ, 252, 455
- Schweizer, F. 1998, in Galaxies: Interactions and Induced Star Formation, eds. D. Friedli, L. Martinet & D. Pfenniger (Springer-Verlag, Berlin)
- Scoville, N.Z. et al. 1986, ApJ, 311, L47
- Shier, L. M., & Fischer, J. 1998, ApJ, 497, 163
- Small, T. A., & Blandford, R. D. 1992, MNRAS, 259, 725
- Soares, D. S. L., de Souza, R. E., de Carvalho, R. R., & Couto da Silva, T. C. 1995, A&A, 110, 371
- Soifer, B.T. et al. 1984a, ApJ, 278, L71
- Soifer, B.T. et al. 1984b, ApJ, 283, L1
- Soifer, B.T., Houck, J.R. & Neugebauer, G. 1987, ARA&A, 25, 187
- Somerville, R. S., Primack, J. R., & Faber, S. M. 2001, MNRAS, 320, 504
- Somerville, R. S., et al. 2004a, ApJ, 600, L135
- Somerville, R. S., Lee, K., Ferguson, H. C., Gardner, J. P., Moustakas, L. A., & Gialalisco, M. 2004b, ApJ, 600, L171
- Springel, V. 2005, MNRAS, submitted, [astro-ph/0505010]
- Springel, V., Di Matteo, T., & Hernquist, L. 2005a, ApJ, 620, L79
- Springel, V., Di Matteo, T., & Hernquist, L. 2005b, MNRAS, 361, 776
- Springel, V. & Hernquist, L. 2002, MNRAS, 333, 649
- Springel, V. & Hernquist, L. 2003a, MNRAS, 339, 289
- Springel, V. & Hernquist, L. 2003b, MNRAS, 339, 312
- Springel, V. & Hernquist, L. 2005, ApJ, in press [astro-ph/0411379]
- Stockton, A. 1978, ApJ, 223, 747
- Stockton, A. & MacKenty, J. 1987, ApJ, 316, 584
- Stockton, A. & Ridgway, S. 1991, AJ, 102, 488
- Strateva, I., Brandt, N., Schneider, D. P., Vanden Berk, D. G., Vignali, C. 2005, AJ, in press [astro-ph/0503009]
- Straughn, A. N., Cohen, S. H., Ryan, R. E., Hathi, N. P., Windhorst, R. A., & Jansen, R. A. 2005, ApJ, accepted [astro-ph/0511423]
- Sulentic, J. W., & Rabaca, C. R. 1994, ApJ, 429, 531
- Surace, J. A., Sanders, D. B., & Evans, A. S. 2000, ApJ, 529, 170
- Telfer, R. C., Zheng, W., Kriss, G. A., & Davidsen, A. F. 2002, ApJ, 565, 773
- Toledo, H. M. H., Dultzin-Hacyan, D., Gonzalez, J. J., & Sulentic, J. W. 1999, AJ, 118, 108
- Toomre A., 1977, in Evolution of Galaxies and Stellar Populations, 401, Yale Univ. Obs: New Haven
- Toomre A. & Toomre J., 1972, ApJ, 178, 623
- Ueda, Y., Akiyama, M., Ohta, K., & Miyaji, T. 2003, ApJ, 598, 886
- Urrutia, T., Lacy, M., Gregg, M. D., & Becker, R. H. 2005, ApJ, 627, 75
- Vanden Berk, D. E., et al. 2001, AJ, 122, 549
- Vanden Berk, D. E., et al. 2005, AJ, in press [astro-ph/0509332]
- van Dokkum, P. G. 2005, AJ, 130, 2647
- Viel, M., Matarrese, S., Theuns, T., Munshi, D. & Wang, Y. 2003, MNRAS, 340, L47
- Viel, M., Haehnelt, M.G. & Springel, V. 2004, MNRAS, 354, 684
- Vignali, C., Brandt, W. N., & Schneider, D. P. 2003, AJ, 125, 433
- Vitvitska, M., Klypin, A. A., Kravtsov, A. V., Wechsler, R. H., Primack, J. R., & Bullock, J. S. 2002, ApJ, 581, 799
- Volonteri, M., Haardt, F., & Madau, P. 2003, ApJ, 582, 559
- Walker, I. R., Mihos, J. C., & Hernquist, L. 1996, ApJ, 460, 121
- Wilkes, B. J., Tananbaum, H., Worrall, D. M., Avni, Y., Oey, M. S., & Flanagan, J. 1994, ApJS, 92, 53
- Wolf, C., et al. 2005, ApJ, 630, 771
- Worthey, G., Faber, S. M., & Gonzalez, J. J. 1992, ApJ, 398, 69
- Wyithe, J. S. B. & Loeb, A. 2003, ApJ, 595, 614
- Xu, C., & Sulentic, J. W. 1991, ApJ, 374, 407
- Xu, C. K., Sun, Y. C., & He, X. T. 2004, ApJ, 603, L73
- Yee, H. K. C., & Ellington, E. 1995, ApJ, 445, 37
- Yip, C. W., et al. 2004, AJ, 128, 2603

Zepf, S. E., & Koo, D. C. 1989, ApJ, 337, 34

Zhang, Y., Anninos, P., & Norman, M. L. 1995, ApJ, 453, L57

TABLE 1
BEST-FIT OBSERVED MERGER LUMINOSITIES

Band	¹ $\langle M_{\text{BAND}} \rangle = M_{10} + \alpha \log \left(\frac{M_{*,\text{new}}}{10^{10} M_{\odot}} \right)$			² $\langle M_{\text{BAND}} \rangle = M_{11} + \alpha \log \left(\frac{M_{*,\text{tot}}}{10^{11} M_{\odot}} \right)$			³ $\langle M_{\text{BAND}} \rangle = M_8 + \alpha \log \left(\frac{M_{\text{BH}}}{10^8 M_{\odot}} \right)$			σ
	M_{10}	α	χ^2/ν	M_{11}	α	χ^2/ν	M_8	α	χ^2/ν	
280/40	-20.7 ± 0.1	-2.0 ± 0.1	0.61	-22.0 ± 0.2	-2.0 ± 0.3	2.29	-22.3 ± 0.2	-1.5 ± 0.2	2.76	0.62 ± 0.06
U	-19.7 ± 0.2	-2.0 ± 0.3	0.76	-20.9 ± 0.2	-2.3 ± 0.3	1.47	-21.3 ± 0.2	-1.9 ± 0.2	1.59	0.67 ± 0.32
B	-20.2 ± 0.2	-2.0 ± 0.2	0.97	-21.2 ± 0.1	-2.3 ± 0.2	0.83	-21.7 ± 0.1	-1.7 ± 0.2	0.77	0.49 ± 0.25
V	-20.7 ± 0.1	-2.0 ± 0.2	1.66	-21.6 ± 0.1	-2.2 ± 0.2	0.74	-22.1 ± 0.1	-1.7 ± 0.2	1.13	0.34 ± 0.28
R	-21.0 ± 0.1	-1.9 ± 0.2	2.40	-21.8 ± 0.1	-2.2 ± 0.2	0.88	-22.3 ± 0.1	-1.7 ± 0.1	1.61	0.52 ± 0.28
I	-21.2 ± 0.1	-1.9 ± 0.1	3.40	-21.9 ± 0.1	-2.3 ± 0.1	0.97	-22.5 ± 0.1	-1.7 ± 0.1	2.24	0.45 ± 0.26
J	-22.2 ± 0.1	-2.0 ± 0.1	6.40	-22.9 ± 0.1	-2.2 ± 0.1	1.51	-23.5 ± 0.1	-1.7 ± 0.1	3.69	0.47 ± 0.18
H	-22.6 ± 0.1	-2.1 ± 0.1	6.15	-23.4 ± 0.1	-2.2 ± 0.1	1.67	-24.1 ± 0.1	-1.7 ± 0.1	3.96	0.39 ± 0.17
K	-22.7 ± 0.1	-2.1 ± 0.1	5.18	-23.6 ± 0.1	-2.3 ± 0.1	1.47	-24.3 ± 0.1	-1.7 ± 0.1	3.42	0.29 ± 0.21
SDSS <i>u</i>	-19.3 ± 0.2	-2.2 ± 0.3	0.85	-20.7 ± 0.2	-2.2 ± 0.3	1.29	-21.1 ± 0.1	-1.7 ± 0.2	0.84	0.76 ± 0.41
SDSS <i>g</i>	-20.5 ± 0.2	-2.0 ± 0.2	1.15	-21.5 ± 0.1	-2.2 ± 0.2	0.80	-22.0 ± 0.1	-1.7 ± 0.2	0.85	0.52 ± 0.25
SDSS <i>r</i>	-20.9 ± 0.1	-1.9 ± 0.2	2.38	-21.7 ± 0.1	-2.2 ± 0.2	0.83	-22.3 ± 0.1	-1.7 ± 0.1	1.58	0.52 ± 0.27
SDSS <i>i</i>	-21.1 ± 0.1	-2.0 ± 0.1	3.19	-21.9 ± 0.1	-2.2 ± 0.1	0.88	-22.5 ± 0.1	-1.7 ± 0.1	2.08	0.48 ± 0.26
SDSS <i>z</i>	-21.3 ± 0.1	-2.0 ± 0.1	4.46	-22.0 ± 0.1	-2.3 ± 0.1	1.04	-22.6 ± 0.1	-1.7 ± 0.1	2.65	0.48 ± 0.22

¹Distribution of observed luminosities of mergers, as a function of new stellar mass $M_{*,\text{new}}$ formed during the merger. This assumes the probability of viewing a merger at some magnitude in the given band is a Gaussian with median $\langle M_{\text{BAND}} \rangle$ and dispersion σ in the band.

²Same, as a function of total, final stellar mass $M_{*,\text{tot}}$ after the merger.

³Same, as a function of final black hole mass M_{BH} after the merger.